The spatial distribution of typhoon wind fields as observed by CYGNSS and AMSR2

顧, 德欣
九州大学大学院総合理工学府大気海洋環境システム学専攻

出版情報：Kyushu University, 2021, 修士, 修士
バージョン：
権利関係：

The spatial distribution of typhoon wind fields as observed by CYGNSS and AMSR2

Dexin Gu

Supervisor: Ichikawa Kaoru

Interdisciplinary Graduate School of Engineering Sciences

Kyushu University

Contents

1. Introduction 4
1.1 Purpose and composition 5
2. Data and Methodology 6
2.1 Digital Typhoon 6
2.2 CYGNSS and data processing 6
2.2.1 CYGNSS 6
2.2.2 CYGNSS data processing 8
2.3 AMSR2 all-weather product and data processing 13
2.3.1 AMSR2 all-weather product 13
2.3.2 AMRS2 data processing 15
2.4 ERA5 and CFSRv2 20
2.4.1 ERA5 model 20
2.4.2 CFSR2 model 20
2.4.3 ERA5 and CFSRv2 models data processing 20
2.5 Target typhoon 22
2.6 Wind speed distribution 26
2.6.1 Setting of degree interval 26
2.6.2 Setting of distance interval 28
2.6.3 Normalization and generalization of wind speed distributions 29
3.Results 32
3.1 Normalized wind speed distribution in storm range 32
3.2 Normalized wind speed distribution in gale range 35
4.Discussions 38
4.1 AMSR2 show different pattern in storm range of Jebi 38
4.2 Peak angles in CYGNSS are shifted in Jebi 41
5.Conclusion 43
6.Acknowledgement 44
7.Reference 45
Appendix 47

A.1 Daily distributions under 45 degree interval 47
A.2 Daily distributions under 90 degree interval 71

1. Introduction

Typhoons are natural phenomena that are extremely powerful and destructive. In addition to direct disasters caused by strong winds, it can also cause secondary disasters such as storm surges, heavy rains, floods, landslides, mudslides, and landslides, or compound disasters caused by several reasons. According to the 10-year statistical data of the Japan Meteorological Agency from 2011 to 2020, the average number of typhoons per year is 26.1. 12.3 of them approached Japan. An average of 3.5 landed in Japan per year affected the lives of many people and caused huge economic losses. In recent years, the frequency of typhoons has been on the rise, and the requirements for accurate monitoring and timely warning of typhoons are imminent. However, it is still difficult to predict the intensity of typhoons. One of the key problems in the current research is the lack of more accurate wind distribution observations of the typhoon to help in-depth understanding of its physical process.

However, since direct observations of a typhoon wind field are practically difficult. Indirect observation by satellite is a feasible method, but strong winds are difficult to observe even by satellite, such as satellite with altimeter observe wind waves. Wind waves are saturated under strong winds. Moreover, the measurements are affected by various factors associated with high sea states, such as big winds, high waves, especially atmospheric rains, and ocean surface foams.

For now, strong winds can only be observed by two types of satellites: CYGNSS and AMSR2.They have many advantages such as global coverage, low cost, all-weather, near real-time. And can penetrate clouds and heavy rainfall under any type of weather conditions, so it is very useful to monitor ocean wind speed during typhoons.

Several research have been undertaken using the CYGNSS and AMSR2 datasets; however, past evaluations and analyses of CYGNSS wind speed have primarily been based on simulated storms or limited stages of tropical cyclones.[1][2]

Furthermore, CYGNSS and AMSR2 dataset's accuracy and reliability are not verified in the actual super typhoon cases. An important feature of the typhoon wind fields: 'Right-hand strengthening' in the movement, was considered as this study's focal point.

1.1 Purpose and composition

For relative wind speed distribution in a typhoon field, it is known that moving wind field has an Ideal asymmetry pattern: which is generally stronger to the right of moving direction due to superimposing background winds. (Fig.1-1)

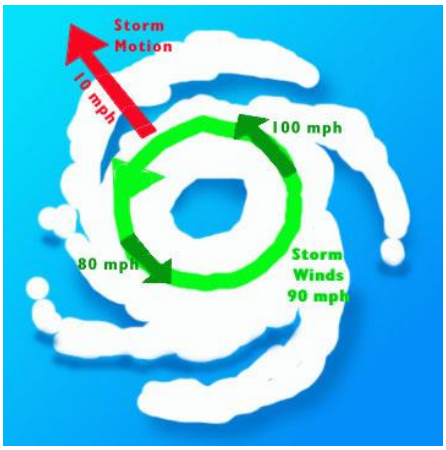

Fig.1-1 Typhoon's asymmetric wind fields

(From Tropical cyclone windspeed climatology, Wikipedia)

In this study, CYGNSS and AMSR2 wind speed distribution were analyzed and compared with numerical models throughout the life cycles of the two super typhoons, Typhoon Jebi (T1821) and Typhoon Trami (T1824), of the 2018 Pacific typhoon season.

Section 2 shows basic introduction and numerical sources of satellite products and numerical models, data processing methods and basic information of the target typhoons. In section 3, results are presented by comparing with the numerical models. In section 4, the discussions are given. Finally, conclusions are given in section 5.

2. Data and Methodology

For these two satellite products and two models, after a brief introduction about their observation methods and limitations, typhoon coordinate maps were made first. Then consider the range of years that different products can provide, two representative typhoons were selected, and their path and basic information are given. Finally, combining the data characteristics of different products and typhoon information, a method of analyzing the distribution of wind fields is given in this section.

2.1 Digital Typhoon

For the analysis of typhoon, data visualization is an essential step. In the visualization process, information such as the location and scope of the typhoon is necessary. So data from Digital Typhoon was used in this study.

Digital Typhoon Detailed Track Information is provided by the National Institute of Informatics (NII), Japan. Detailed Track Information records metadata related to the typhoon such as center location, radius, and maximum wind speed for every three or six hours. Digital typhoon also provides information including typhoon path, satellite image, etc. This information will be used in subsequent data processing and analysis.

2.2 CYGNSS and data processing

2.2.1 CYGNSS

One satellite product that can observe strong winds is CYGNSS. CYGNSS is a NASA Cyclone Global Navigation Satellite System mission operates eight micro-satellites in the same orbit measures the strength of GPS signals reflected at the sea surface to provide frequent observations of the wind speeds. Each of the 8 micro-satellites receives 4 signals from different GPS satellites, corresponding to a total of 32 GPS satellites. This makes each micro-satellite can provides four observational lines along trails of GPS refection points during its fly-over movements. [3] And the reflected GPS signals are reversely proportional to the sea surface gradient so that wind speed can be retrieved. (Fig. 2-1)

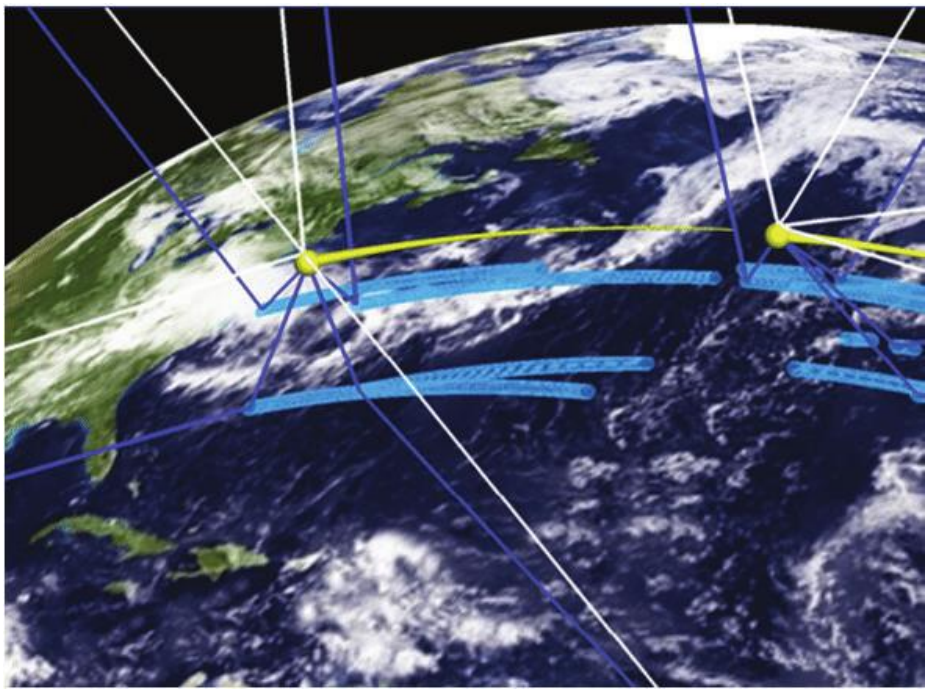

Fig. 2-1 CYGNSS satellite observation method

(From Satellite Missions introduction, ESA Earth Observation Portal)

CYGNSS satellites use an orbital inclination of approximately 35° from the equator. Because of this inclination, CYGNSS can monitor ocean surface winds between 38° N and 38° S latitude. This range includes the critical latitude band for tropical cyclone formation and movement.

Through the above methods, satellites have the capability to measure the ocean surface wind field with unprecedented temporal resolution and spatial coverage, under all precipitating conditions, and over the full dynamic range of wind speeds experienced in a typhoon. (Fig.2-2)

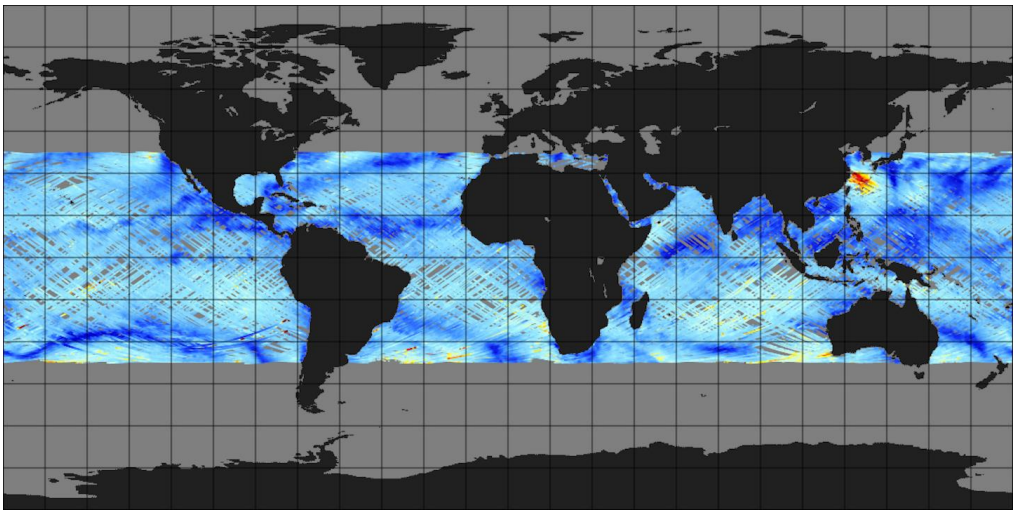

Fig. 2-2 CYGNSS satellite observation range

(From CYGNSS Dataset, PO. DAAC, NASA)

CYGNSS can obtain many-time frequent observation at about 12-minute interval. In this study, CYGNSS Level 2 Science Data Record Version 3.0 (2018-Aug-01 to Present) was used for analysis, which is freely available from the following URL.

https://podaac.jpl.nasa.gov/dataset/CYGNSS_L2_V3.0

2.2.2 CYGNSS data processing

As already stated, CYGNSS provides linear continuous observation without mention of typhoon center position. To visualize CYGNSS according to the typhoon center, typhoon time information, latitude, and longitude of typhoon center from information Digital Typhoon Detailed Track Information (Table.2-3) was used to interpolate to reckon the center position of every CYGNSS observation time. (Fig.2-4)

Time(hour)	latitude	longitude
0	15.4	157.0
6	16.2	156.3
12	16.6	155.6
18	16.7	154.4
24	17.0	153.5

Table.2-3 Sample of Digital Typhoon Detailed Track Information in one day

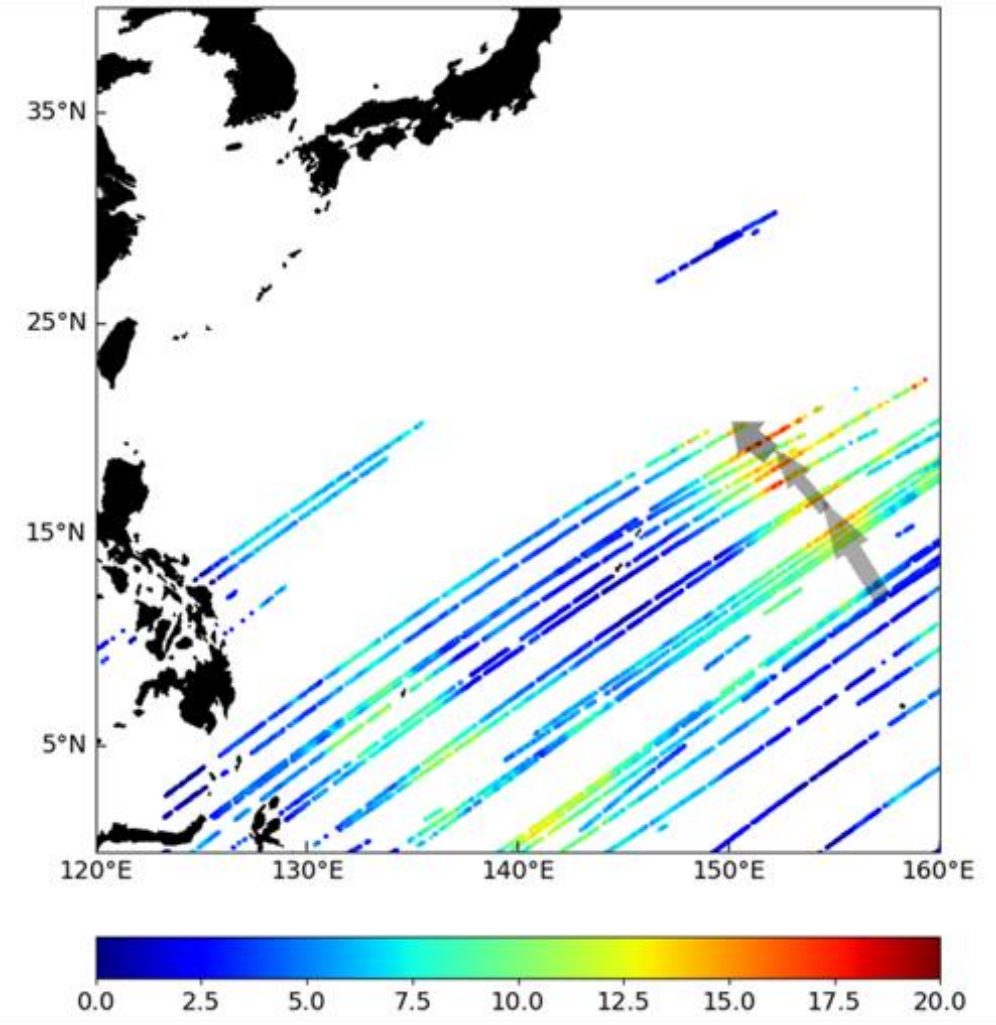

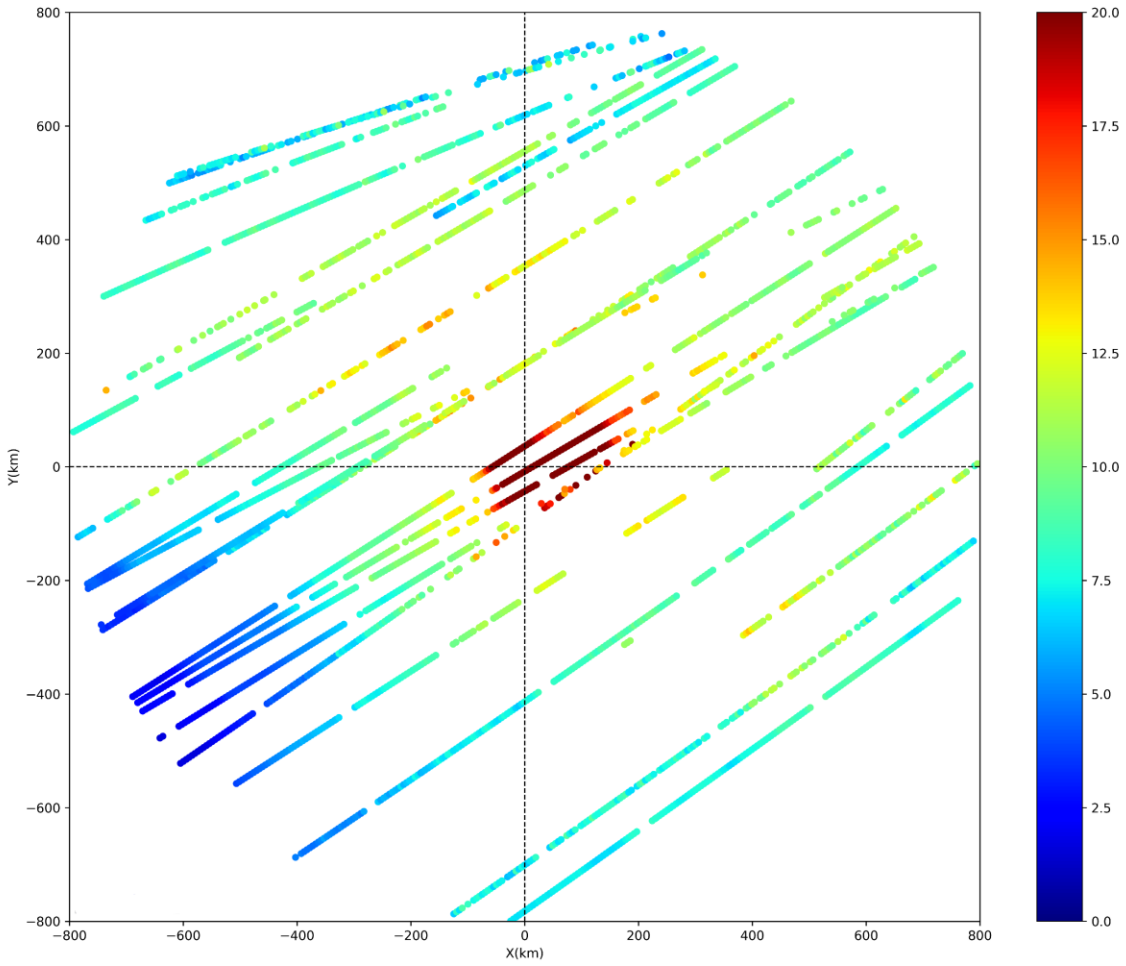

Fig.2.4 A sample set of CYGNSS raw data visualization and processed typhoon center map (units [m/s])

In the left figure is the raw data of CYGNSS for half a day, during this half day, the position of the typhoon center changes as indicated by the arrow, so in order to get the position of all points relative to the center at different observation times in half a day, as in the right figure, the interpolation calculation was required as follows.

The Estimated latitude Lat_i and Estimated longitude Lon_i of center position were calculated as:

$$Lat_i = Lat_0 + \frac{\Delta Lat}{\Delta t} \cdot (t_i - t_0) \qquad Lon_i = Lon_0 + \frac{\Delta Lon}{\Delta t} \cdot (t_i - t_0), \qquad (2.5)$$

where t_0 denote the start time in each interval from Digital Typhoon, Lat_0 and Lon_0 denote latitude and longitude at the start time, Δt denote the length of a time interval, ΔLat and ΔLon denote the change of latitude and longitude during the interval. t_i denote the specific observation time that needs to be estimated.

After interpolation, the typhoon center coordinates at each observation time are obtained. Making a typhoon coordinate map is a feasible method, which provides for a more accurate comparison of CYGNSS data with other products. Since the position of the typhoon center at each observation time of CYGNSS has been obtained, assuming that the earth is a sphere, the distance $Dist.$and bearing $Brng.$between the coordinates of the observation point and the center of the typhoon at each observation time of CYGNSS were calculated by $haversine\ formula.$

$$a = \sin\left(\frac{Lat_i - Lat_c}{2}\right)^2 + \cos(Lat_i) \cdot \cos(Lat_c) \cdot \sin\left(\frac{Lon_i - Lon_c}{2}\right)^2 \qquad (2.6)$$

$$Dist. = \mathrm{R} \cdot \arctan\left(\frac{\sqrt{a}}{\sqrt{1-a}}\right) \qquad (2.6)$$

$$Brng. = \arctan\left(\frac{\sin(Lon_c - Lon_i) \cdot Lat_c}{cosLat_i \cdot Lon_C - sinLon_i \cdot cosLat_c \cdot \cos(Lon_c - Lon_i)}\right) \qquad (2.7)$$

where Lat_i , Lon_i denote interpolated latitude and longitude;Lat_c, Lon_c denote the longitude and latitude of the CYGNSS observation point. R denote the radius of the earth, set to 6373km. After determining the distance and bearing from the typhoon center, since

the two numerical models are daily aggregates data, the CYGNSS data was plotted as daily typhoon coordinate maps base on the calculated distance, bearing and wind speed value from the data.

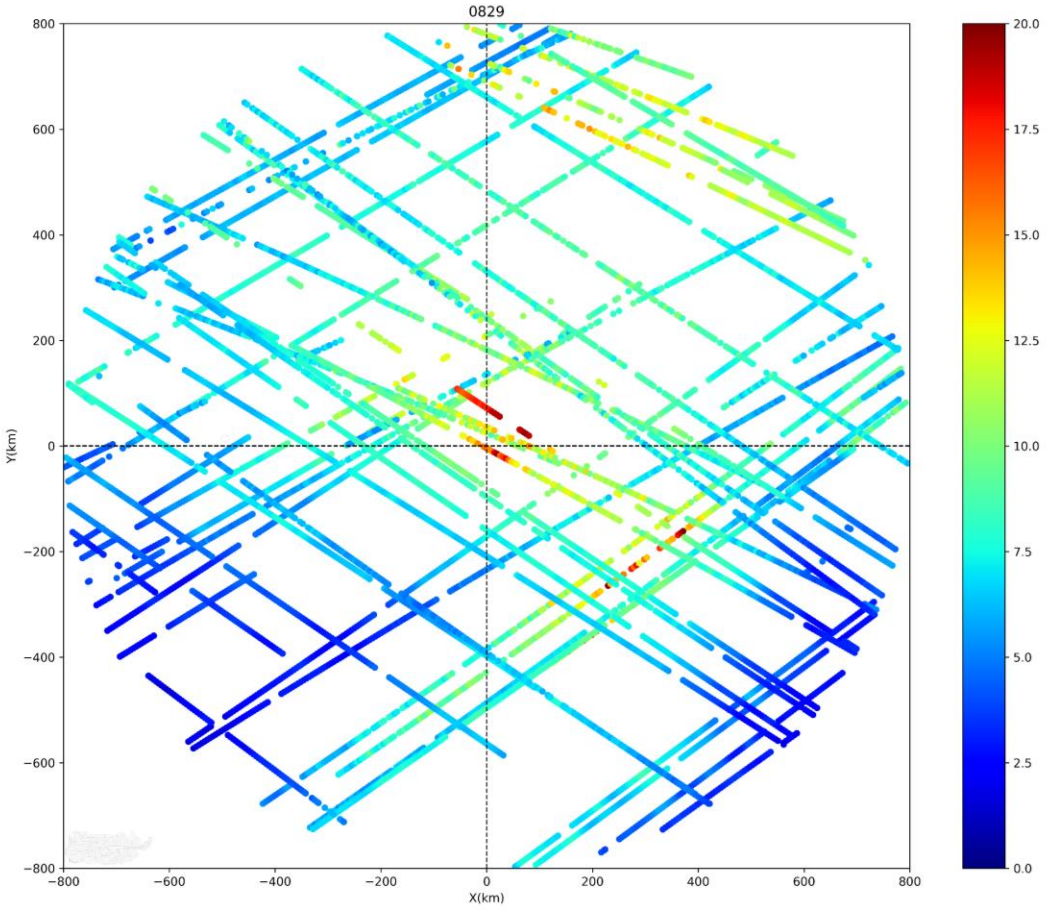

Fig.2-8 Typhoon coordinate map on August 29 (units [m/s])

The horizontal and vertical axis represents the range from the center of the typhoon. The color bar from blue to red indicates that the wind speed is from weak to strong. It can be found in the figure that the observations of CYGNSS are very sparse, and there are many overlapping places, even in the same orbit. In addition, strong wind can be observed in the

lower right part of the center, but not in the surroundings. This may be due to the large temporal variations in the observation of CYGNSS in a whole day.

2.3 AMSR2 all-weather product and data processing

2.3.1 AMSR2 all-weather product

Another satellite product that can observe strong winds is AMSR2 All-weather Sea surface Wind speed (ASW) product. ASW product is one of the data products provided by The Advanced Microwave Scanning Radiometer 2 (AMSR2) on GCOM-W1 spacecraft by JAXA measures microwave radiation. ASW product is different from the standard product by using low-frequency channels as 6-GHz and 10-GHz.

From about 700 km above the Earth, scanner on the satellite will provide us highly accurate measurements. And the antenna rotates once per 1.5 seconds and obtains data over a 1450 km swath. This conical scan mechanism enables this satellite to acquire data with adequate earth coverage. (Fig.2-9)

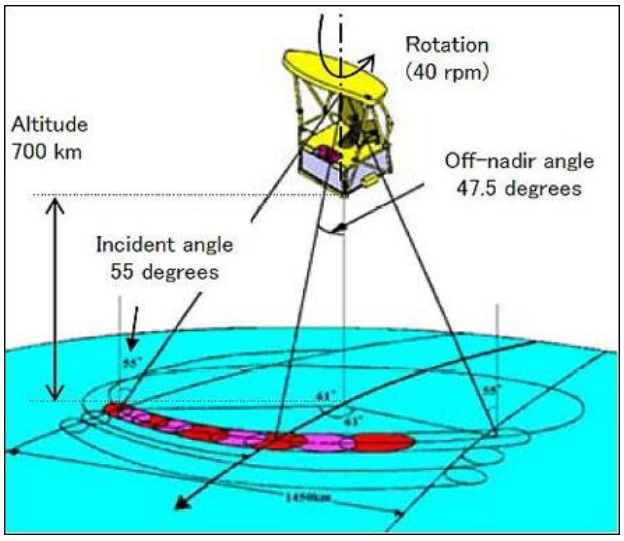

Fig. 2-9 Observation method (From GCOM, eoPortal Directory)

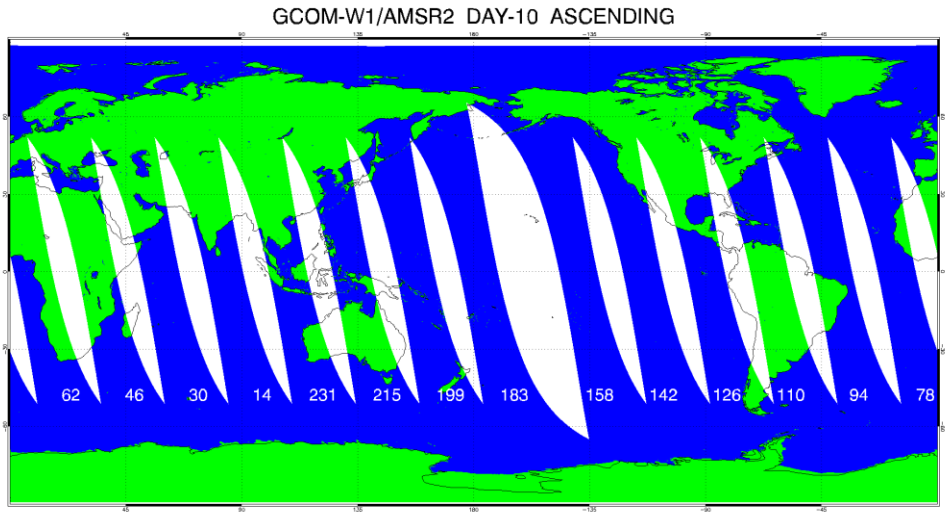

Fig.2-10 AMSR2 on GCOM-W1 spacecraft observation range on Aug.29, 2018 (Ascending) (From observation area of AMSR2, GCOM)

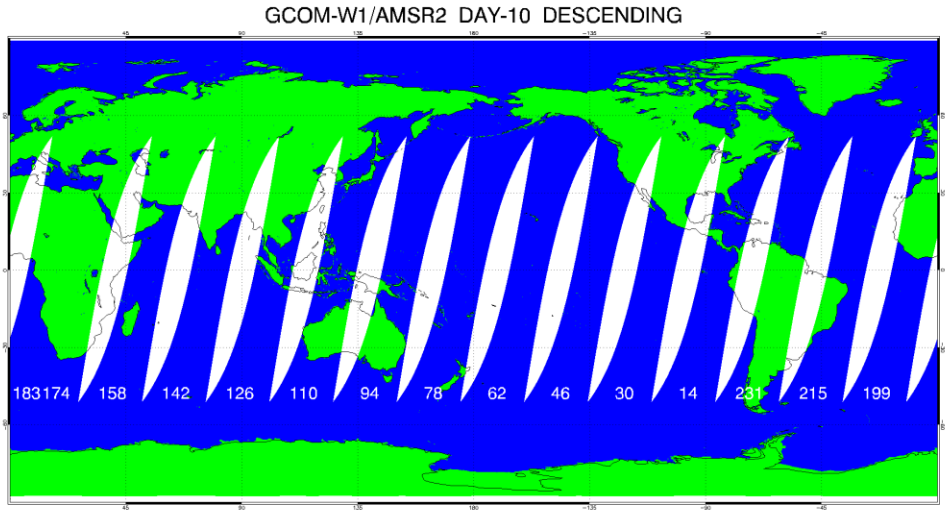

Fig.2-11 AMSR2 on GCOM-W1 spacecraft observation range on Aug.29, 2018 (Descending) (From observation area of AMSR2, GCOM)

As described earlier, ASW product is one of GCOM-W1 research product, have the same observation range as the standard product, and contains wind speeds in the best track of

typhoons announced by Japan Meteorological Agency and NOAA National Hurricane Center, realized the inversion of sea surface wind speed more than 70 m/s.

In this product provided, 2-dimensional snapshot wind speed distribution map can be obtained every half day even under heavy wind conditions. In this study, Dr. Hiroyuki Tomita, Hokkaido Univ provided ASW data for analysis.

2.3.2 AMRS2 data processing

As mentioned above, AMSR2 can provide two snapshots a day at most, in the ascending orbit and the descending orbit. (Fig.2-12)

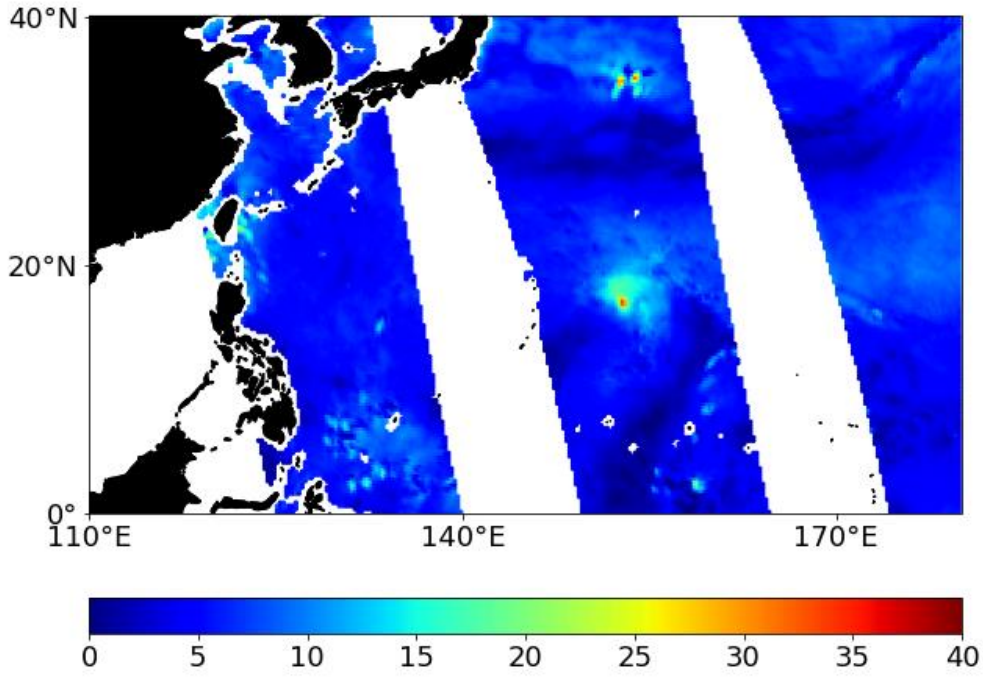

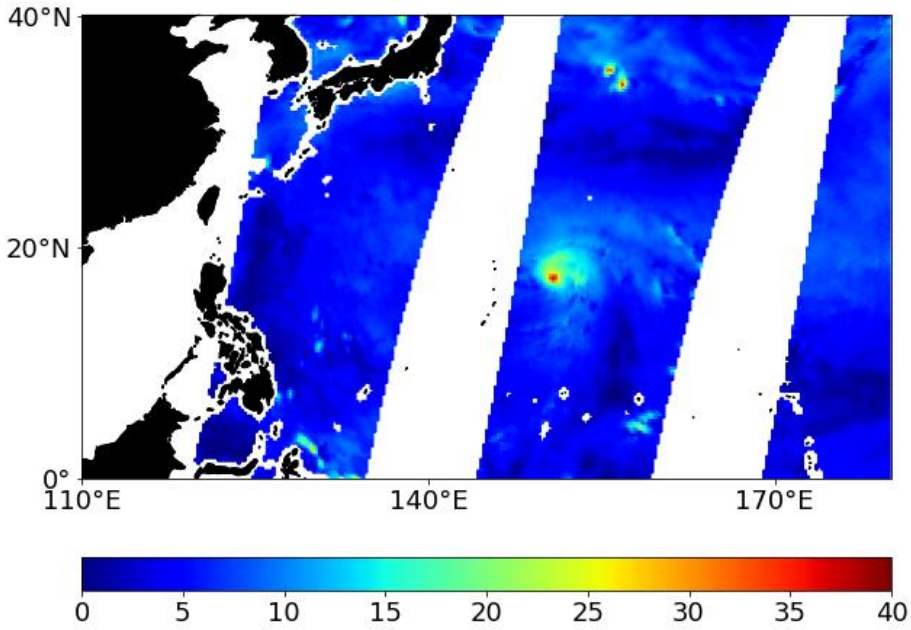

Fig.2-12 AMSR2 ascending orbit and the descending orbit observation on August 29 (units [m/s])

It can be noticed that in one observation orbit, the observation range of AMSR2 cannot cover all places. When observing a typhoon, it will be possible to observe the position of the typhoon once a day. In the most extreme case, the typhoon may not be observed, such as August 31. (Fig.2-13)

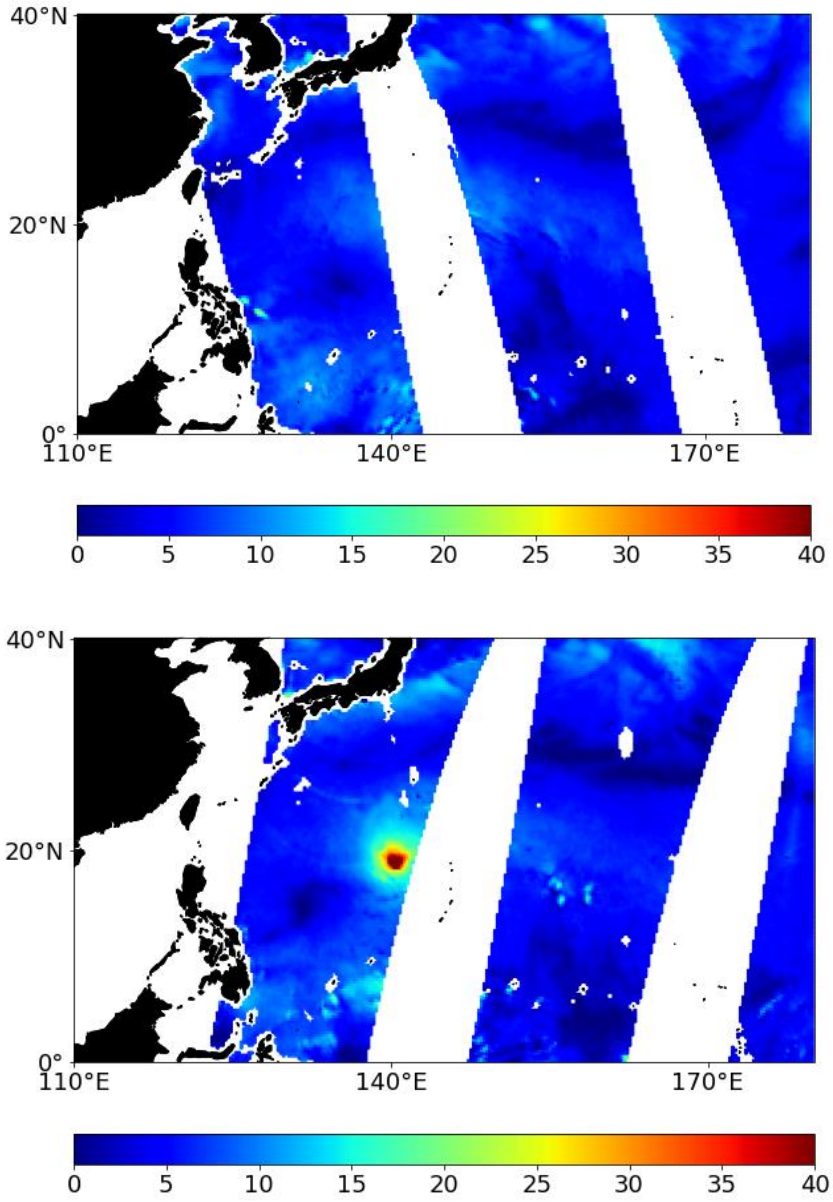

Fig.2-13 AMSR2 ascending orbit and the descending orbit observation on August 31 (units [m/s])

Based on recognizing this situation of AMSR2, refer to the typhoon center location in Digital Typhoon Detailed Track Information, AMSR2 had also been made into typhoon coordinate maps. These are the typhoon coordinates on August 29 as a sample for explanation. (Fig.2-14)

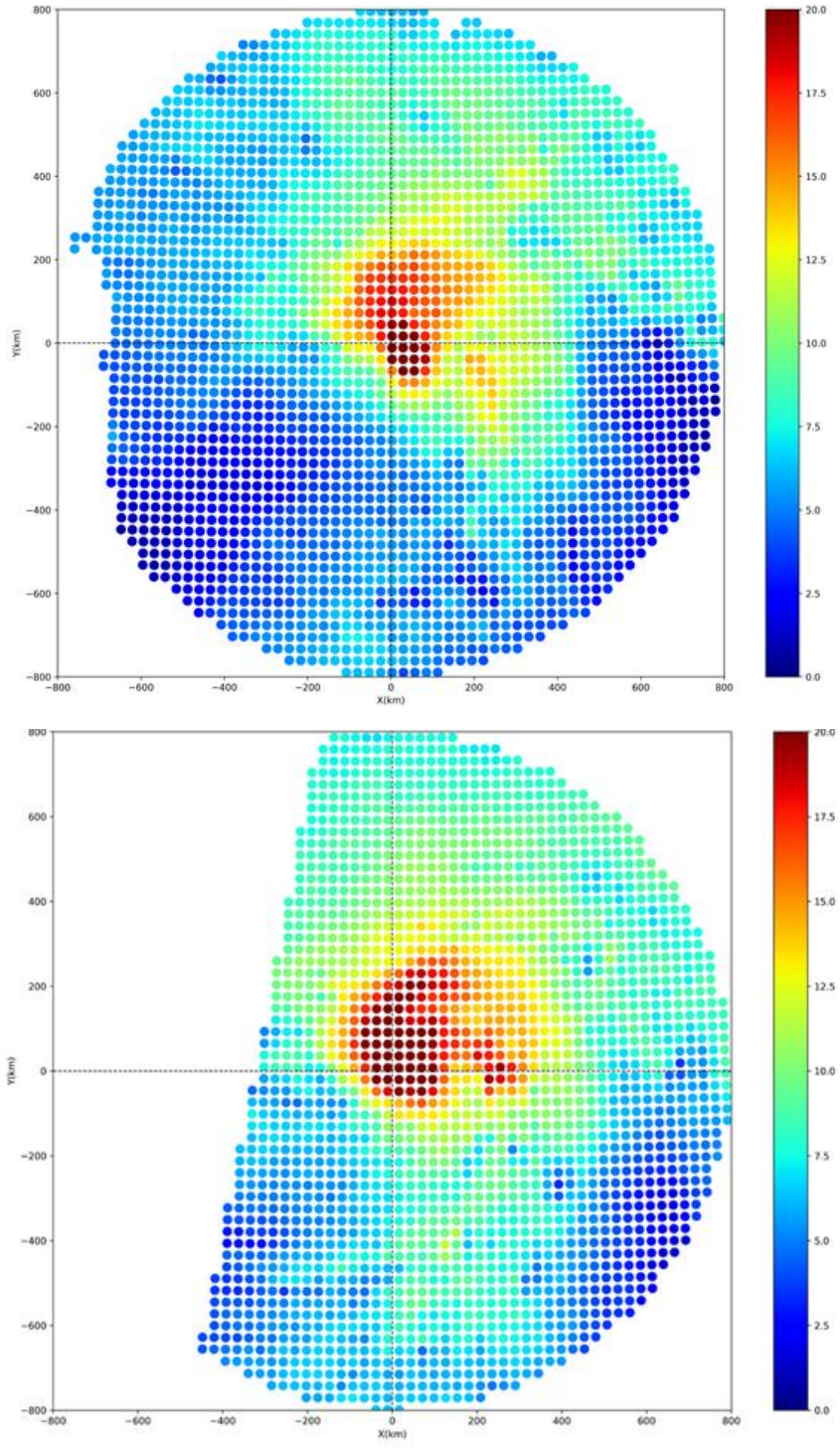

Fig.2-14 AMSR2 typhoon coordinate maps on August 29 (units [m/s]. Left: 4:30UTC; Right: 16:30UTC)

2.4 ERA5 and CFSRv2

2.4.1 ERA5 model

ERA5 is a comprehensive reanalysis produced by the Copernicus Climate Change Service (C3S) at ECMWF covering the period from January 1950 to present, which assimilates as many observations as possible in the upper air and near surface. The ERA5 atmospheric model is coupled with a land surface model and a wave model. ERA5 combines vast amounts of historical observations including various types of satellite data and In-situ data into global estimates using advanced modelling and data assimilation systems. It provides hourly estimates of atmospheric, land and oceanic climate variables. The data cover the Earth on a 30km grid and resolve the atmosphere using 137 levels from the surface up to a height of 80km.

2.4.2 CFSR2 model

CFSRv2 is another comprehensive reanalysis produced by National Centers for Environmental Prediction (NCEP) covering the period from April 2011 to present. CFS also uses the latest scientific approaches for taking in, or assimilating, observations from data sources including surface observations, upper air balloon observations, aircraft observations, and satellite observations. This model offers hourly data with a horizontal resolution down to one-half of a degree (approximately 56 km) around Earth for many variables. Daily aggregates grid data of the ERA5 and CFSRv2 hourly grid data provided by Dr. Shinichiro Kako, Faculty of Engineering, Kagoshima University, was used for analysis in this study.

2.4.3 ERA5 and CFSRv2 models data processing

For ERA5 and CFSR2, their data format is grid value as AMSR2, and the values are a daily averaged, so they were processed as AMSR2. (Fig.2-15)

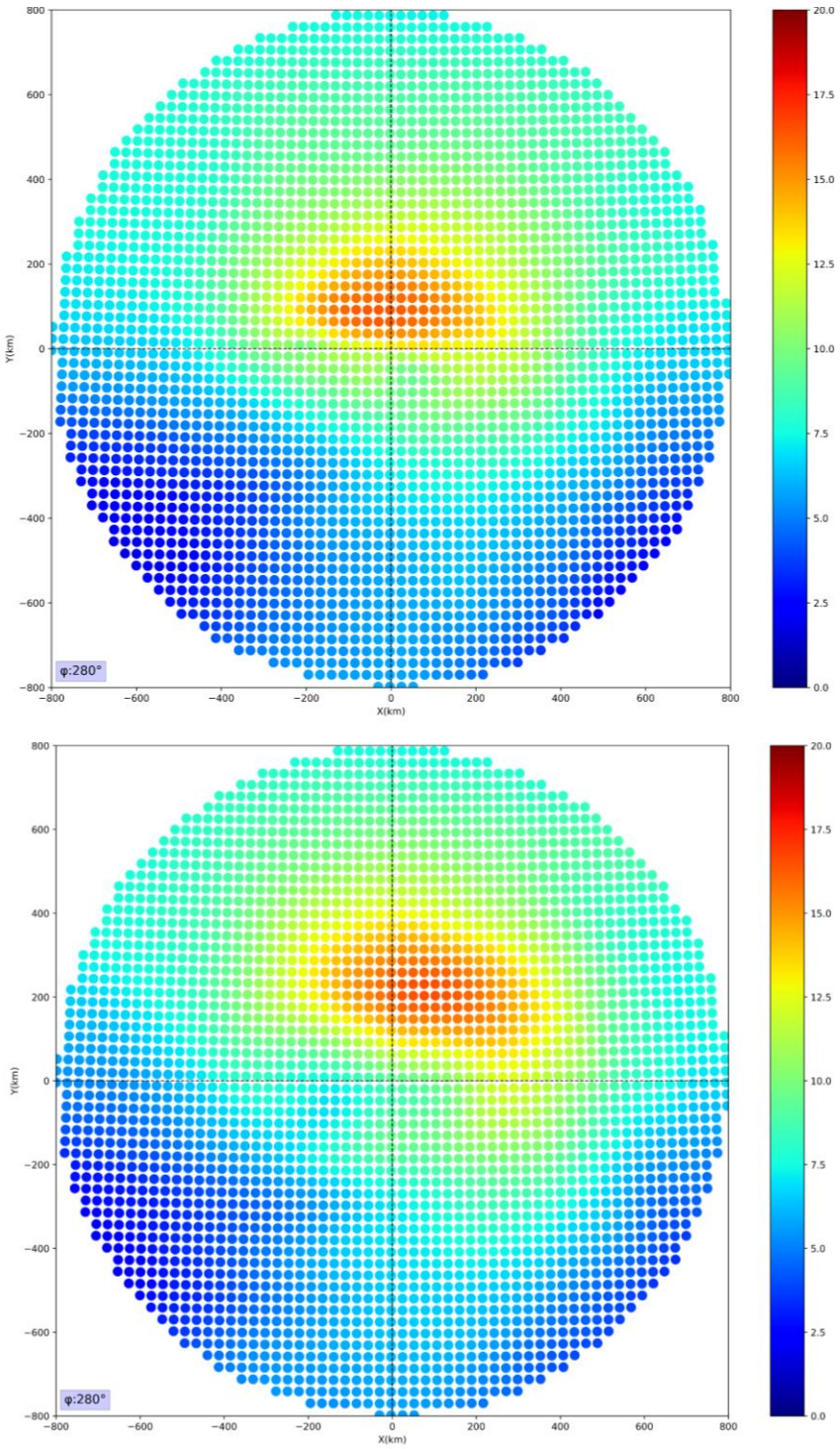

Fig.2-15 ERA5 and CFSRv2 typhoon coordinate maps on August 29(units [m/s]. Left: ERA5; Right: CFSRv2)

2.5 Target typhoon

Considering the date range and observation range included in the data product, the following two representative strong typhoons were selected to be target of this study.

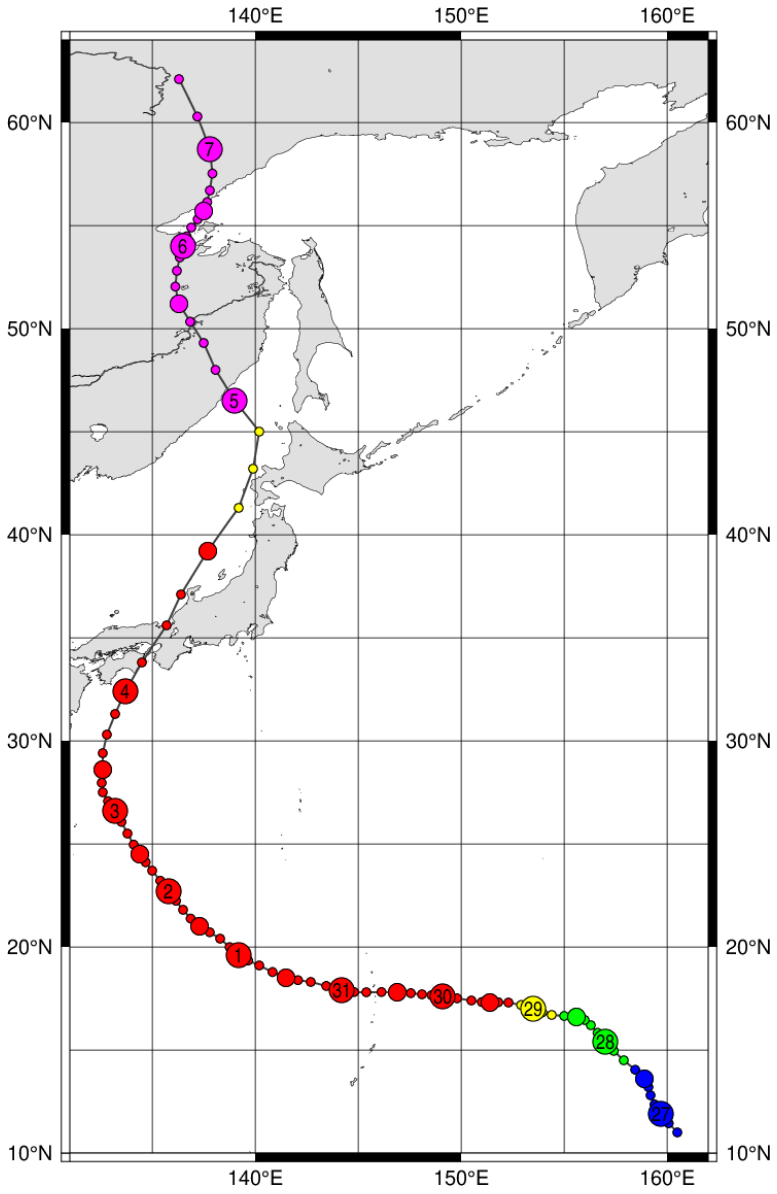

Fig.2-16 Path of Typhoon Jebi (T1821) (From Digital typhoon)

Jebi began to intensify on August 29, reaching typhoon status at 06:00 UTC. Jebi intensified into a super typhoon by 18:00 UTC on August 30 with winds of 260 km/h,

representing an increase of 95 km/h in the past 24 hours. Jebi reached its peak intensity at 00:00 UTC on August 31 with winds of 195 km/h and a central pressure of 915 hPa. Jebi's winds continued to increase and peaked at 285 km/h at 06:00 UTC. Jebi's intensity leveled off thereafter. Jebi had weakened below super typhoon status by 18:00 UTC on September 1. Travelling northwestwards, Jebi entered the Philippine Area of Responsibility (PAR) at 06:00 UTC on September 2 Jebi exited the PAR roughly 12 hours later. Slow weakening continued through September 3. Jebi made landfall over southern Tokushima Prefecture at around 03:00 UTC on September 4, possessing winds of around 155 km/h. In the next two hours, Jebi crossed Osaka Bay and made another landfall around 05:00 UTC near Kobe, Hyōgo Prefecture. (Fig.2-16)

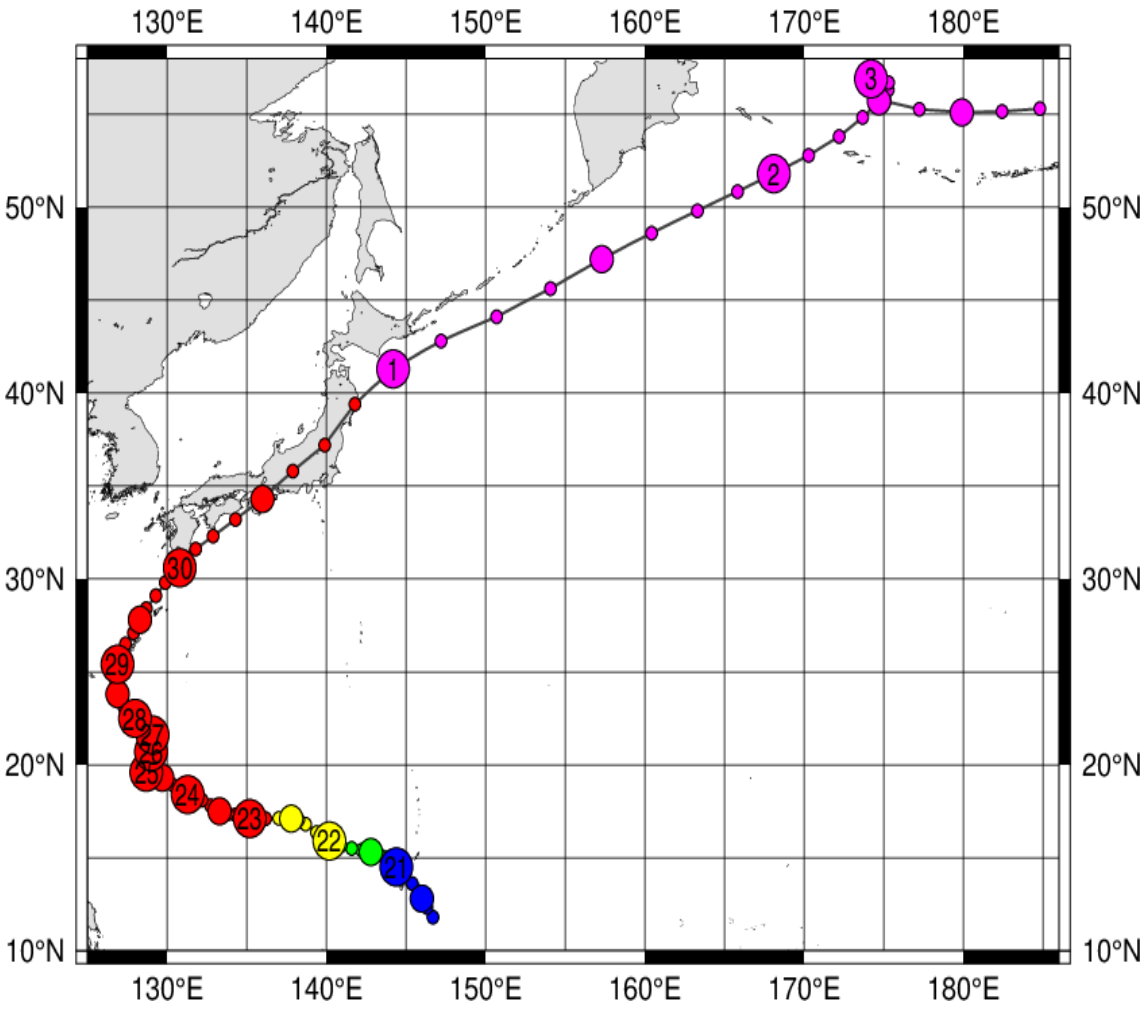

Fig.2-17 Path of Typhoon Trami (T1824) (From Digital typhoon)

On September 22, Trami gradually intensified, attaining severe tropical storm on the morning, and became the tenth typhoon of the annual typhoon season later that day. Continued moving west-northwestward, Trami kept on intensifying thanks to favorable environmental condition. The storm achieved its peak intensity at 18:00 UTC that day, with 10-minute maximum sustained winds of 195 km/h, and a central pressure of 915 hPa. Trami has become a Category 5-equivalent super typhoon three hours later, with 1-minute sustained winds of 260 km/h. Soon afterwards, Trami lost its steering current and slowed.

The typhoon's persistence over the same location for several days. Trami dropping below super typhoon status late on September 25. However, the previously small eye of Trami expanded dramatically. On September 28, Trami accelerated to the northwest. Trami turned to the northeast along a wester lies on September 29 and passed just west of the Okinawa Island. The typhoon made landfall near Tanabe, Wakayama at 11:00 UTC on September 30 with winds of 150 km/h. (Fig.2-17)

2.6 Wind speed distribution

After plotting all the coordinate maps about Jebi and Trami, the wind speed distribution in the maps were areal averaged as follow.

2.6.1 Setting of degree interval

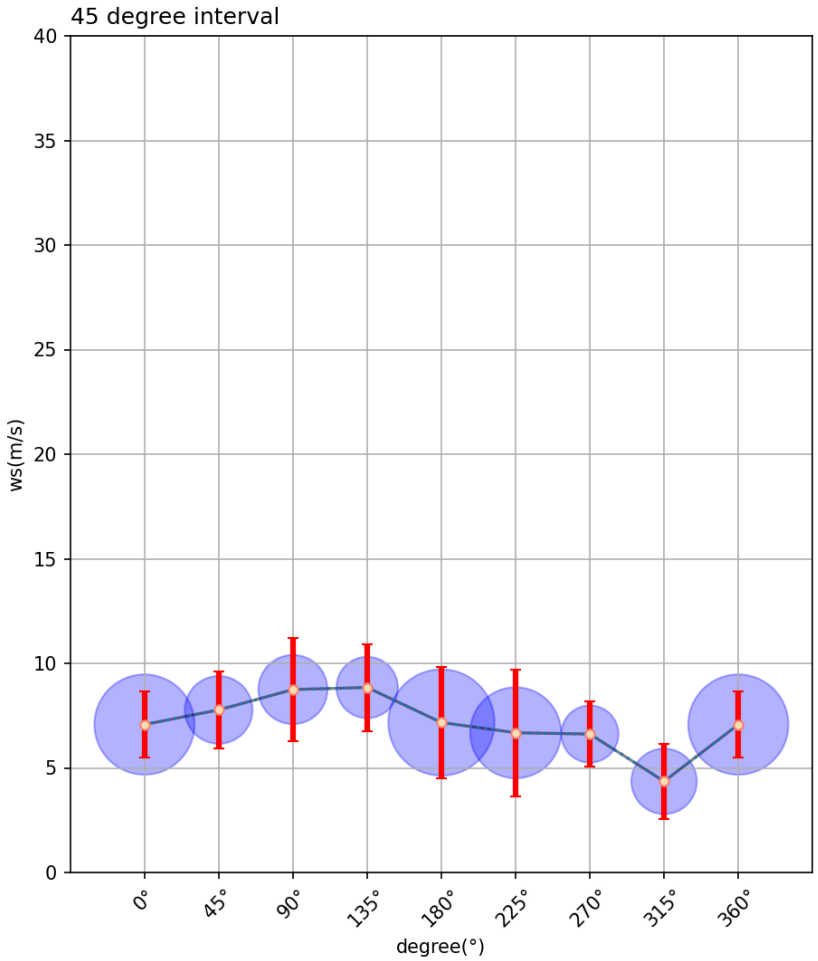

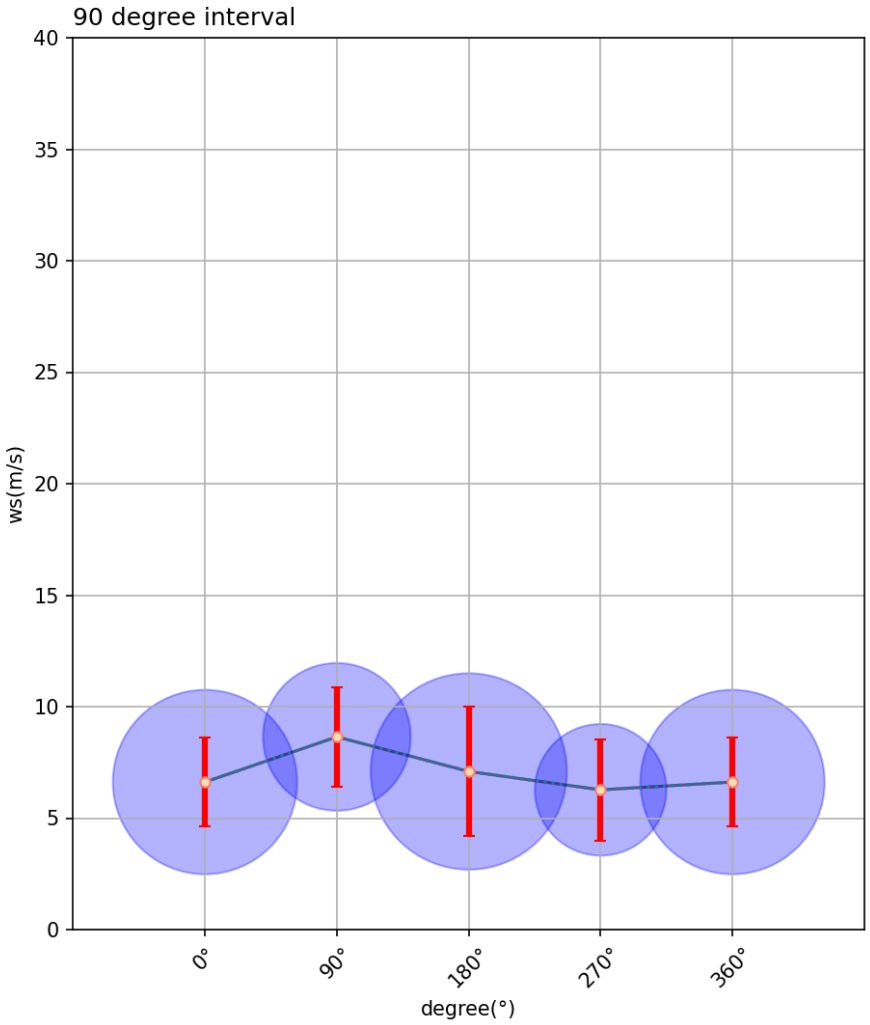

Fig.2-18 CYGNSS 45-degree and 90-degree interval samples on Aug.29

(orange bars represent the standard deviations, blue circles at each point represent the amount of data)

As a sample, all CYGNSS data points on August 29 were carried out at three angular intervals. The horizontal axis of each subgraph represents the angle, from 0 to 360, clockwise from the bin where typhoon moving direction is located. The vertical axis

represents the average wind speed of every bin. It can find three subgraphs show the same angular dependence.

In the range of 0~180 degree, which is the right-hand side of the typhoon, the wind speed is higher. And it can also be found there is less data in 45-degree interval graph, so the graph looks noisy. Consider the signal-to-noise ratio, temporarily choose a 90-degree interval for the next processing. (Fig.2-18)

2.6.2 Setting of distance interval

Since the size of each typhoon is different, to discuss the same relative position, the sizes of the two typhoons were checked. (L1= R of Major Storm Axis, L2= R of Minor Storm Axis, L3= R of Major Gale Axis, L4= R of Minor Gale Axis.)

Date	L1(km)	L2(km)	L3(km)	L4(km)
8.29	75.932	55.56	333.36	185.2
8.30	90.748	83.34	333.36	185.2
8.31	133.344	133.344	400.032	251.872
9.1	166.68	166.68	437.072	277.8
9.2	181.496	181.496	444.48	322.248
9.3	196.312	127.788	501.892	275.948

Table.2-19 the axes of Typhoon Jebi (T1821)

Date	L1(km)	L2(km)	L3(km)	L4(km)
9.22	71.765	71.765	388.92	222.24
9.23	142.604	142.604	433.368	266.688
9.24	174.088	174.088	477.816	348.176
9.25	185.2	185.2	500.04	477.816
9.26	192.608	192.608	500.04	500.04
9.27	222.24	222.24	533.376	533.376

Table.2-20 the axes of Typhoon Trami (T1824)

Refer to the above information of Typhoon Jebi and Trami from Digital Typhoon,0~L1, L1~L3 were selected as Storm range and Gale range for the next distribution analysis.

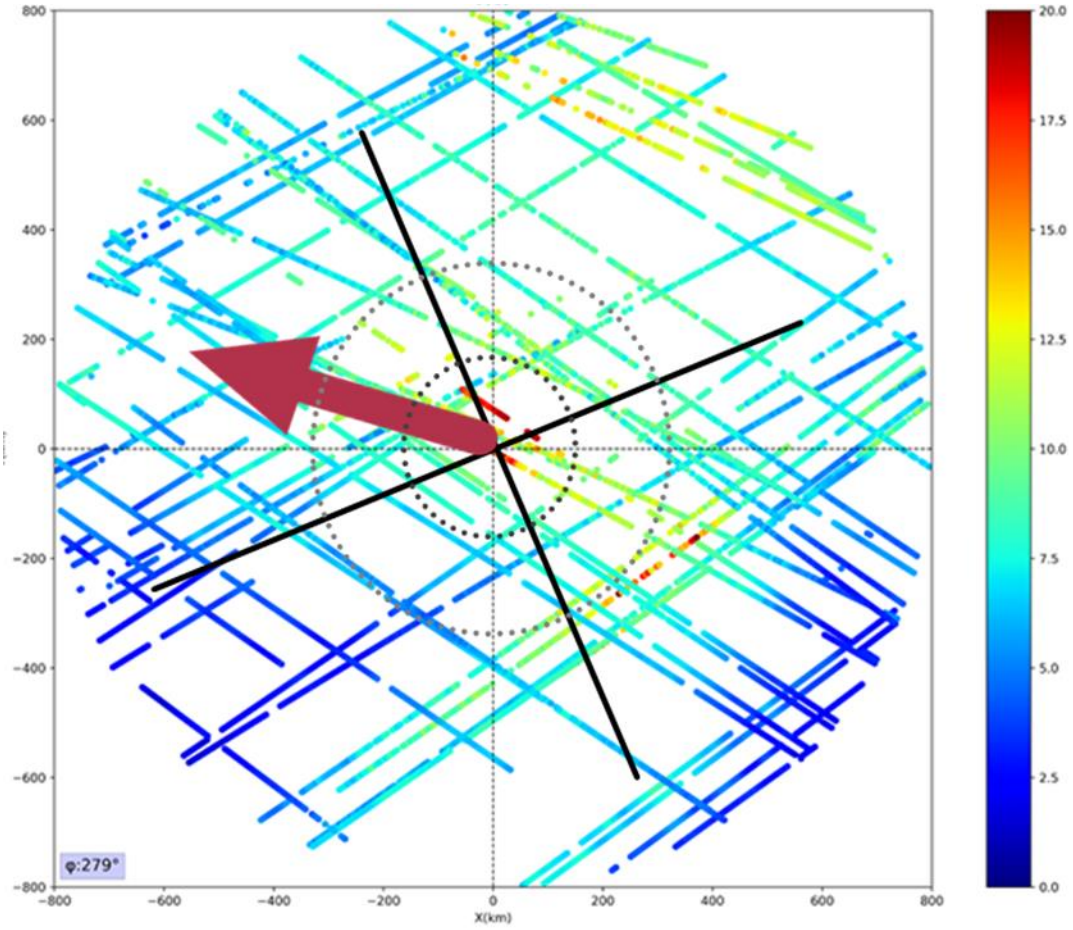

Figure.2-21 Areal averaging method

2.6.3 Normalization and generalization of wind speed distributions

As above method, together with CYGNSS and AMSR2 observations, ERA5 and CFSRv2 model results were plotted. (Fig.2-22)

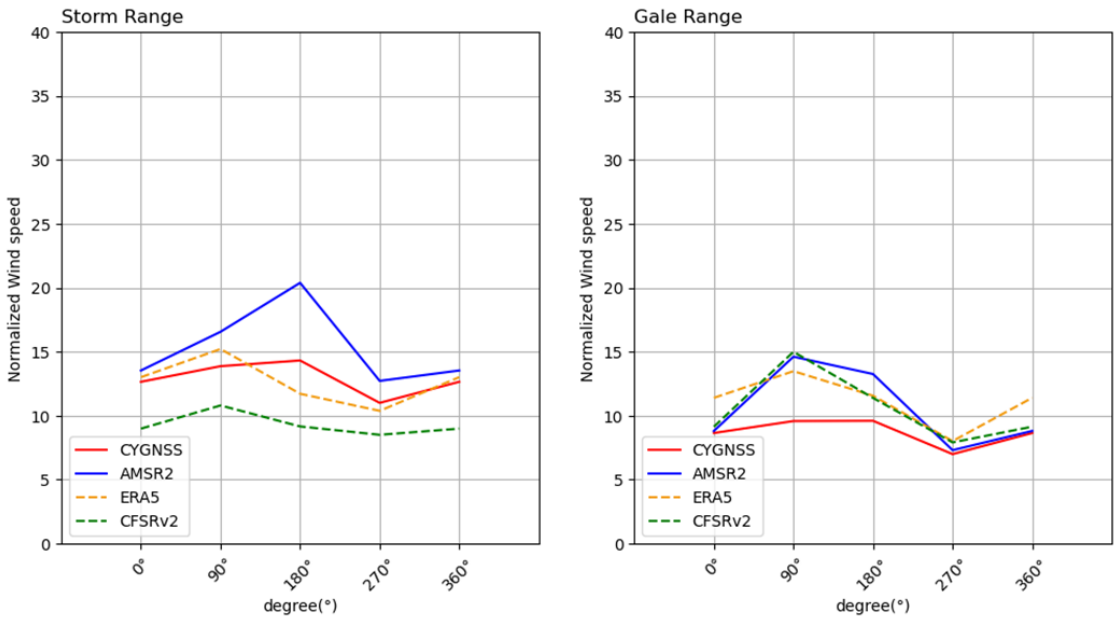

Figure.2-22 Example of daily wind speed distribution

An example of daily wind speed distribution on 2 September 2018 is plotted in Fig.2-22. The horizontal axis represents the clockwise angle in degree from the direction of typhoon Jebi's movement. The vertical axis represents wind speed, is m/s. Together with CYGNSS and AMSR2 observations, ERA5 and CFSRv2 model results were plotted. It can be noticed that different products have different wind speed ranges. In storm range, AMSR2 wind speed is significantly larger than other products. In gale range, wind speeds of four products become similar, but maximum and minimum peaks of CYGNSS are slightly shifted than the other products.

To generalize these daily comparisons, daily wind speed distribution of each product was normalized by its maximum speed. (Fig.2-23)

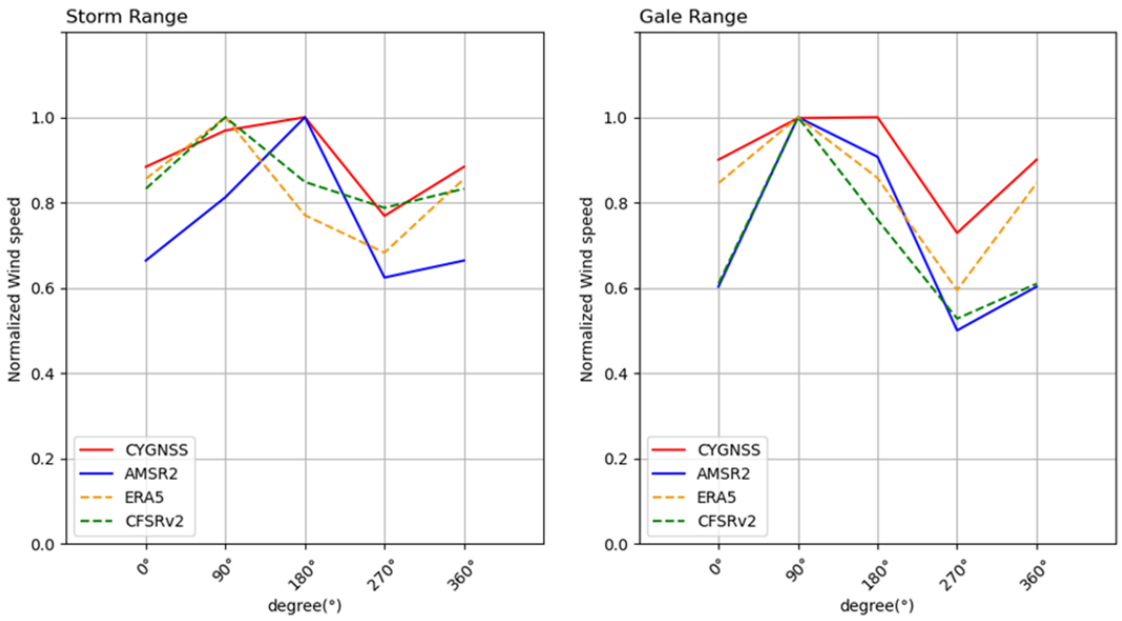

Fig.2-23 Sample of normalized daily wind speed distribution

It can be found that AMSR2 and CYGNSS show maximum values at 180 degree in storm range. And in gale range, wind speeds of four products become similar and consistent with 'Ideal asymmetry pattern'.

Since this kind of distributions are different every day. In order to generalize, daily distributions were weight averaged during the whole period of a typhoon by the number of data points in each bin to make overall wind speed distributions during each typhoon.

3.Results

3.1 Normalized wind speed distribution in storm range

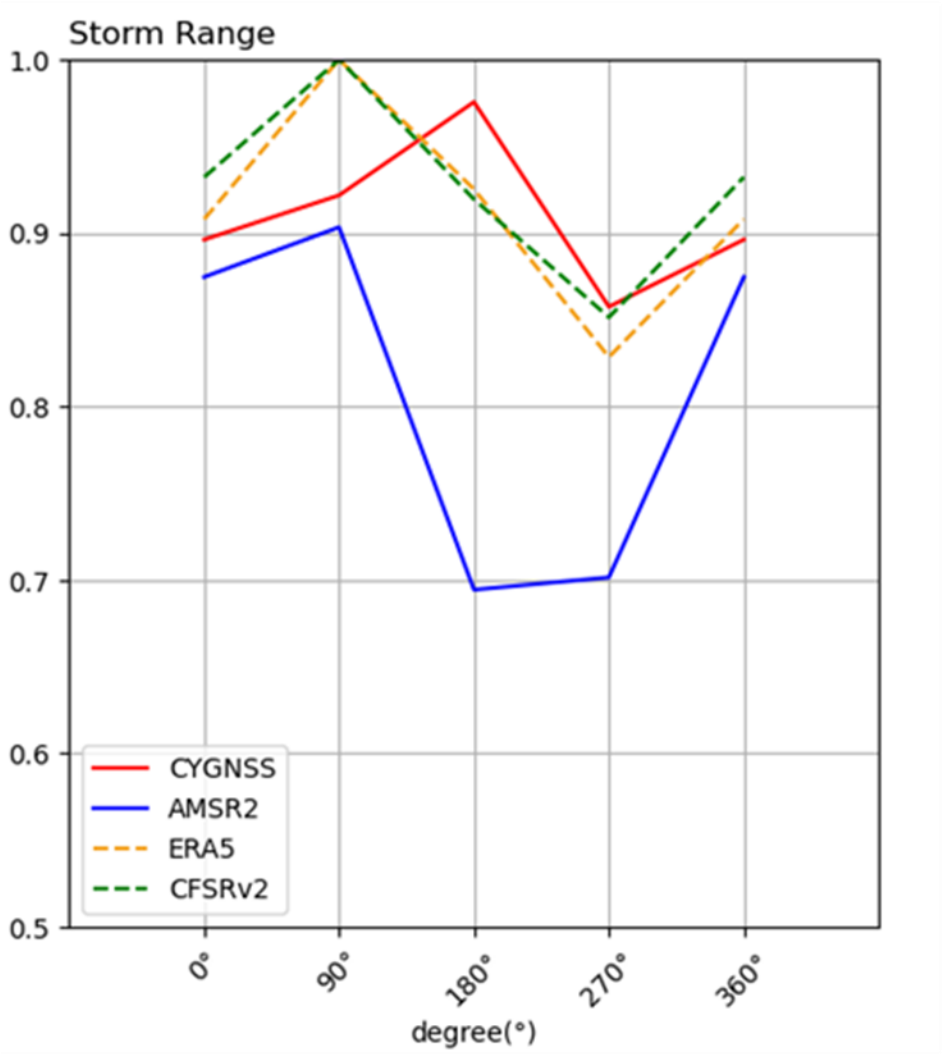

Fig.3-1 Normalized wind speed distribution in Jebi’s storm range

In Jebi's storm range, ‘Ideal asymmetry pattern’ can be recognized in all products, although peaks of CYGNSS are shifted clockwise direction. And AMSR2 has a different shape which shows minimum values at 180 degree. (Fig.3-1)

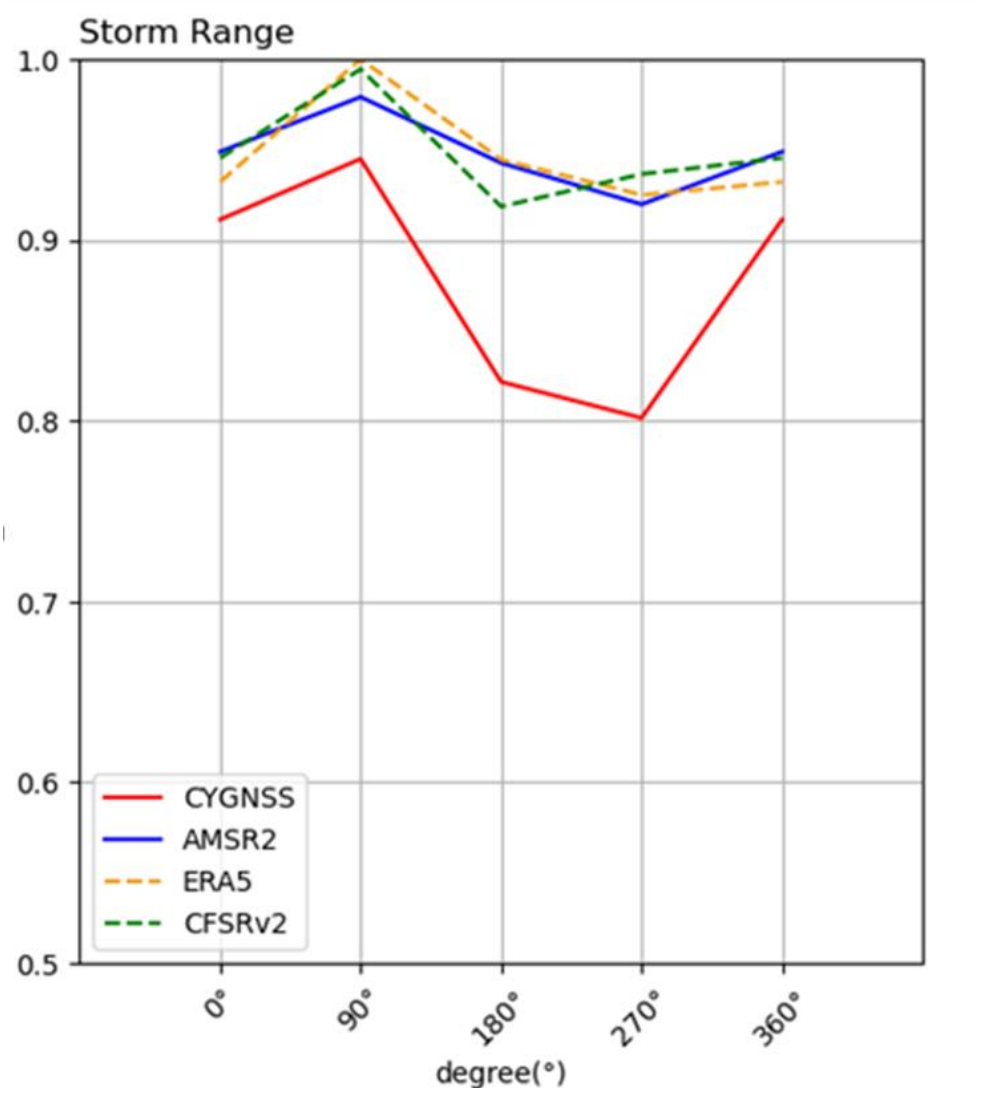

Fig.3-2 Normalized wind speed distribution in Trami's storm range

'Ideal asymmetry pattern' can also be recognized in all products in Trami's storm range. (Fig.3-2)

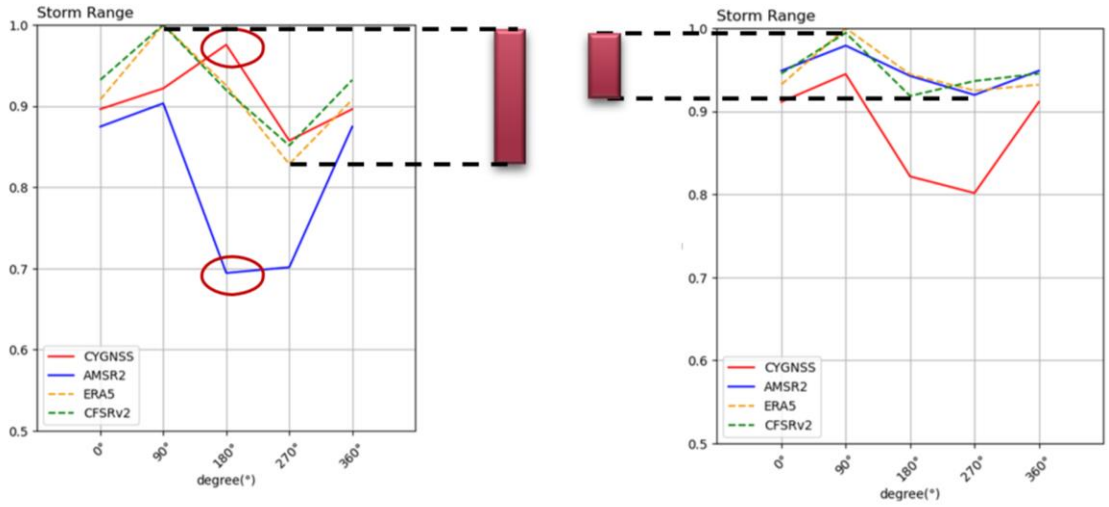

Fig.3-3 Comparison Jebi and Trami's storm ranges (red bars show variation amplitude of models)

Fig.3-3 shows comparison of storm range, 'Ideal asymmetry pattern' can be recognized in all products and in both typhoons' storm range. CYGNSS are shifted clockwise direction in Jebi. AMSR2 has different shape which shows minimum values at 180 degree in Jebi. Variation amplitude for Trami is smaller than Jebi in storm range since Trami moved slower than Jebi.

3.2 Normalized wind speed distribution in gale range

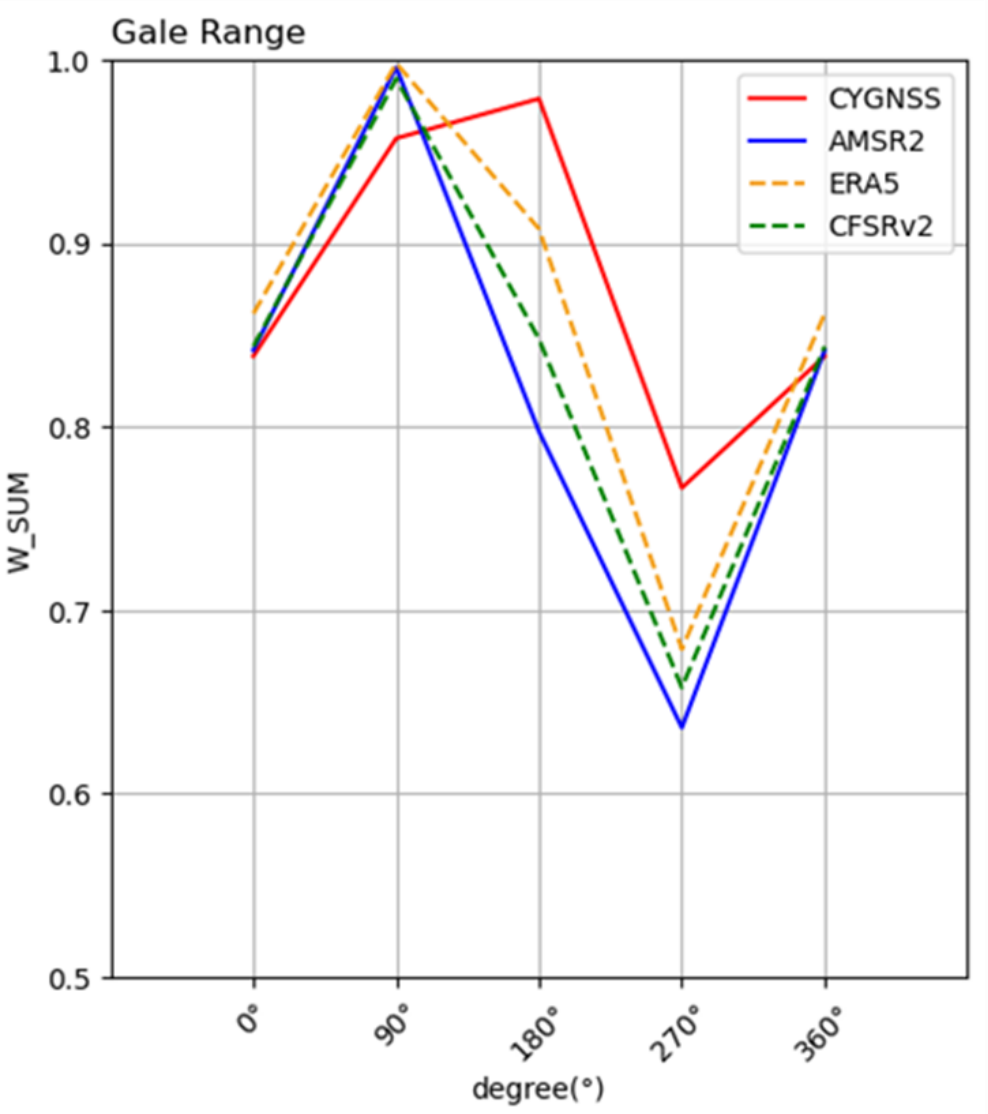

Fig.3-4 Normalized wind speed distribution in Jebi's gale range

'Ideal asymmetry pattern' can also be recognized in all products in Jebi' gale range. Same as in Jebi's storm range, peaks of CYGNSS are shifted clockwise direction in Jebi

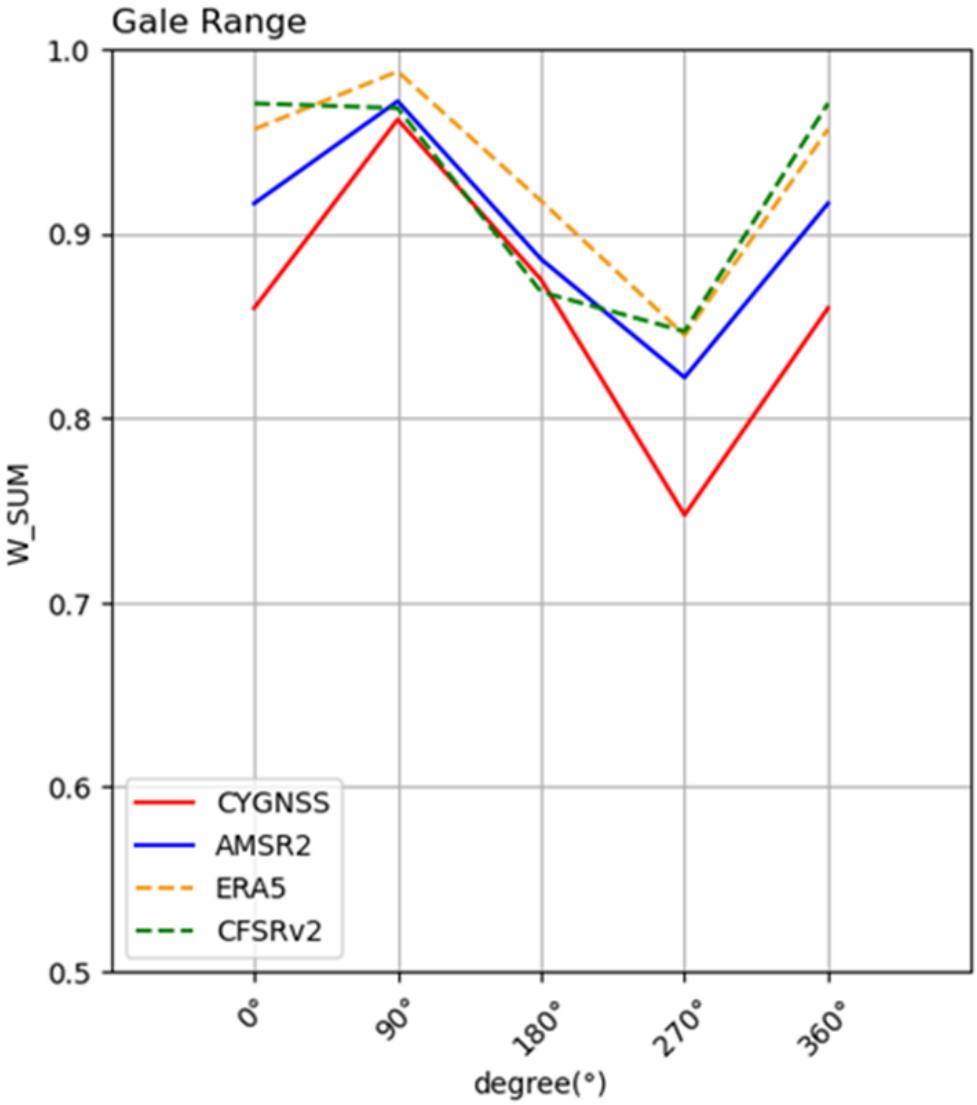

Fig.3-5 Normalized wind speed distribution in Trami's gale range

'Ideal asymmetry pattern' can be recognized in all products and in Trami' gale range.

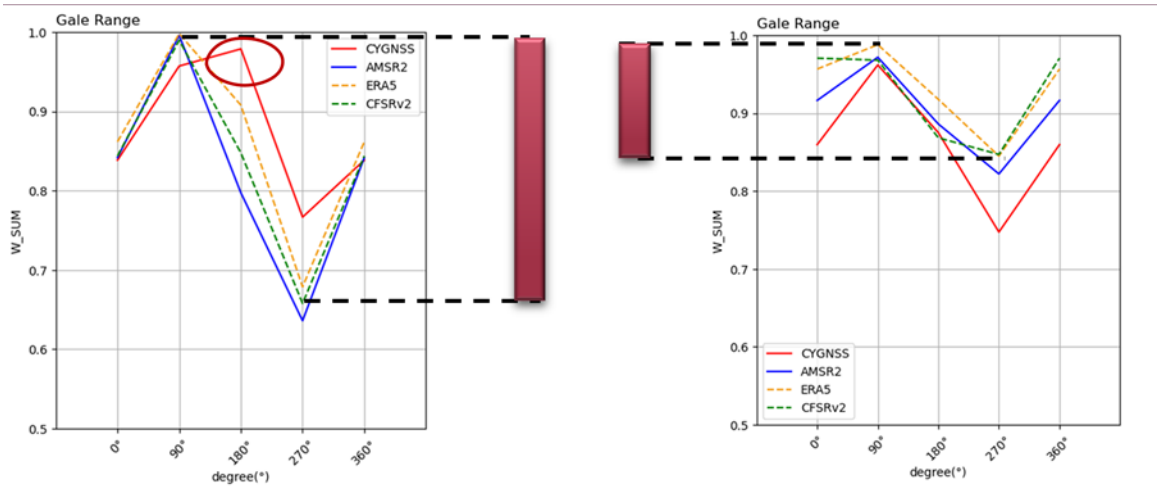

Fig.3-6 Comparison Jebi and Trami's storm ranges

'Ideal asymmetry pattern' are recognized in all products and in both typhoons' gale range.

Same as storm range, peaks of CYGNSS are slightly shifted clockwise direction in Jebi.

Variation amplitude for Trami is also smaller than Jebi in gale range.

4.Discussions

4.1 AMSR2 show different pattern in storm range of Jebi

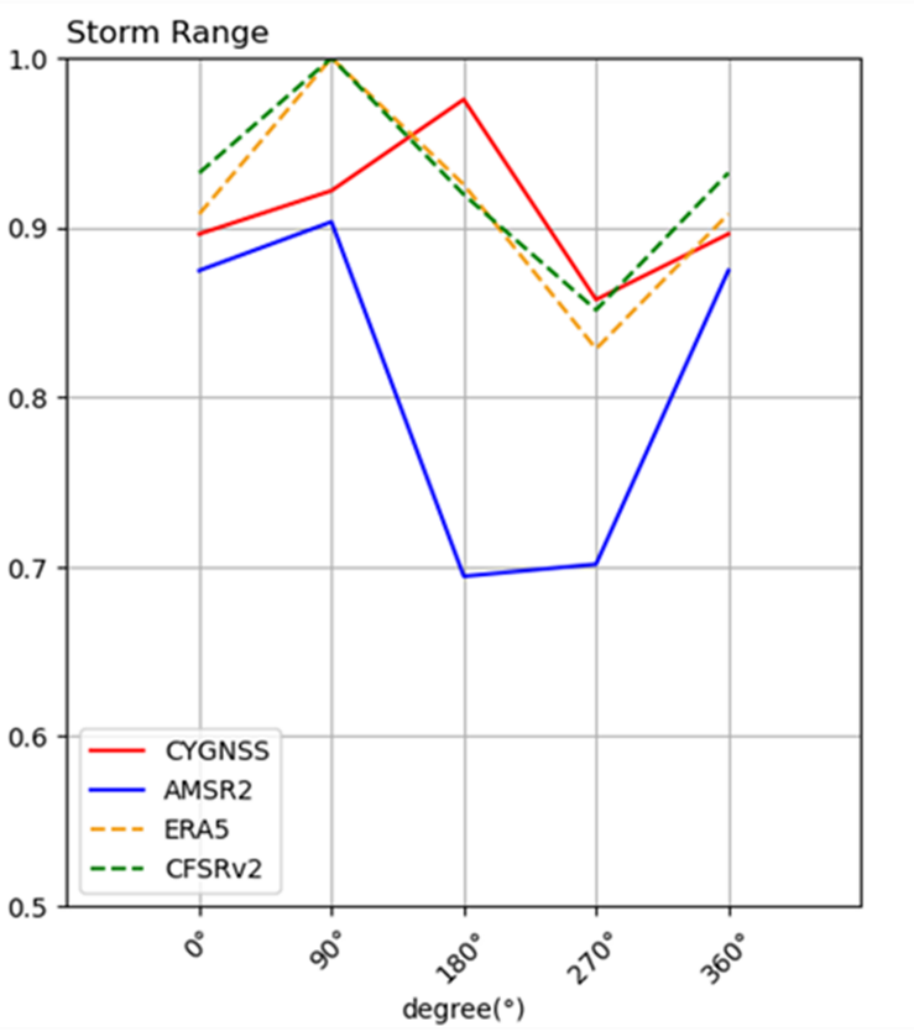

Fig.4-1 Jebi's storm ranges

In Jebi's storm range, AMSR2 shows minimum value at 180 degree. So, we checked its daily wind speed distribution during Jebi, by using the original wind speed data.

Below are all the daily distribution figures of AMSR2 during Jebi. Orange bar presents standard deviation of the wind speed value in each angle bin.

We can find Maximum value of the AMSR2 storm range is not at 90 degrees in some dates.

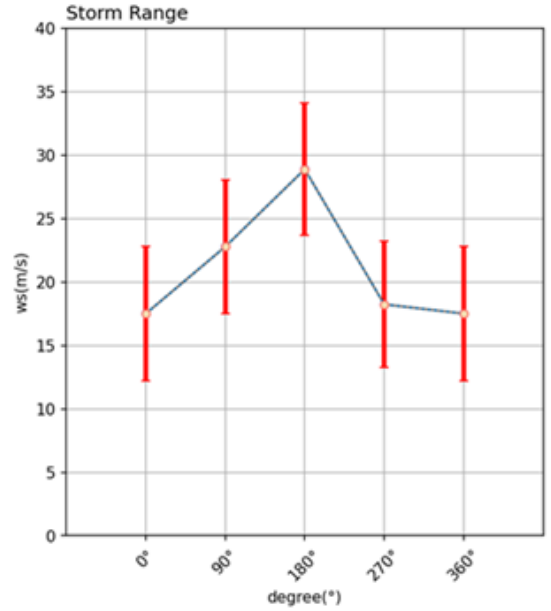
Storm Range
ws(m/s)
degree(°)
0°
90°
180°
270°
360°

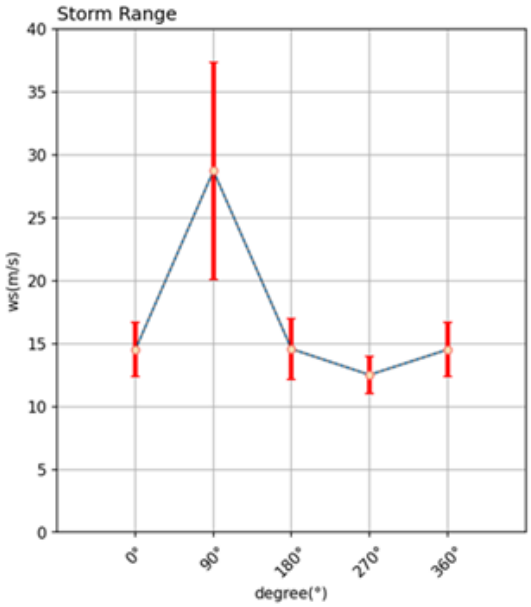
Storm Range
ws(m/s)
degree(°)
0°
90°
180°
270°
360°

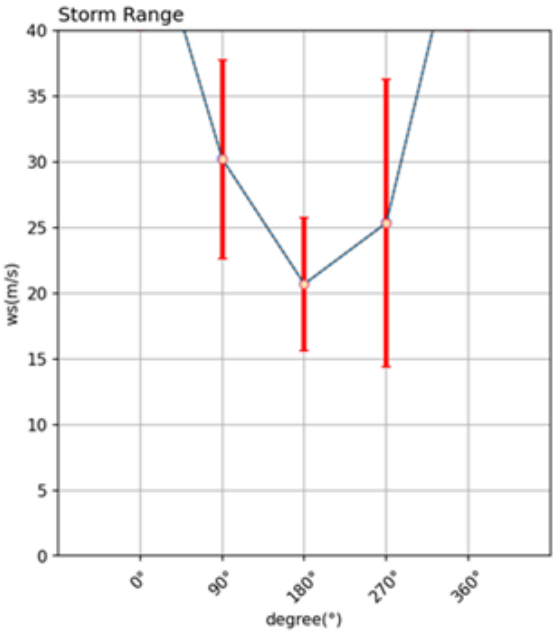
Storm Range
ws(m/s)
degree(°)
0°
90°
180°
270°
360°

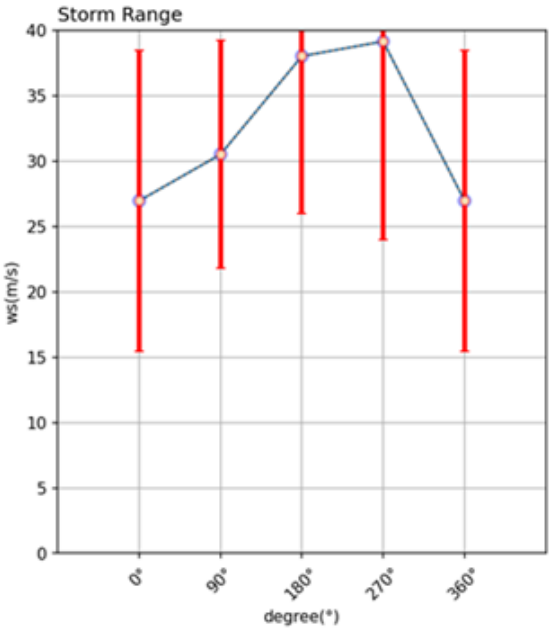
Storm Range
ws(m/s)
degree(°)
0°
90°
180°
270°
360°

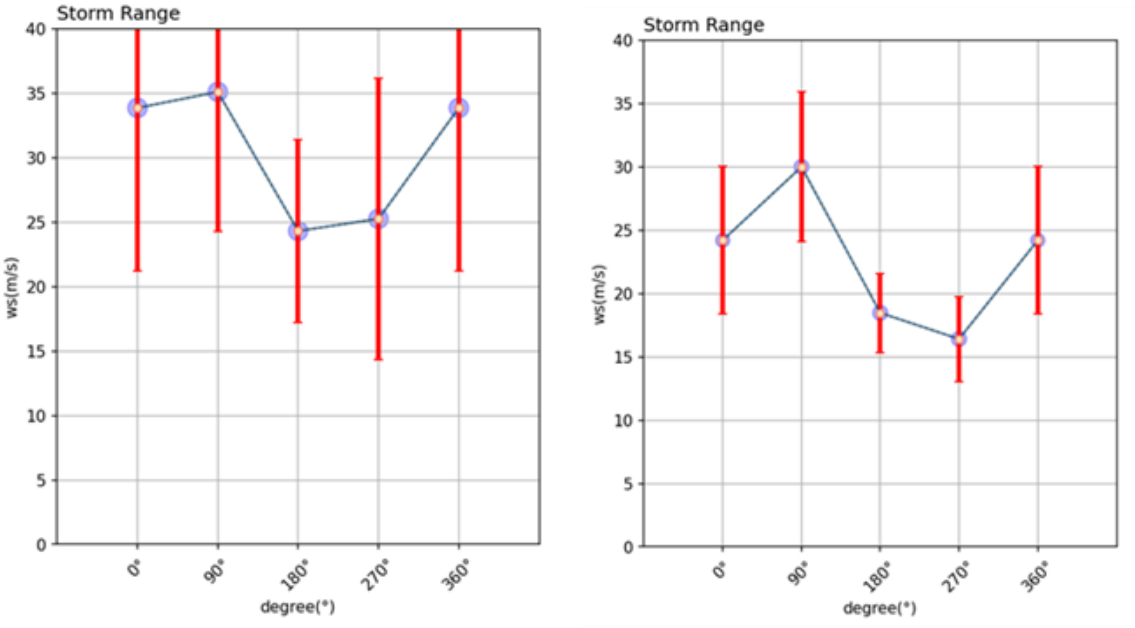

Fig.4-2 AMSR2 daily distributions in storm range of Jebi (Aug.29~Sep.3)

From these figures, it can be found maximum value of the AMSR2 storm range is not at 90 degrees in some dates. Sometimes at 180 degree and 0 degree with extremely large values with big standard deviation. This could be due to AMSR2 snapshot observation that seriously affect the weighted average shape.

4.2 Peak angles in CYGNSS are shifted in Jebi

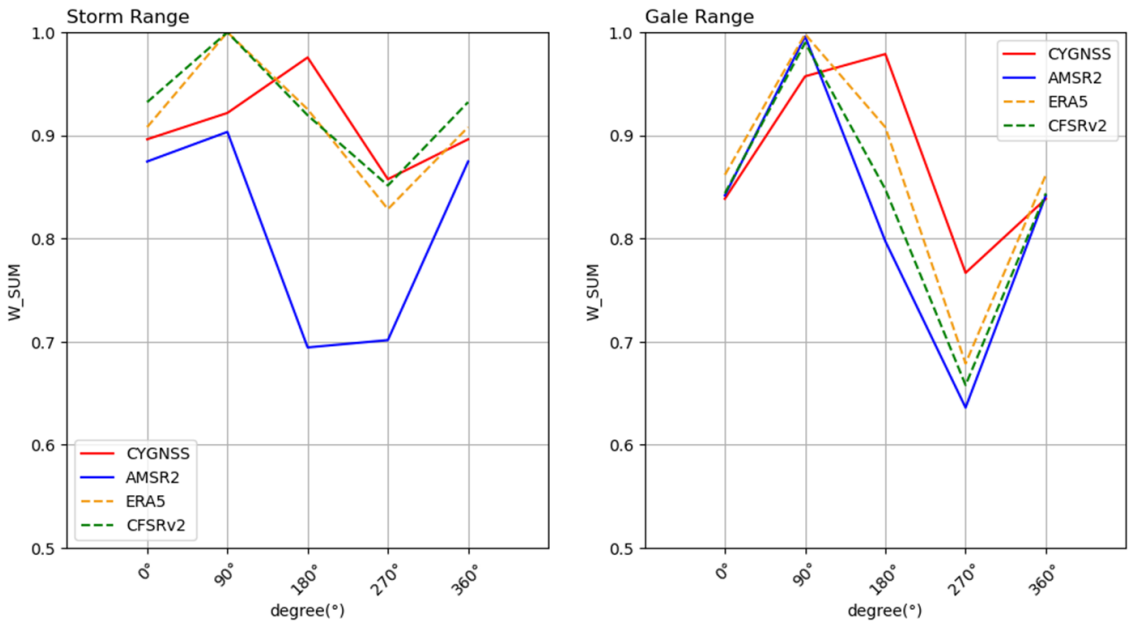

Fig.4-3 Jebi's wind distributions in storm range and gale range

Peak angles in CYGNSS are shifted in Jebi, which show maximum values at 180 degree but not 90 degree. Since CYGNSS measures wind waves to indirectly observe the wind speeds, waves could be affected by other reason expect the direct influence of wind.

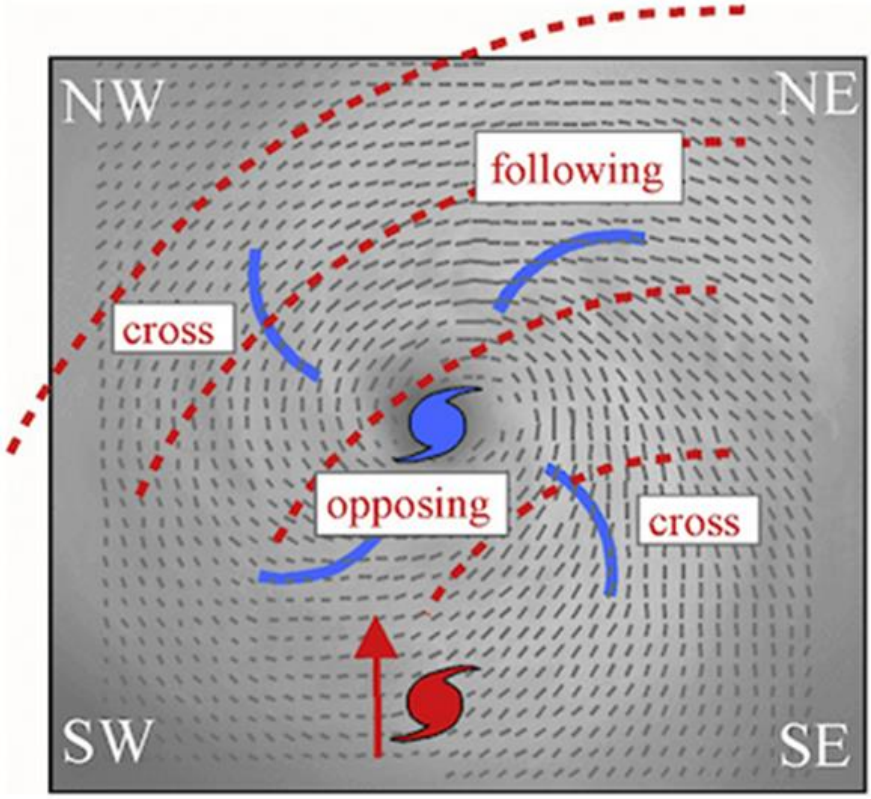

Fig.4-4 Wind field and swell orientation (From figure 3 in Wind and waves in extreme hurricanes, Holthuijsen et al (2012))

Argument in Holthuijsen et al. (2012) showed that swell distribution around moving hurricanes has significant directional dependency. This could explain why CYGNSS tends to have larger winds than expected in 315-deg directions. More research with wave models would be necessary to investigate dependency of CYGNSS winds on swell distribution. (Fig.4-4)

5.Conclusion

Two different types of satellites products, CYGNSS L2 version.3.1 and AMSR2 all-weather product, that can observe strong winds and two models, ERA5 and CFSR2 are investigated for Typhoon Jebi (T1821) and Typhoon Trami (T1824) and compared with models, ERA5 and CFSRv2.

Wind speeds are converted in daily typhoon center coordinate, and then normalized by the maximum speed to produce relative spatial distribution patterns. After weighted average, asymmetry wind speed patterns of each typhoon are obtained.

1.In storm and gale ranges of typhoon Jebi and Trami, they all show ‘Ideal asymmetry pattern’, and consistent with the different moving speeds.

2.Peak angles of CYGNSS maximum speeds are shifted in Jebi’s two ranges, could be affected by complicated swell distribution and ocean current.

3.AMSR2 shows different shape in Jebi’s storm range, could be affected by instantaneous strong wind speeds in snapshot observations.

Since both satellite products are in the research phase, the updated version of the data may be able to expect more ideal results. But ‘Right hand strength’ is only theoretical idea and do not hold under actual circumstances. For example, background wind speed or background wave may not be homogeneous. And ‘Right hand strength’ is only for long term mean wind field thus not applicable for instantaneous wind speeds. Use the updated version of the satellite data to analysis and verify the influence of other factors on the wind speed distributions will be the further works of this study.

6.Acknowledgement

Many people have provided me with guidance, advice, and support throughout my study. Here, I would like to express gratitude.

First, I am greatly indebted to my supervisor, Associate Professor Ichikawa Kaoru from the Research Institute for Applied Mechanics of Kyushu University. Throughout the learning process, he has provided me with insightful advice and helpful suggestions. The completion of this thesis would not have been possible without his patience and constant encouragement. I'm also impressed by his strong sense of duty and commitment to professionalism. This has not only taught me how to conduct academic research but has also served as a model for my future job and life.

Secondly, I want to give my gratitude to Dr. Hiroyuki Tomita, Hokkaido Univ. and Dr. Shinichiro Kako, Kagoshima Univ., to thank them contribution providing AMSR2 ASW product data and programs for CYGNSS and AMSR2 data processing.

Thirdly, I am very indebted to Secretary Takata for her help during my graduate studies.

Fourthly, I would like to give my thanks to my schoolmate Mr.Li Daxing and Ms.Zhang Ganmeng, we exchange opinions with each other in many aspects.

Finally, I would like to conclude this paper with deep gratitude to my parents and my friends for their financial and spiritual support.

7.Reference

1.Leidner, S. M., Annane, B., McNoldy, B., Hoffman, R., and Atlas, R. (2018). 'Variational Analysis of Simulated Ocean Surface Winds from the Cyclone Global Navigation Satellite System (CYGNSS) and Evaluation Using a Regional OSSE', Journal of Atmospheric and Oceanic Technology, vol.35, no. 8, pp.1571-1584, doi: 10.1175/JTECH-D-17-0136.1

2. N. Ebuchi. (2018), 'Evaluation of All-Weather SEA Surface Wind Speed Product from GCOM-W/AMSR2 Microwave Radiometer', IGARSS 2018 - 2018 IEEE International Geoscience and Remote Sensing Symposium, pp. 6659-6662, doi:10.1109/IGARSS.2018.8519042.

3. Ruf, CS, Atlas, R, Chang, PS, Clarizia, MP, Garrison, JL, Gleason, S, Katzberg, SJ, Jelenak, Z, Johnson, JT, Majumdar, SJ, O'Brien, A, Posselt, DJ, Ridley, AJ, Rose, RJ & Zavorotny, (2016), 'New ocean winds satellite mission to probe hurricanes and tropical convection', Bulletin of the American Meteorological Society, vol. 97, no. 3, pp. 385-395, Doi: 10.1175/BAMS-D-14-00218.1

4. Holthuijsen, L. H., Powell, M. D., and Pietrzak, J. D. (2012), 'Wind and waves in extreme hurricanes', J. Geophys. Res., 117, C09003, doi:10.1029/2012JC007983.

Tropical cyclone windspeed climatology, Wikipedia,
https://en.wikipedia.org/wiki/Tropical_cyclone_windspeed_climatology

CYGNSS Dataset, PO. DAAC, NASA,
https://podaac.jpl.nasa.gov/datasetlist

GCOM, eoPortal Directory,
https://directory.eoportal.org/web/eoportal/satellite-missions/g/gcom

Observation area of AMSR2, GCOM,
https://suzaku.eorc.jaxa.jp/GCOM_W/w_amsr2/w_amsr2_orbit.html

Digital typhoon,
http://agora.ex.nii.ac.jp/digital-typhoon/summary/wnp/k/201821.html.en
http://agora.ex.nii.ac.jp/digital-typhoon/summary/wnp/k/201823.html.en

Appendix

A.1 Daily distributions under 45 degree interval

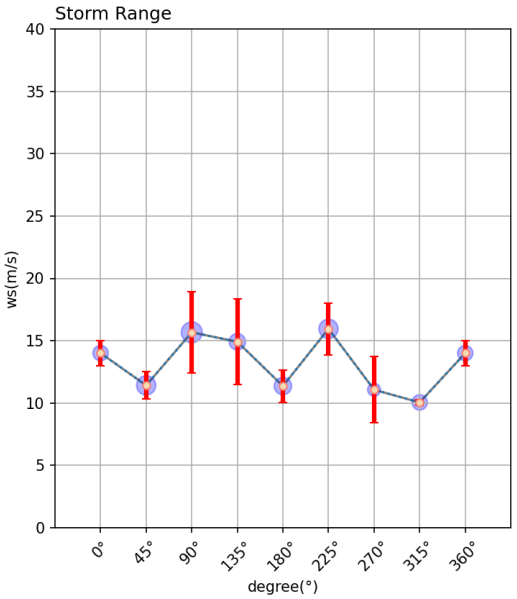

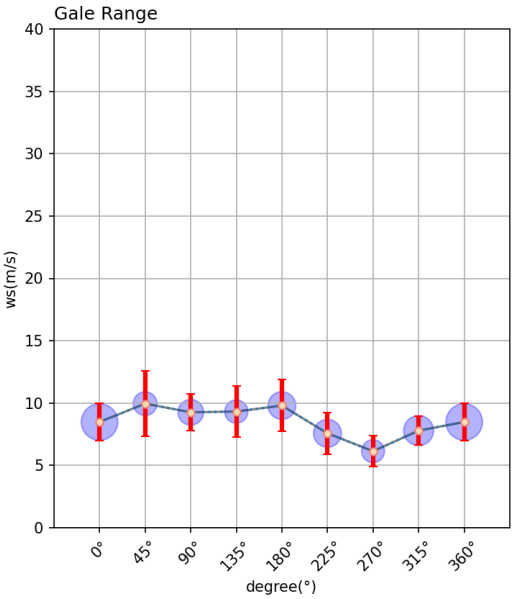

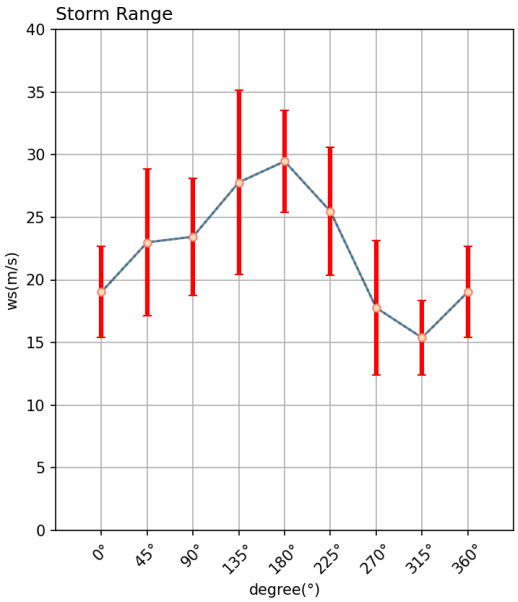

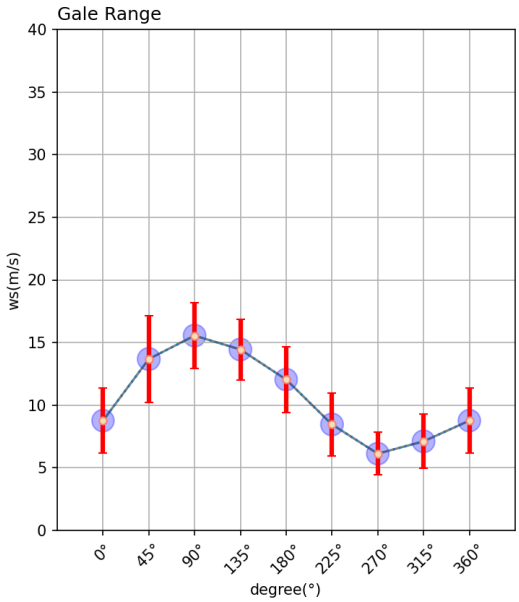

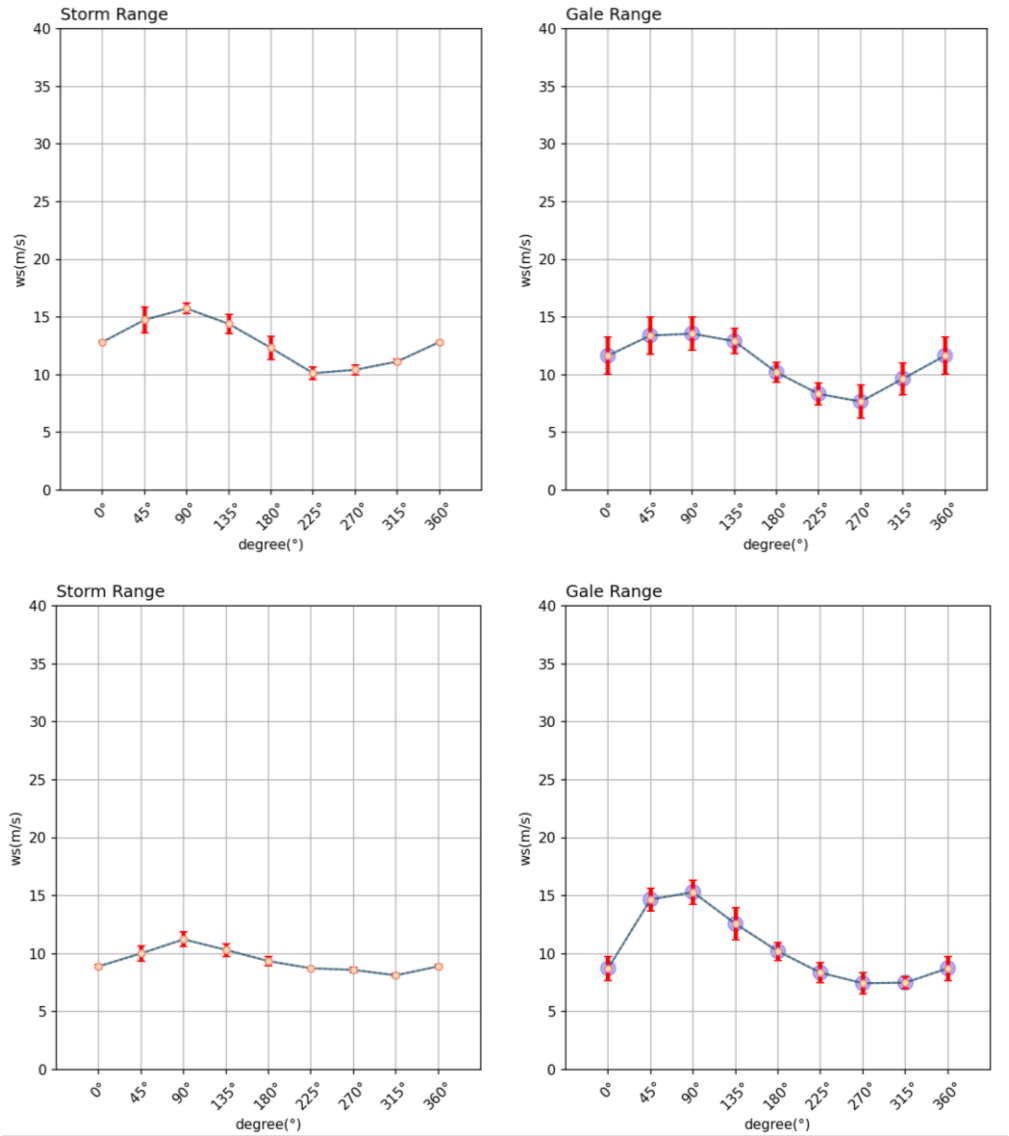

Fig.A-1 Aug.29 Wind speed distribution

(the top set: CYGNSS; the second set: AMSR2; the third set: ERA5; the fourth set: CFSR2)

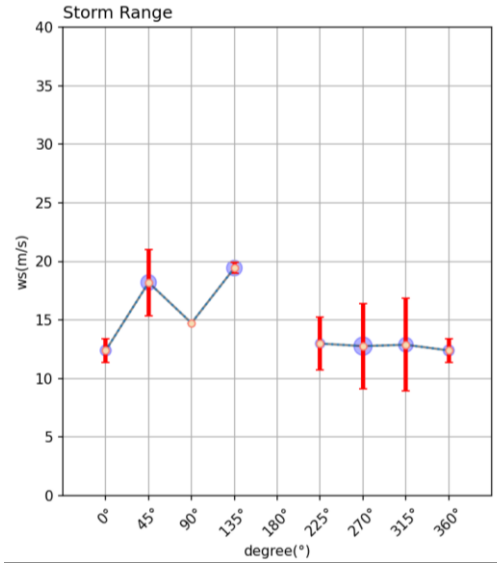
Storm Range
ws(m/s)
degree(°)
0°
45°
90°
135°
180°
225°
270°
315°
360°

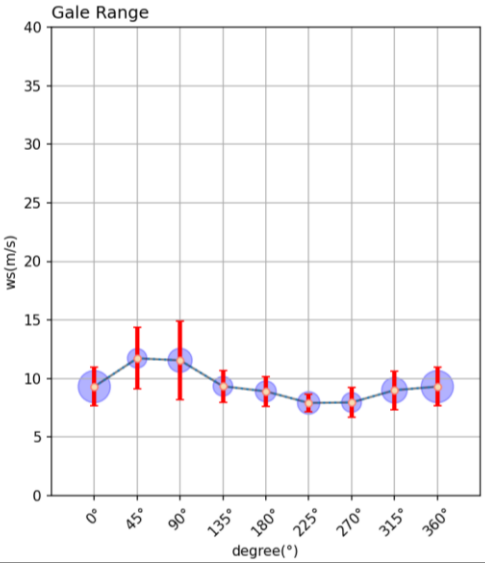
Gale Range
ws(m/s)
degree(°)
0°
45°
90°
135°
180°
225°
270°
315°
360°

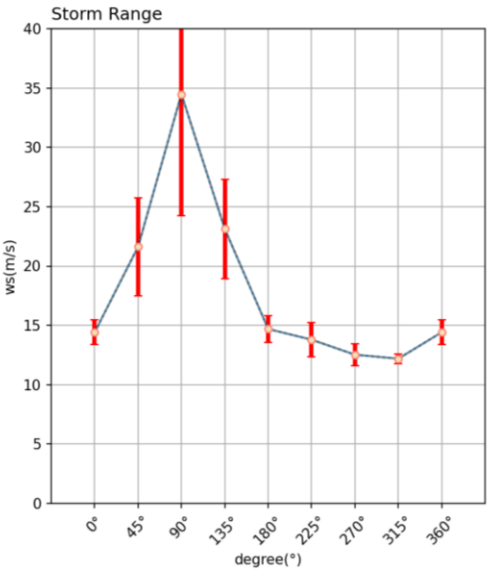
Storm Range
ws(m/s)
degree(°)
0°
45°
90°
135°
180°
225°
270°
315°
360°

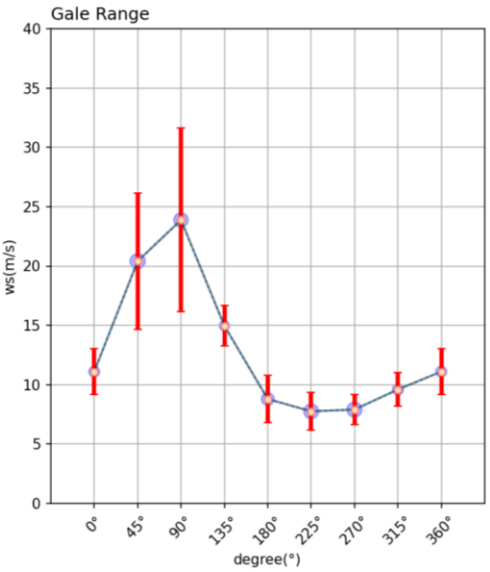
Gale Range
ws(m/s)
degree(°)
0°
45°
90°
135°
180°
225°
270°
315°
360°

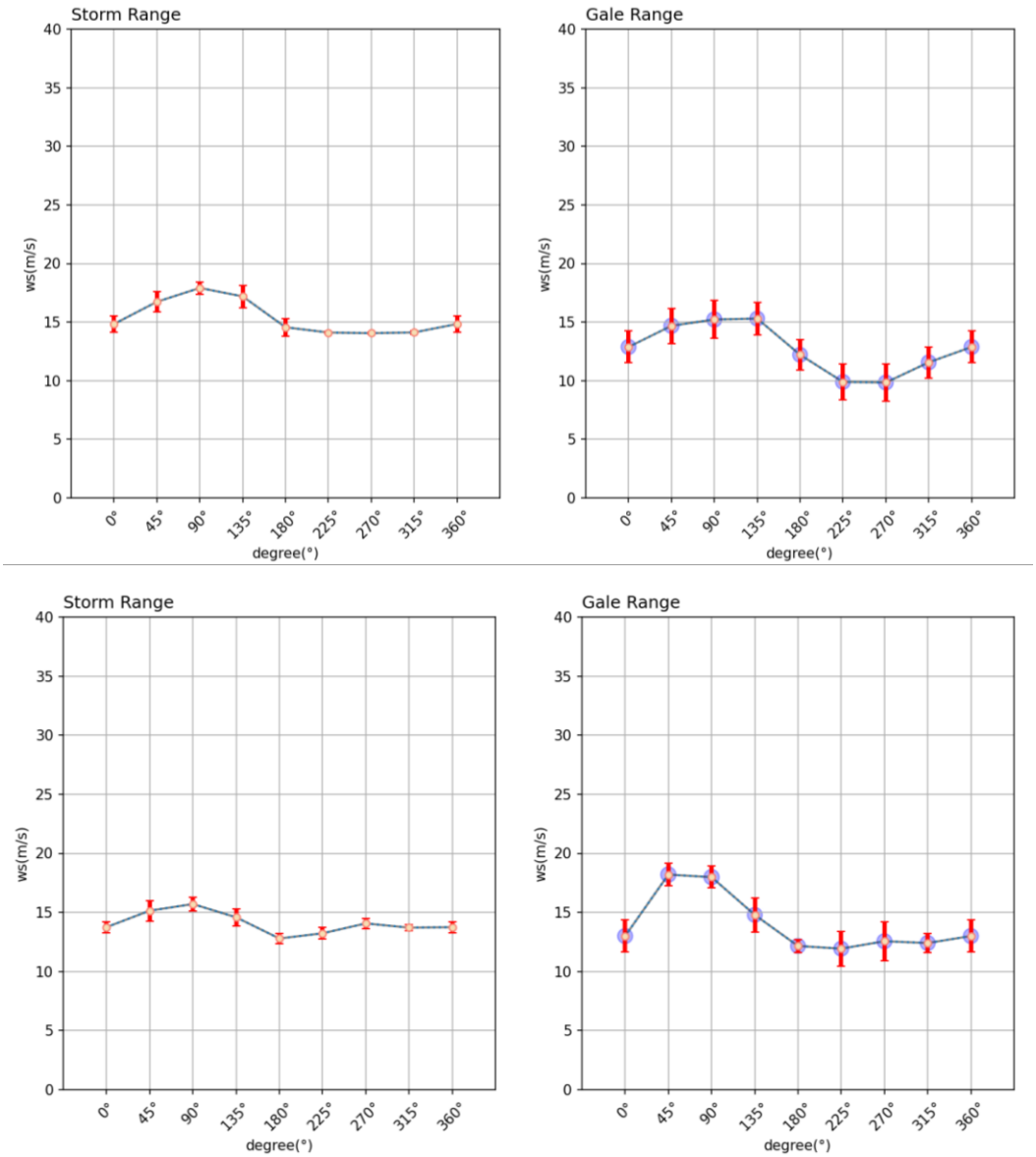

Fig.A-2 Aug.30 Wind speed distribution

(the top set: CYGNSS; the second set: AMSR2; the third set: ERA5; the fourth set: CFSR2)

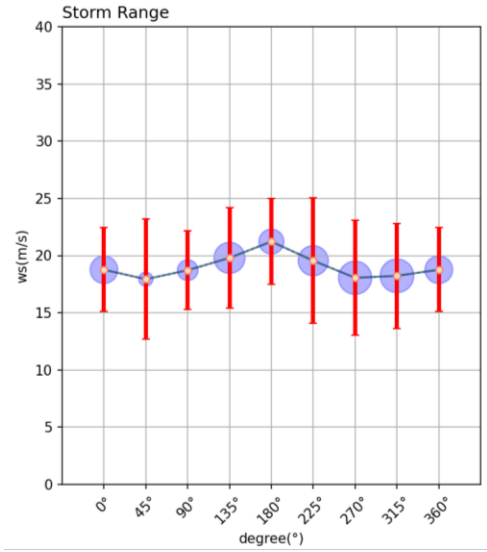
Storm Range
ws(m/s)
degree(°)
0°
45°
90°
135°
180°
225°
270°
315°
360°

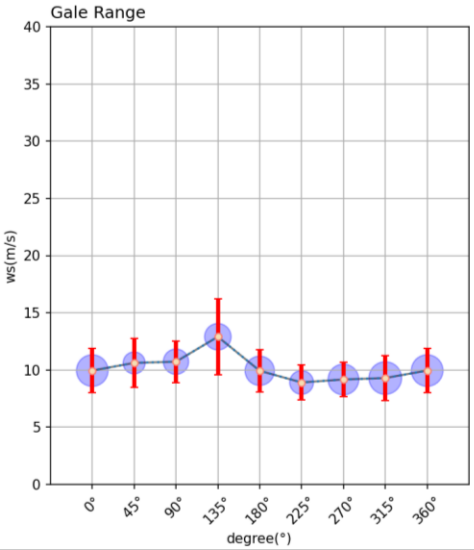
Gale Range
ws(m/s)
degree(°)
0°
45°
90°
135°
180°
225°
270°
315°
360°

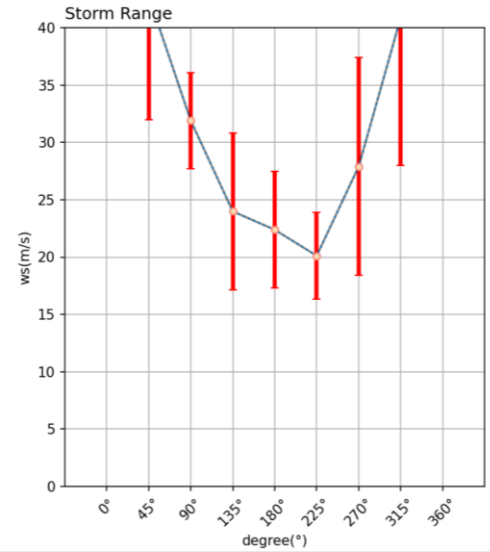
Storm Range
ws(m/s)
degree(°)
0°
45°
90°
135°
180°
225°
270°
315°
360°

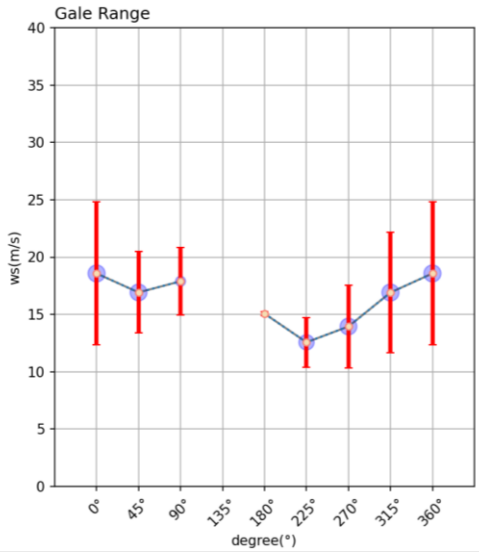
Gale Range
ws(m/s)
degree(°)
0°
45°
90°
135°
180°
225°
270°
315°
360°

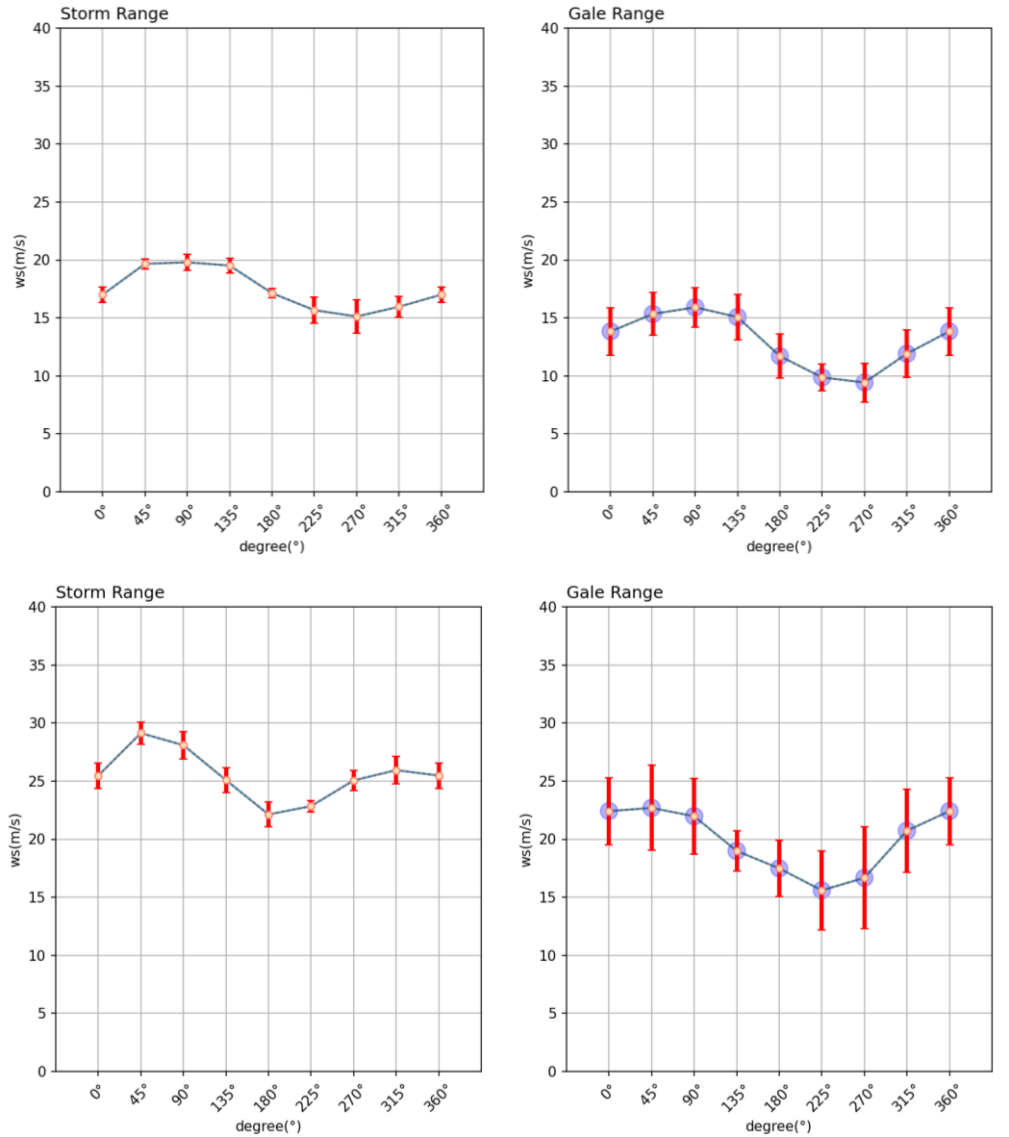

Fig.A-3 Aug.31 Wind speed distribution

(the top set: CYGNSS; the second set: AMSR2; the third set: ERA5; the fourth set: CFSR2)

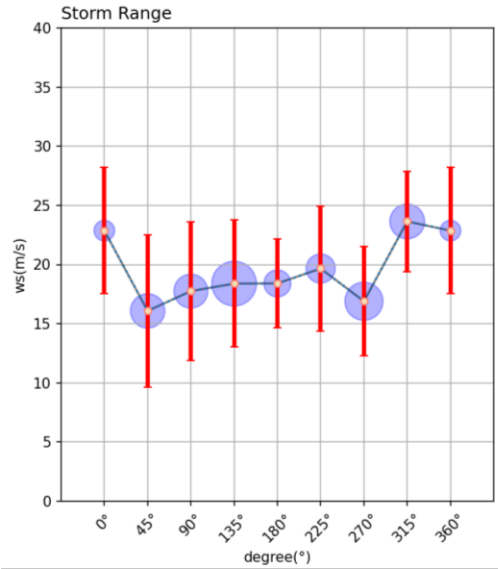
Storm Range
ws(m/s)
degree(°)
0°
45°
90°
135°
180°
225°
270°
315°
360°

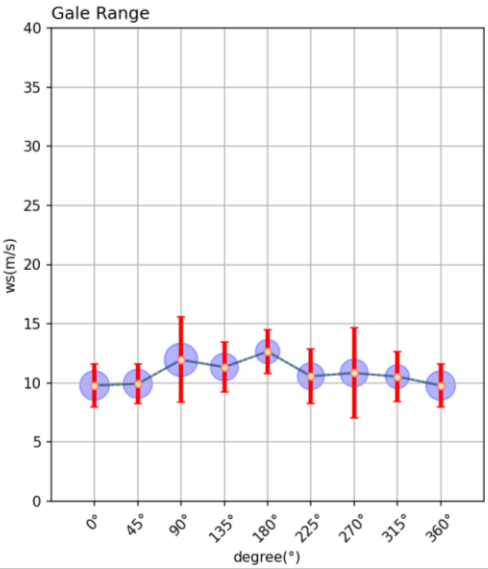
Gale Range
ws(m/s)
degree(°)
0°
45°
90°
135°
180°
225°
270°
315°
360°

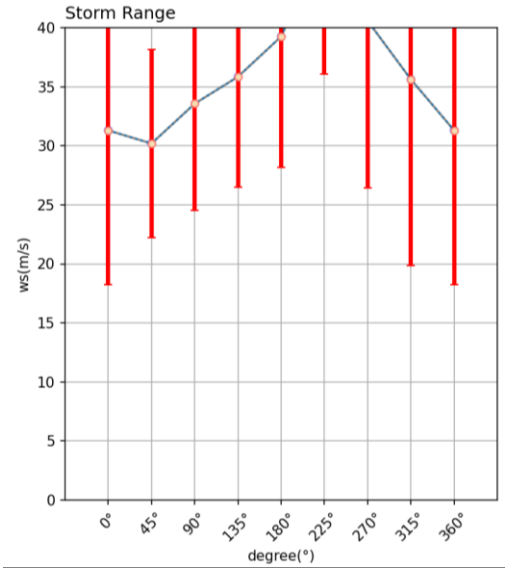
Storm Range
ws(m/s)
degree(°)
0°
45°
90°
135°
180°
225°
270°
315°
360°

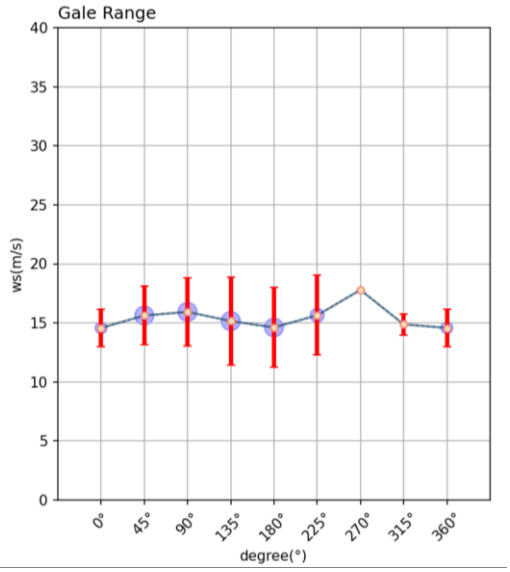
Gale Range
ws(m/s)
degree(°)
0°
45°
90°
135°
180°
225°
270°
315°
360°

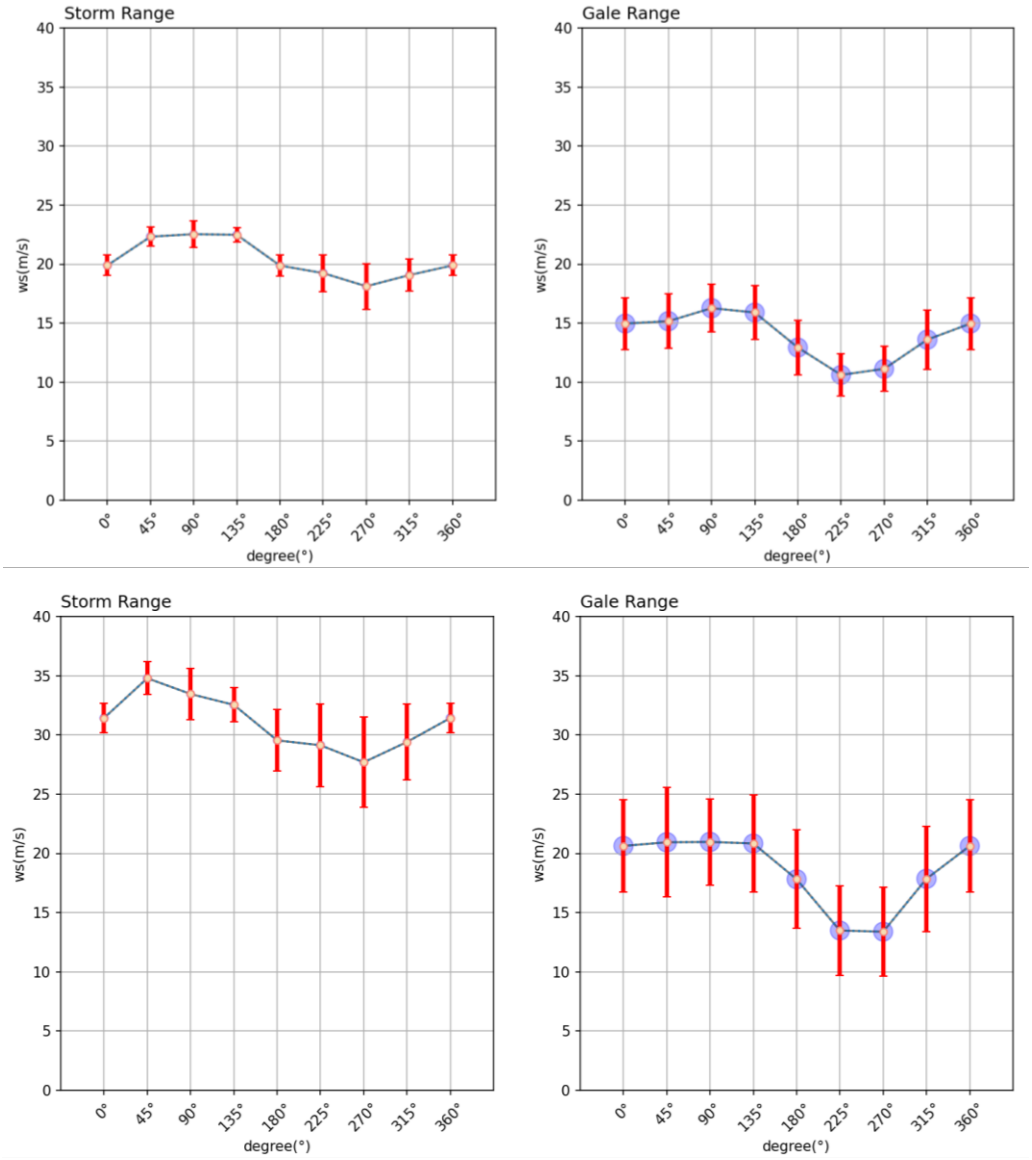

Fig.A-4 Sep.1 Wind speed distribution

(the top set: CYGNSS; the second set: AMSR2; the third set: ERA5; the fourth set: CFSR2)

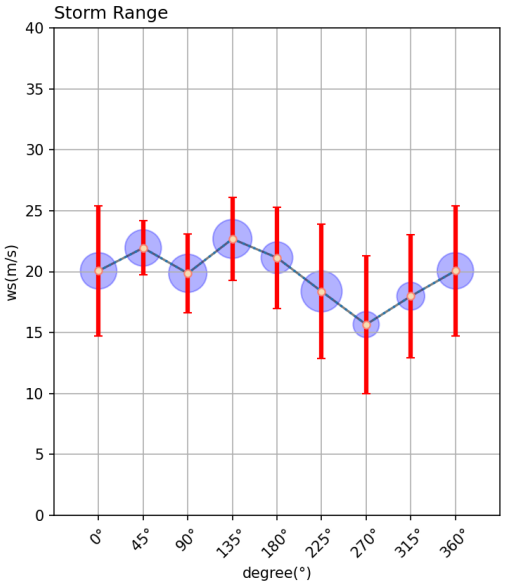
Storm Range
ws(m/s)
degree(°)
0°
45°
90°
135°
180°
225°
270°
315°
360°

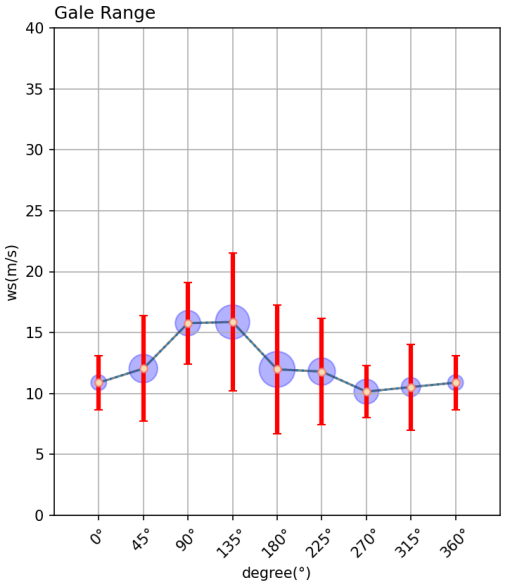
Gale Range
ws(m/s)
degree(°)
0°
45°
90°
135°
180°
225°
270°
315°
360°

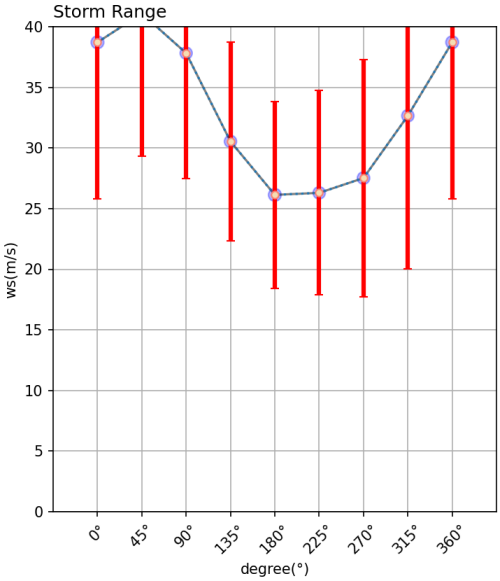
Storm Range
ws(m/s)
degree(°)
0°
45°
90°
135°
180°
225°
270°
315°
360°

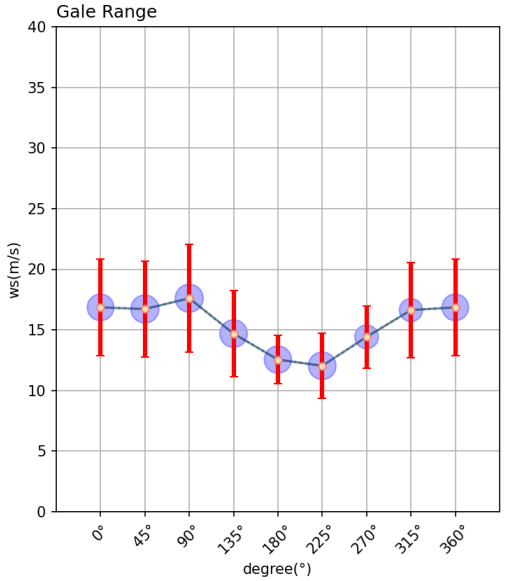
Gale Range
ws(m/s)
degree(°)
0°
45°
90°
135°
180°
225°
270°
315°
360°

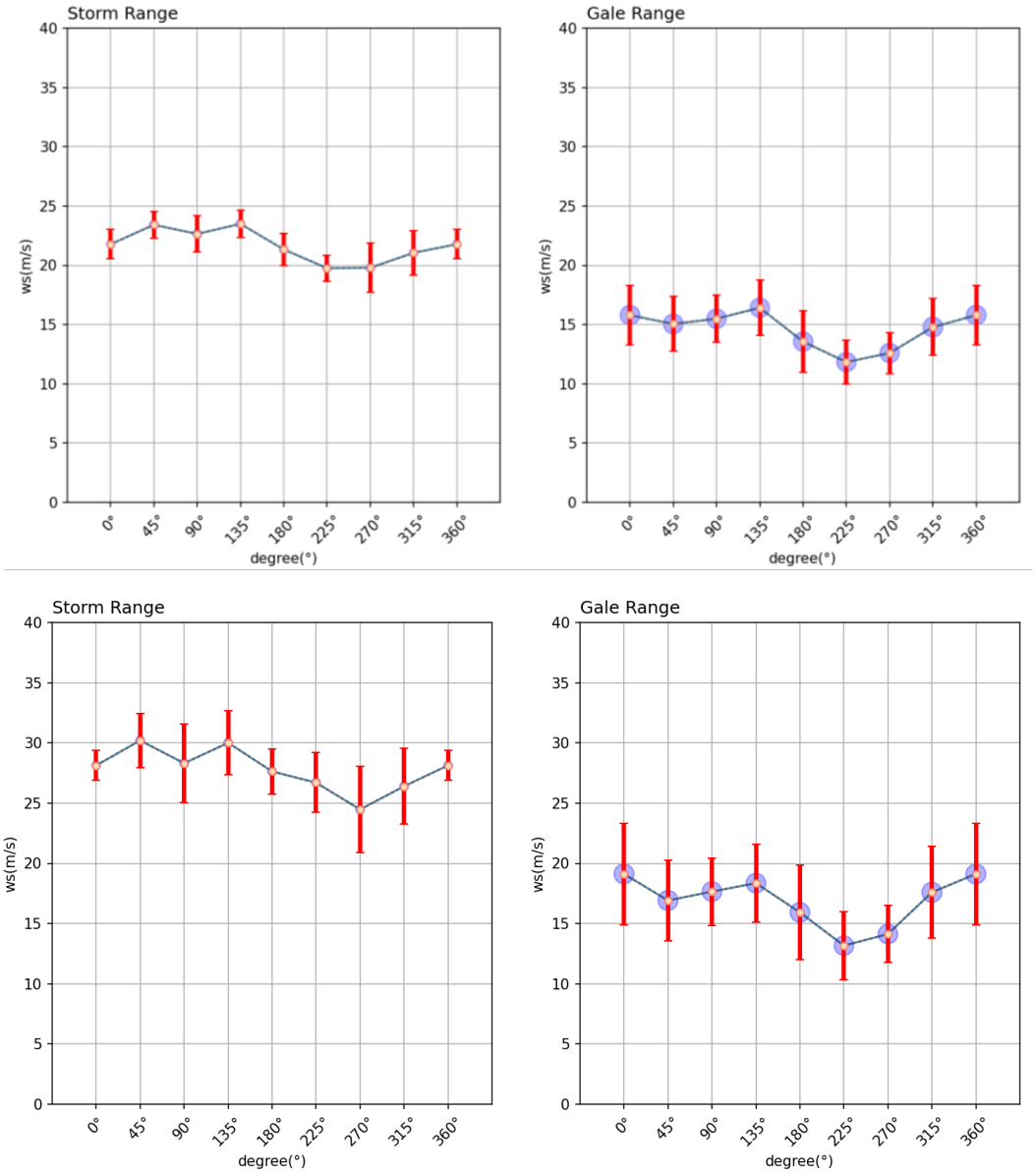

Fig.A-5 Sep.2 Wind speed distribution

(the top set: CYGNSS; the second set: AMSR2; the third set: ERA5; the fourth set: CFSR2)

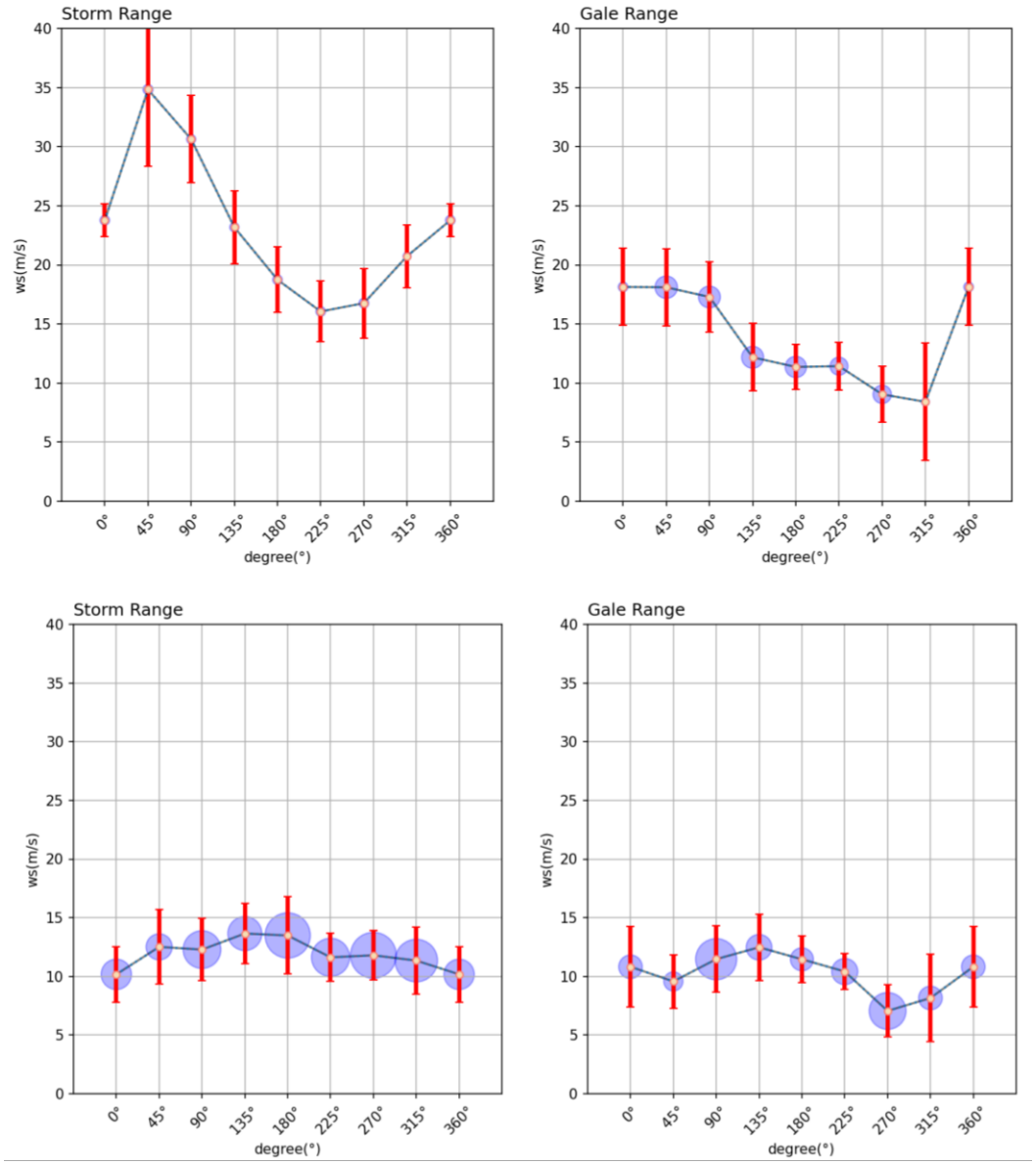
Storm Range
Gale Range
Storm Range
Gale Range
ws(m/s)
degree(°)
0°
45°
90°
135°
180°
225°
270°
315°
360°
0
5
10
15
20
25
30
35
40

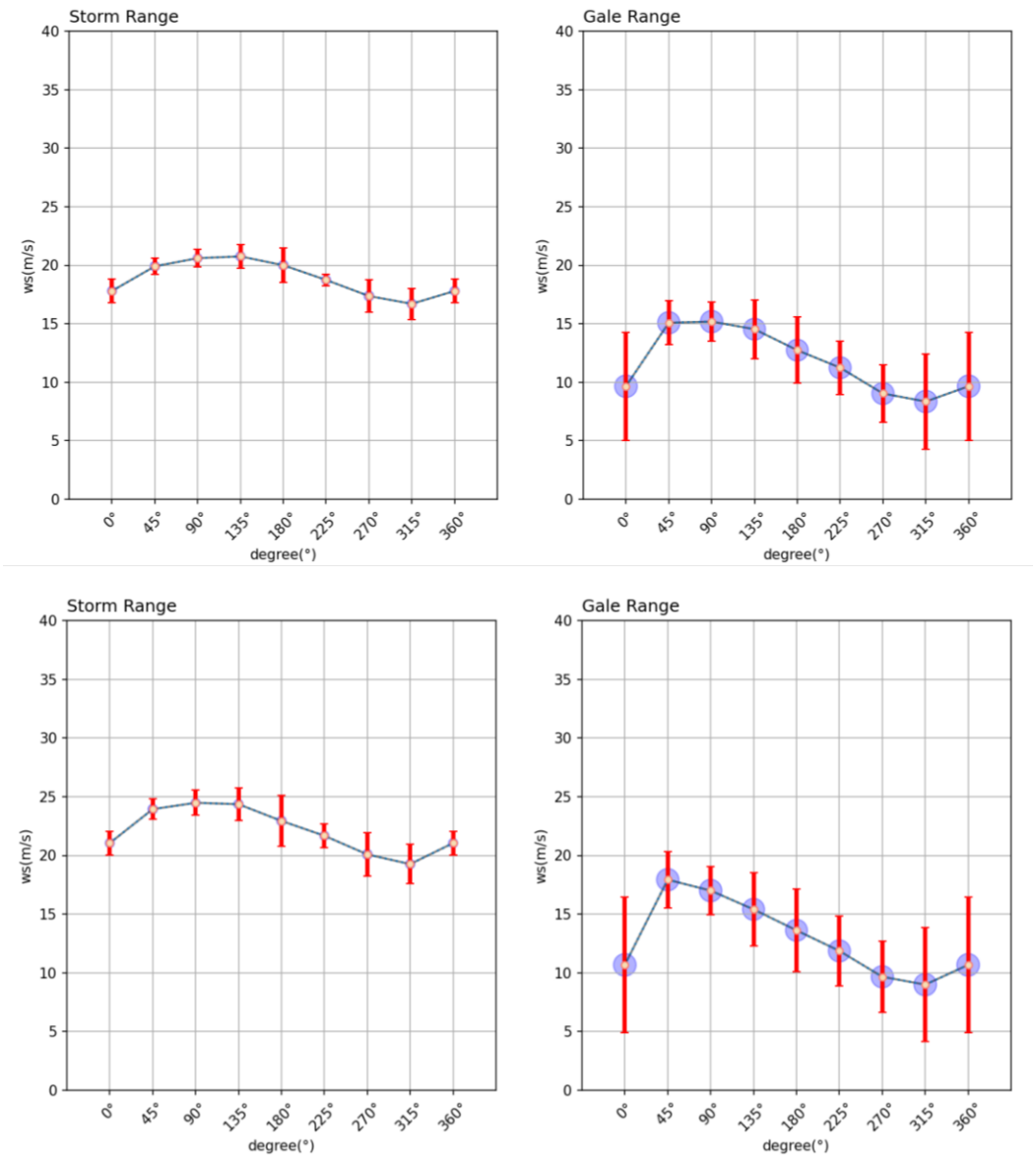

Fig.A-6 Sep.3 Wind speed distribution

(the top set: CYGNSS; the second set: AMSR2; the third set: ERA5; the fourth set: CFSR2)

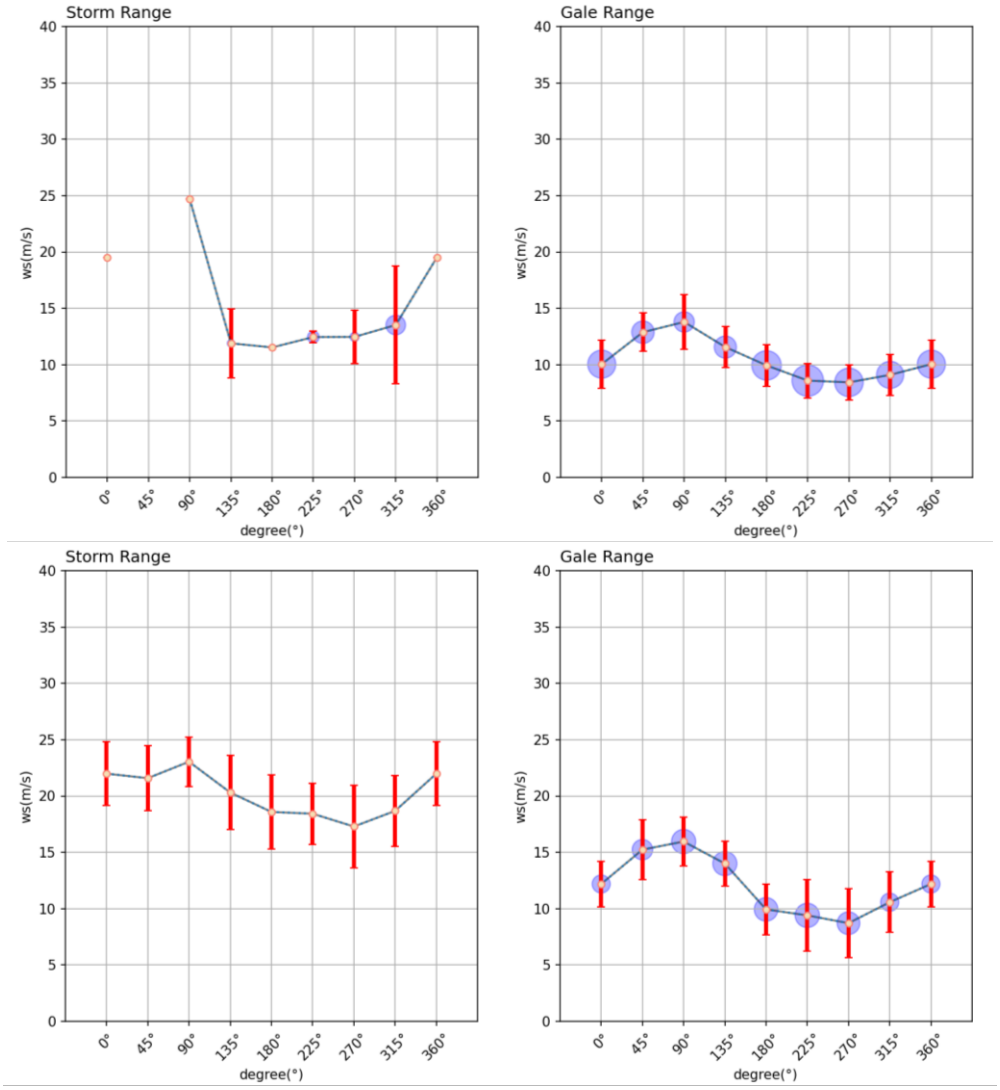
Storm Range
Gale Range
Storm Range
Gale Range
ws(m/s)
degree(°)
0°
45°
90°
135°
180°
225°
270°
315°
360°
0
5
10
15
20
25
30
35
40

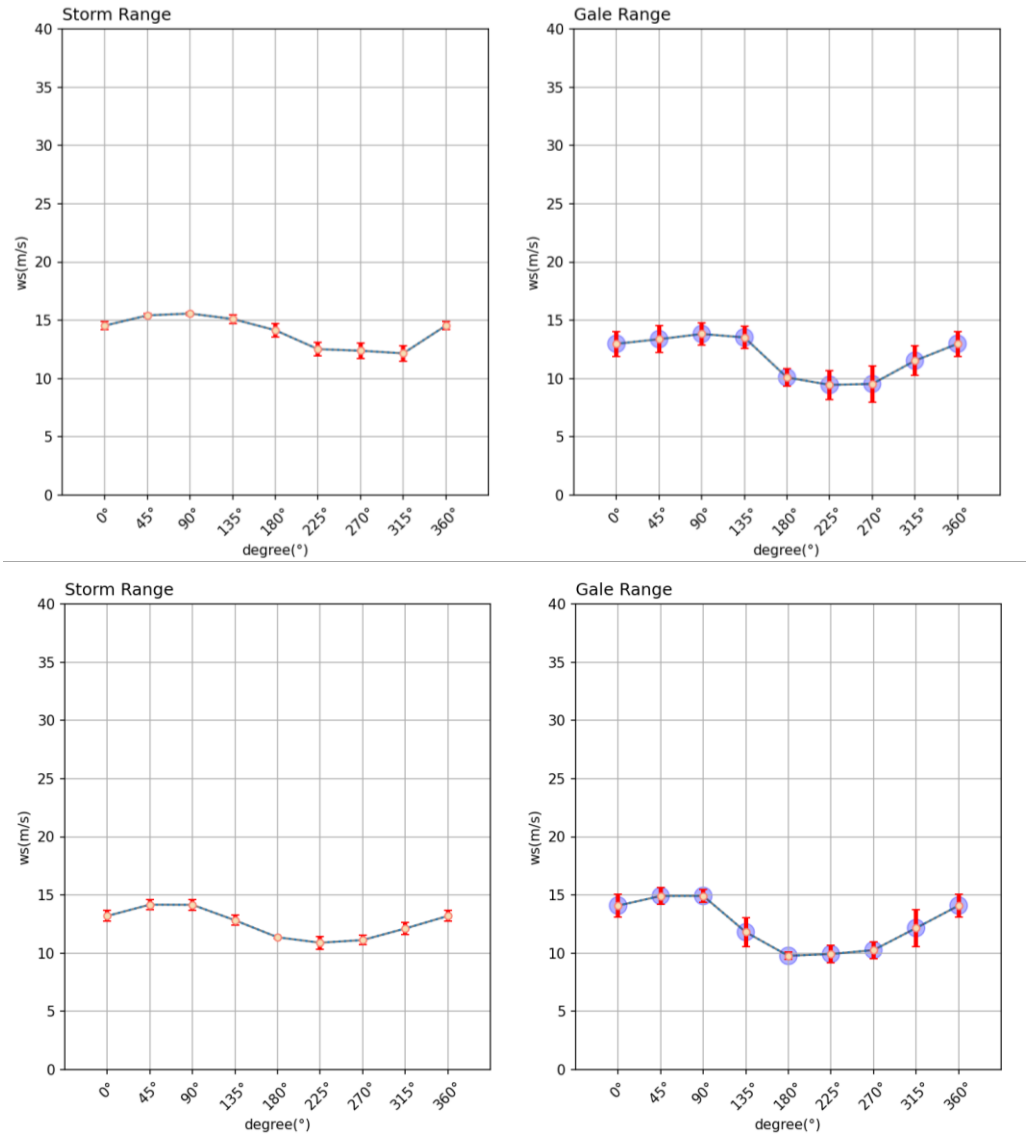

Fig.A-7 Sep.22 Wind speed distribution (the top set: CYGNSS; the second set: AMSR2; the third set: ERA5; the fourth set: CFSR2)

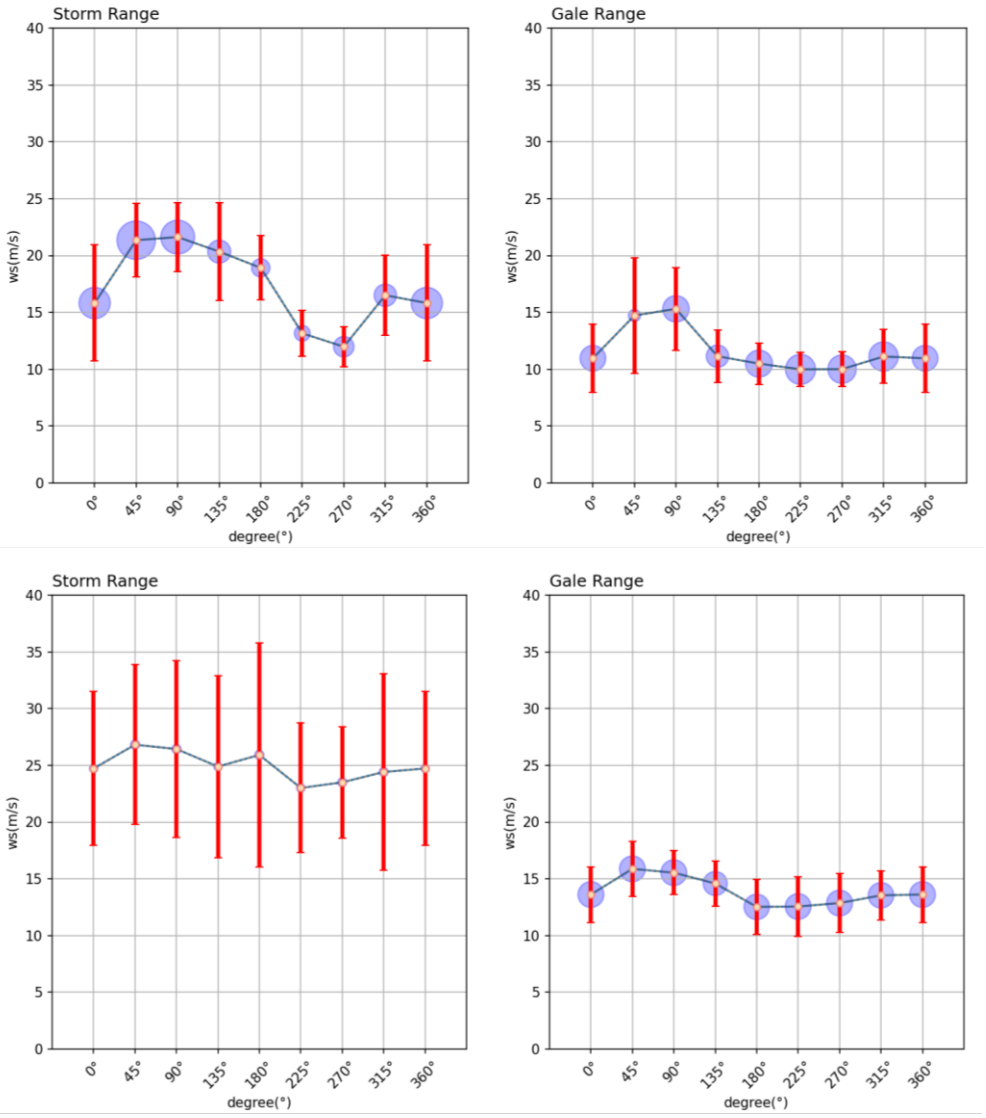
Storm Range
Gale Range
Storm Range
Gale Range
ws(m/s)
degree(°)
0°
45°
90°
135°
180°
225°
270°
315°
360°

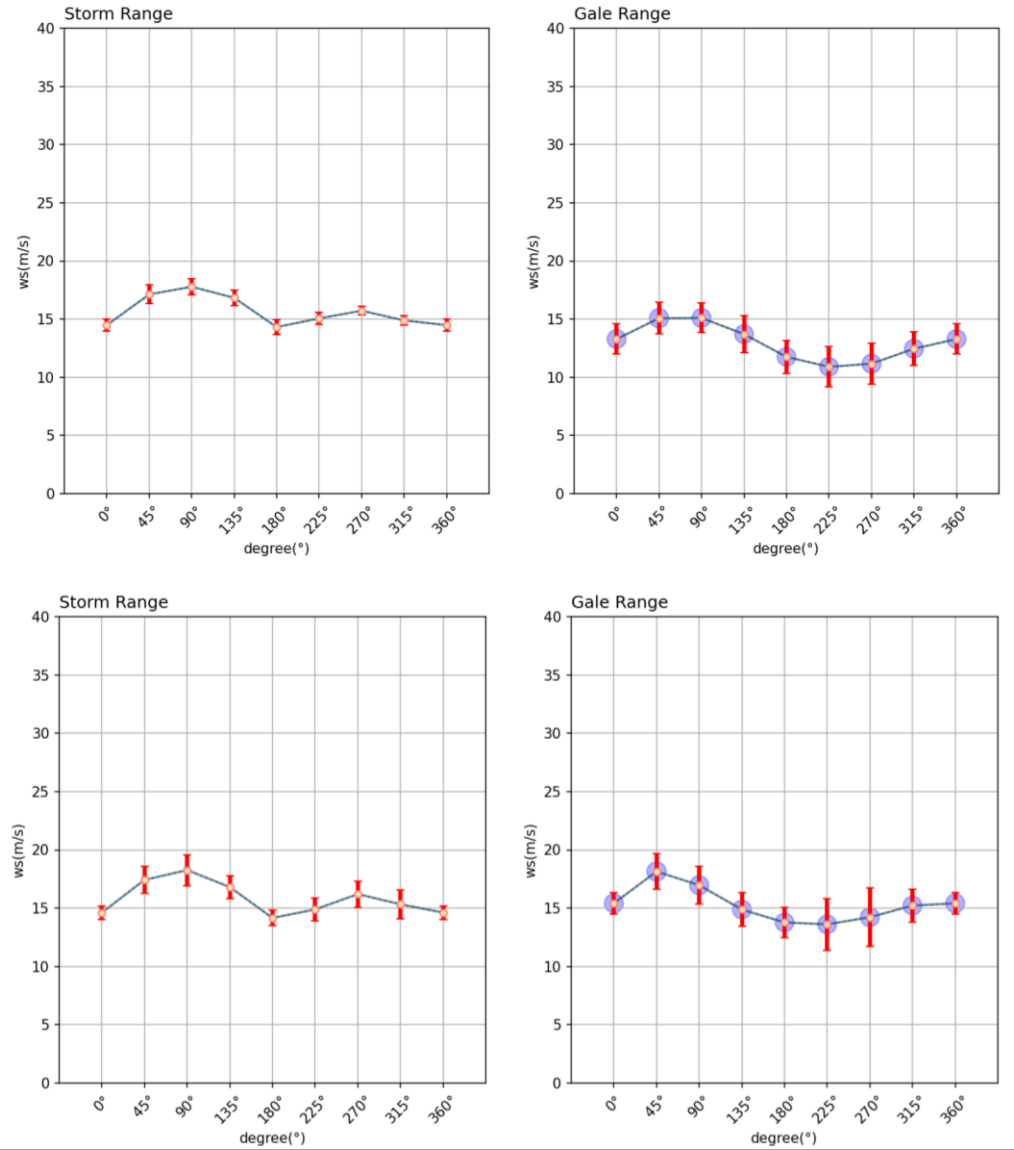

Fig.A-8 Sep.23 Wind speed distribution (the top set: CYGNSS; the second set: AMSR2; the third set: ERA5; the fourth set: CFSR2)

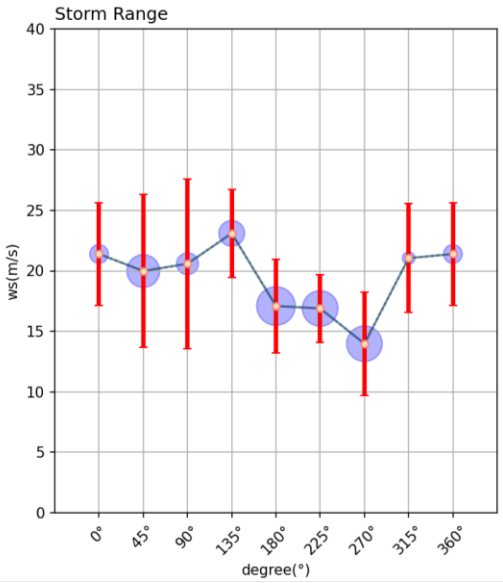
Storm Range
ws(m/s)
degree(°)
0°
45°
90°
135°
180°
225°
270°
315°
360°

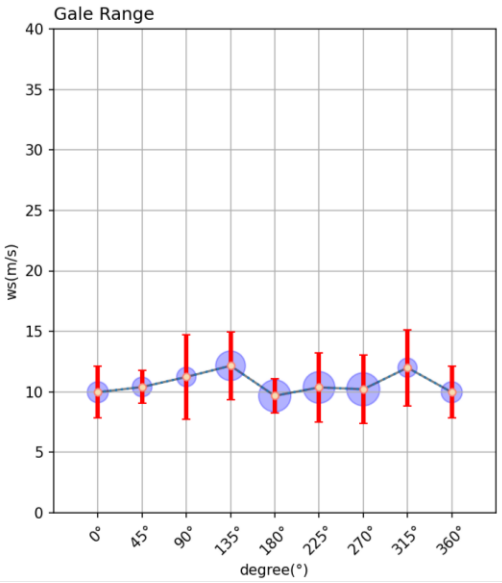
Gale Range
ws(m/s)
degree(°)
0°
45°
90°
135°
180°
225°
270°
315°
360°

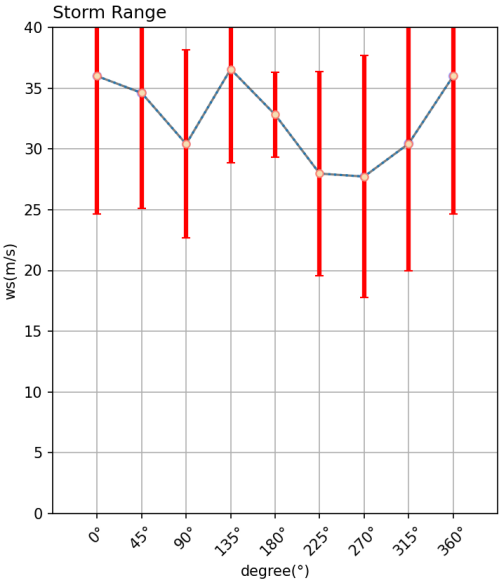
Storm Range
ws(m/s)
degree(°)
0°
45°
90°
135°
180°
225°
270°
315°
360°

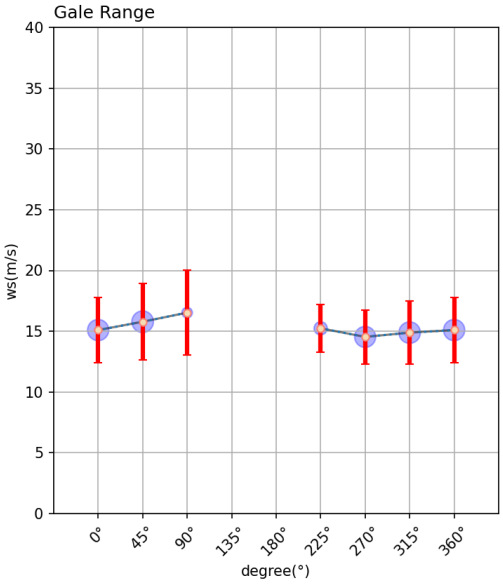
Gale Range
ws(m/s)
degree(°)
0°
45°
90°
135°
180°
225°
270°
315°
360°

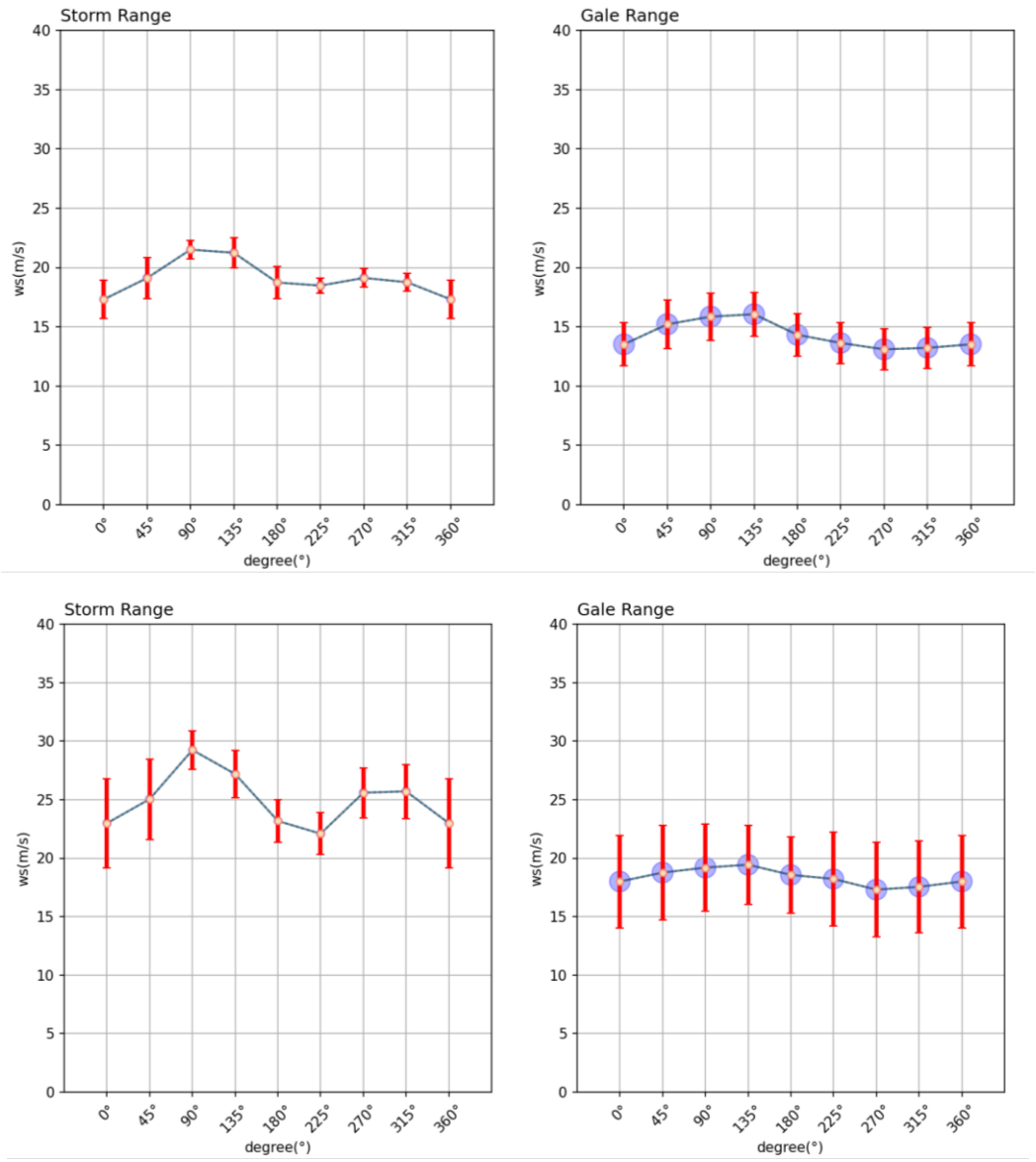

Fig.A-9 Sep.24 Wind speed distribution (the top set: CYGNSS; the second set: AMSR2; the third set: ERA5; the fourth set: CFSR2)

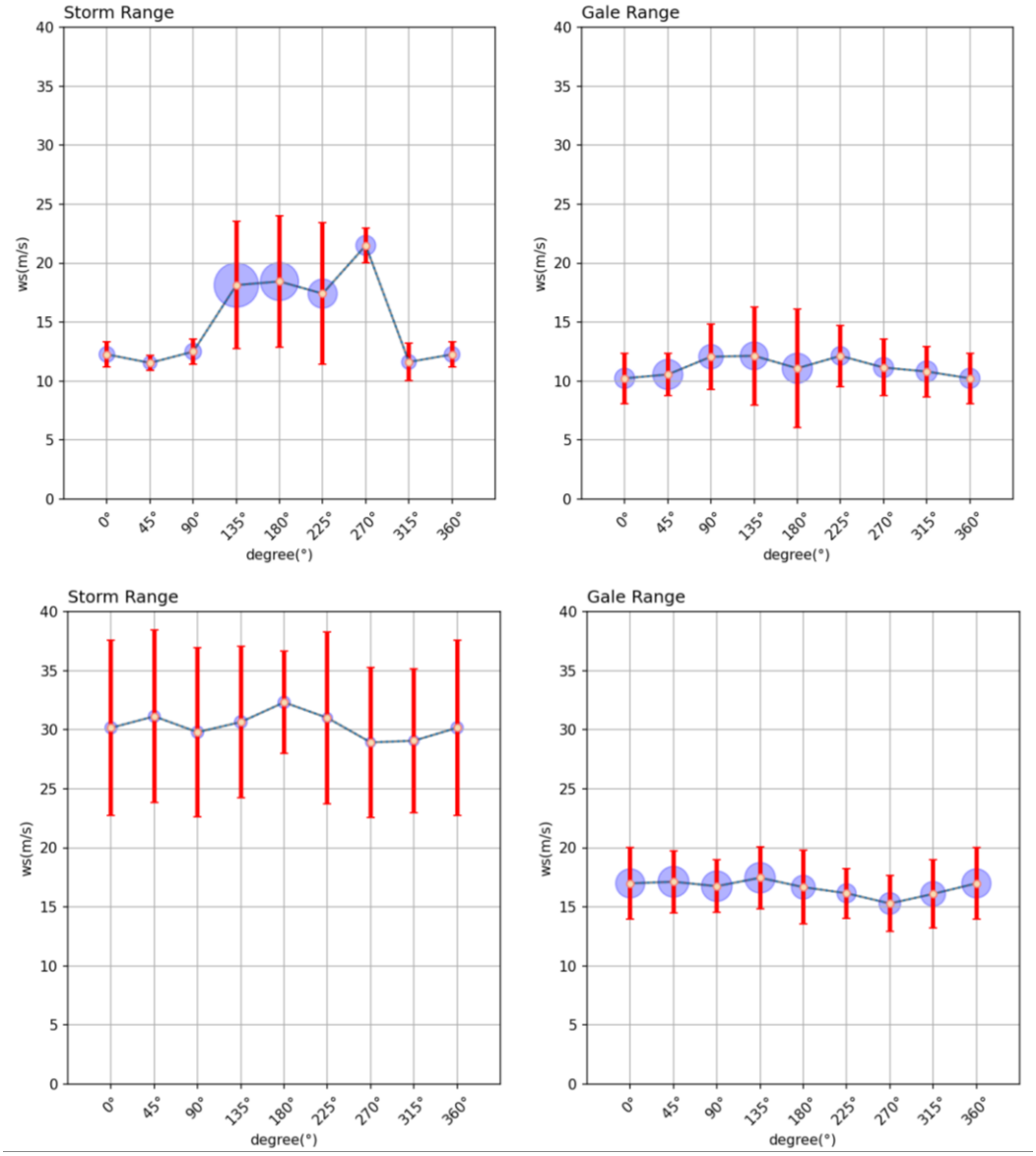
Storm Range
Gale Range
Storm Range
Gale Range
ws(m/s)
degree(°)
0°
45°
90°
135°
180°
225°
270°
315°
360°
0
5
10
15
20
25
30
35
40

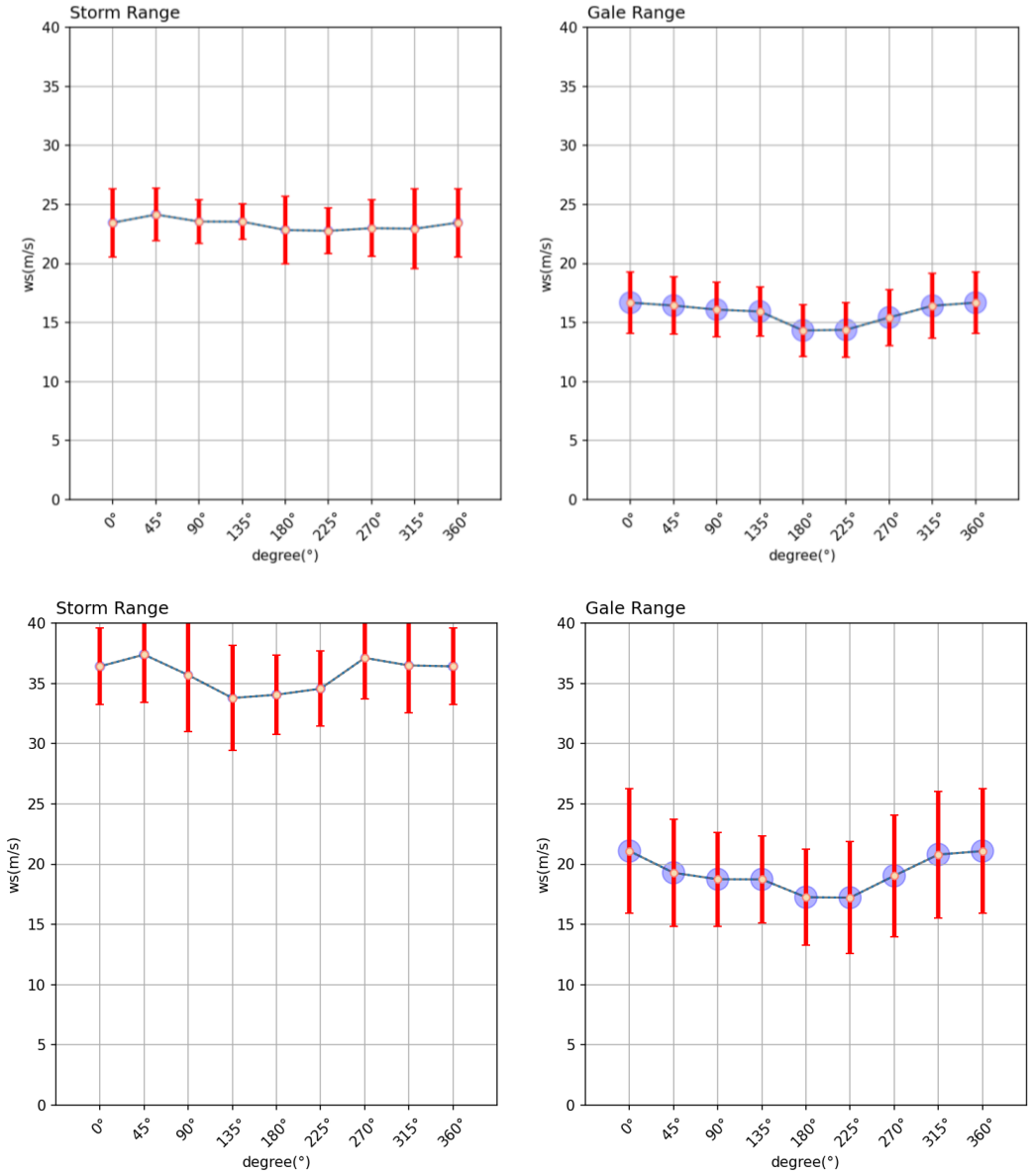

Fig.A-10 Sep.25 Wind speed distribution (the top set: CYGNSS; the second set: AMSR2; the third set: ERA5; the fourth set: CFSR2)

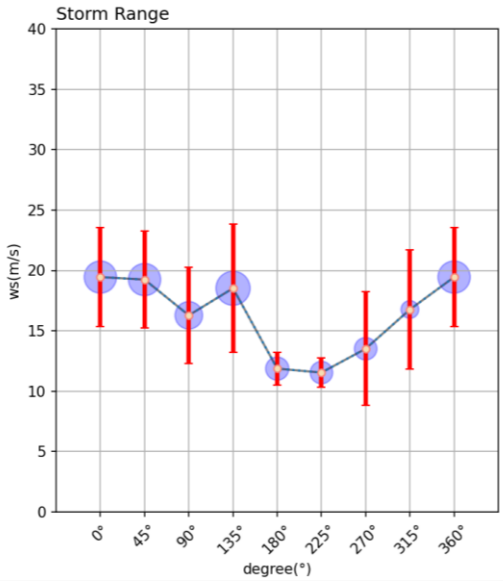
Storm Range
ws(m/s)
degree(°)
0°
45°
90°
135°
180°
225°
270°
315°
360°

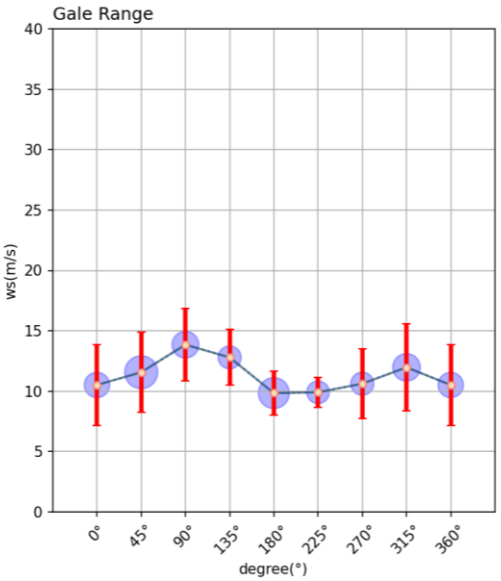
Gale Range
ws(m/s)
degree(°)
0°
45°
90°
135°
180°
225°
270°
315°
360°

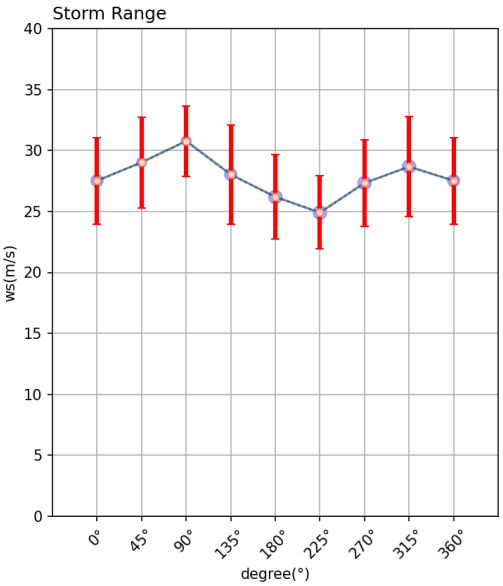
Storm Range
ws(m/s)
degree(°)
0°
45°
90°
135°
180°
225°
270°
315°
360°

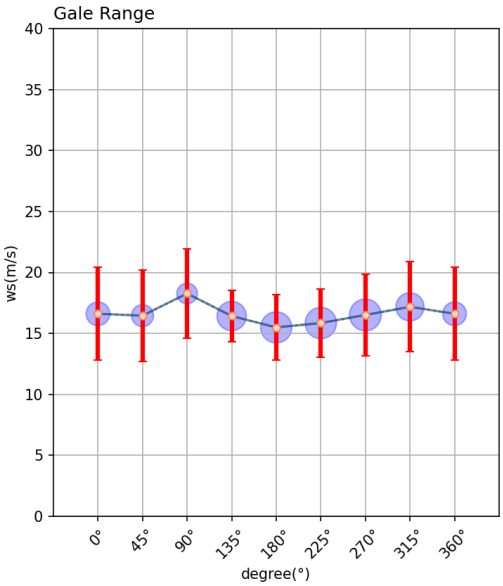
Gale Range
ws(m/s)
degree(°)
0°
45°
90°
135°
180°
225°
270°
315°
360°

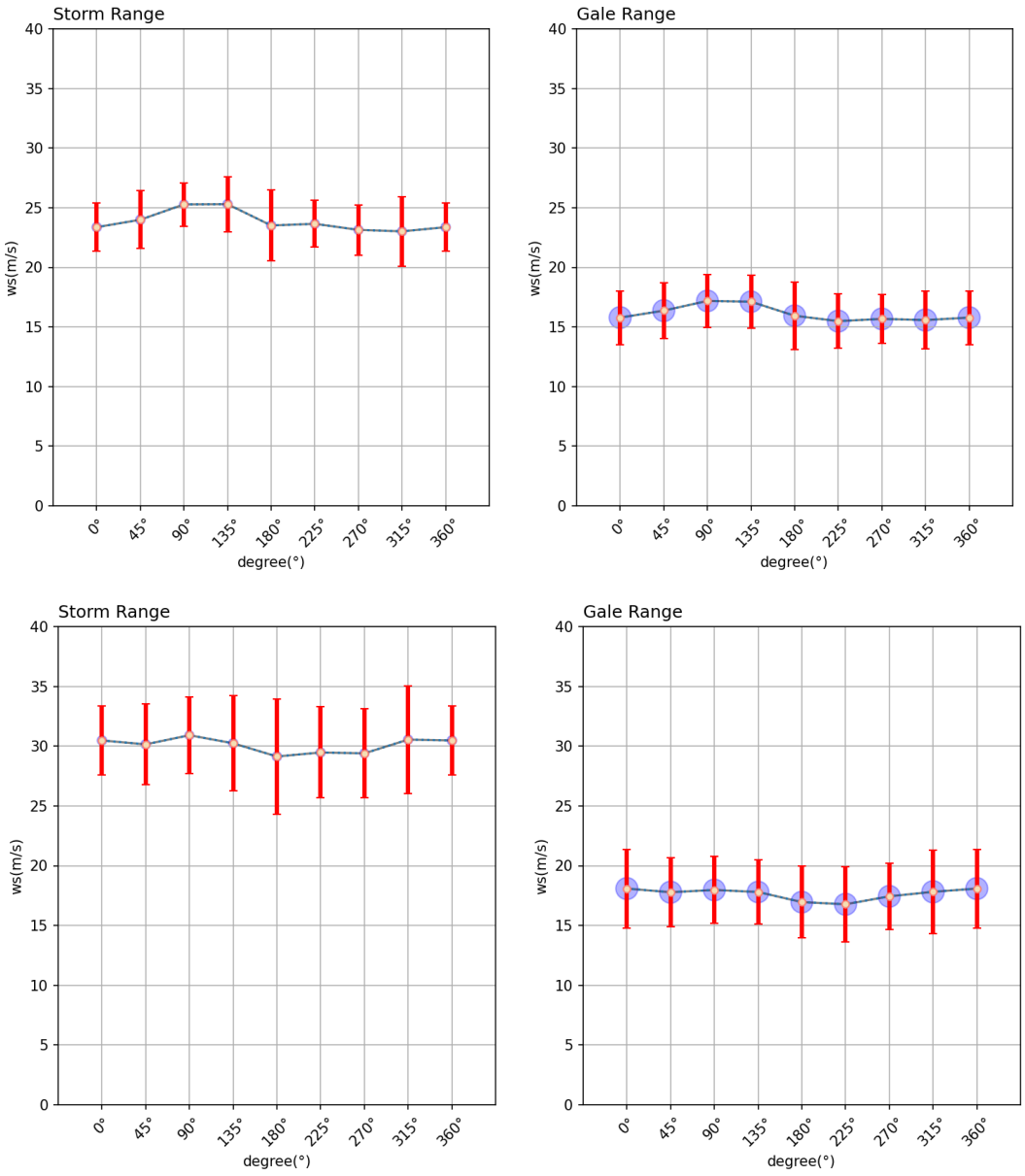

Fig.A-11 Sep.26 Wind speed distribution (the top set: CYGNSS; the second set: AMSR2; the third set: ERA5; the fourth set: CFSR2)

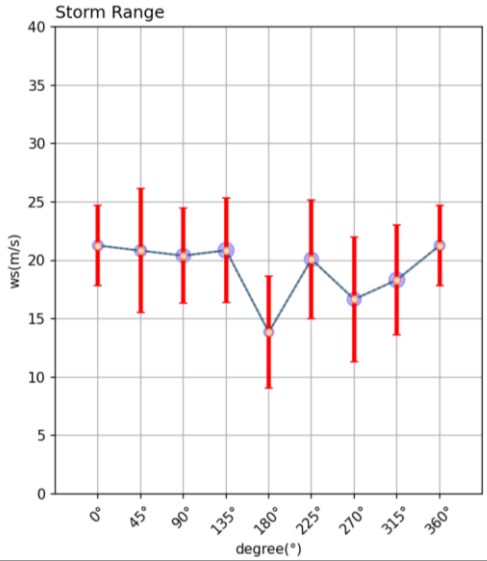
Storm Range
ws(m/s)
degree(°)
0°
45°
90°
135°
180°
225°
270°
315°
360°

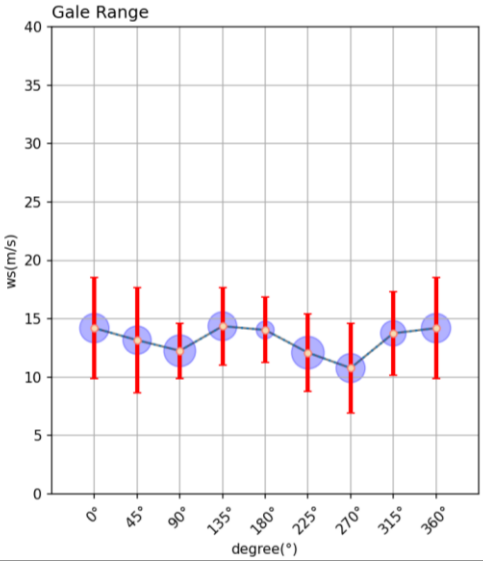
Gale Range
ws(m/s)
degree(°)
0°
45°
90°
135°
180°
225°
270°
315°
360°

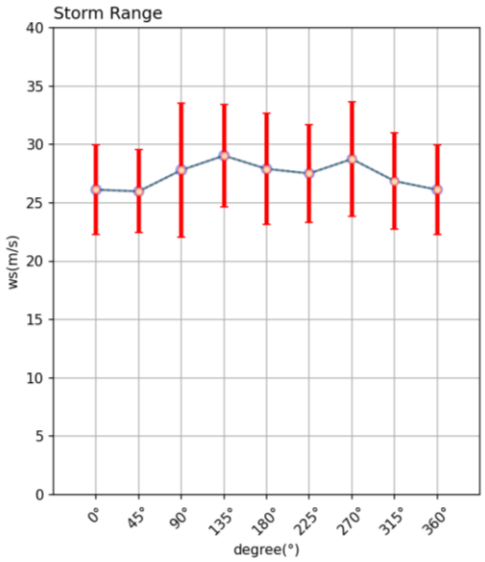
Storm Range
ws(m/s)
degree(°)
0°
45°
90°
135°
180°
225°
270°
315°
360°

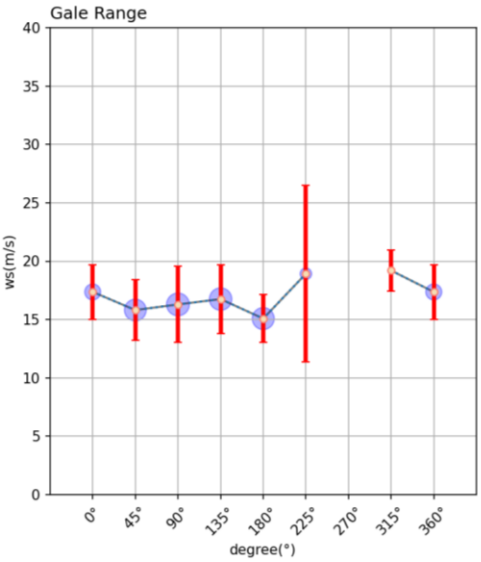
Gale Range
ws(m/s)
degree(°)
0°
45°
90°
135°
180°
225°
270°
315°
360°

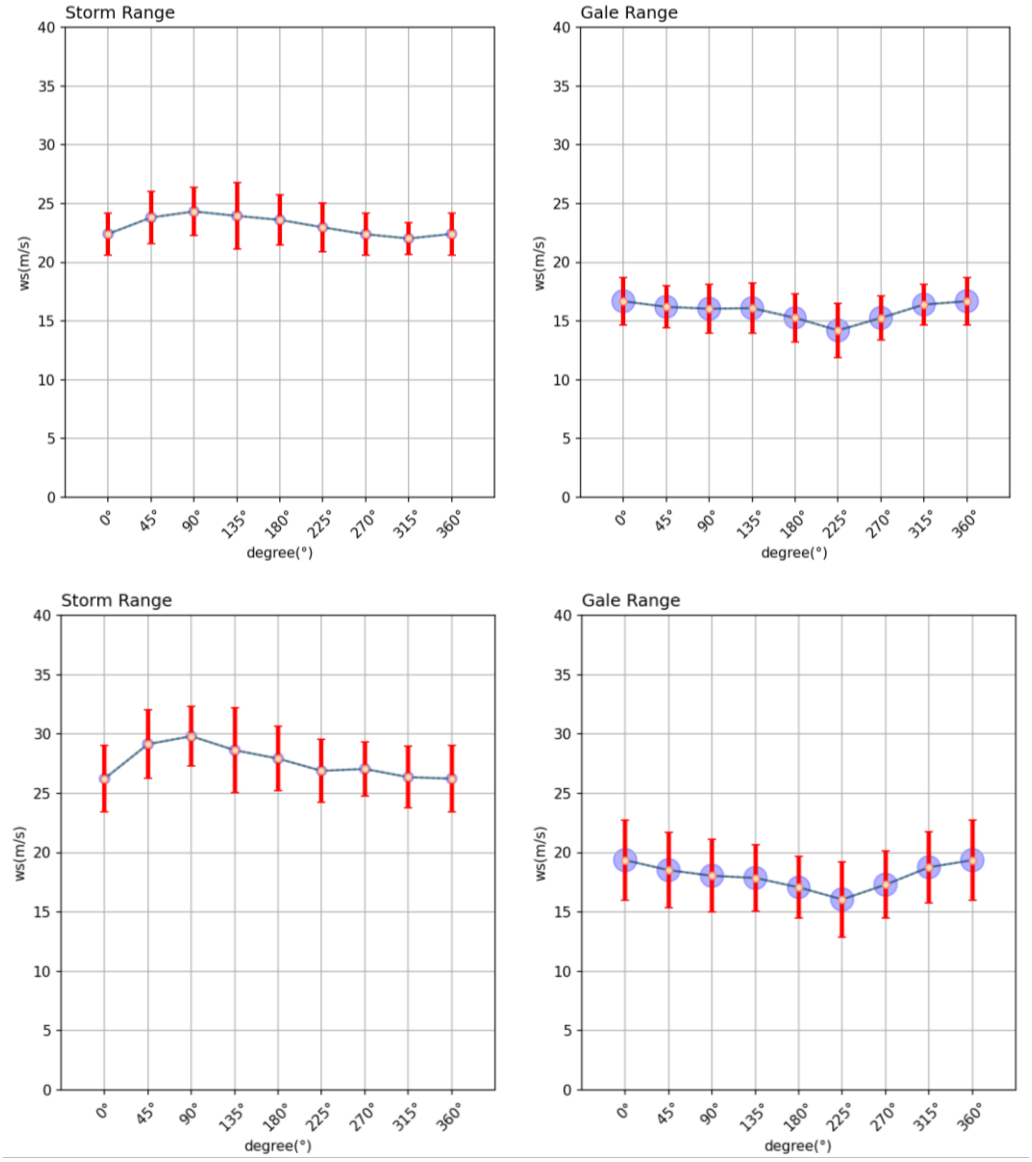

Fig.A-12 Sep.27 Wind speed distribution (the top set: CYGNSS; the second set: AMSR2; the third set: ERA5; the fourth set: CFSR2)

A.2 Daily distributions under 90 degree interval

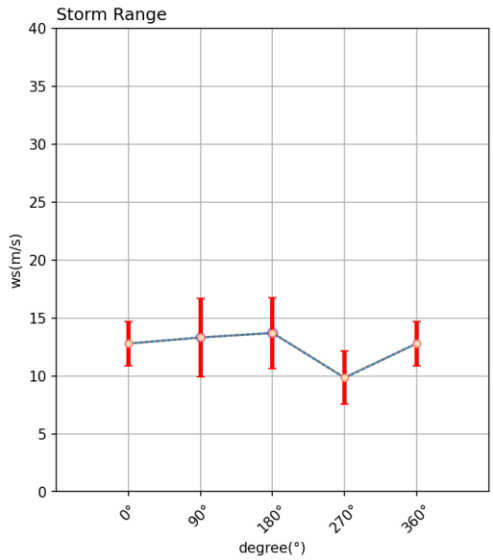

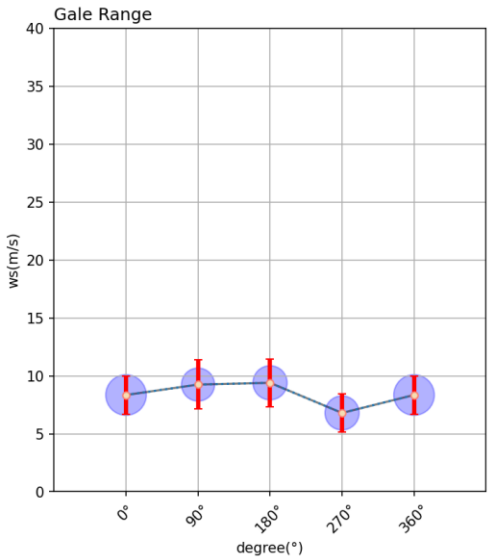

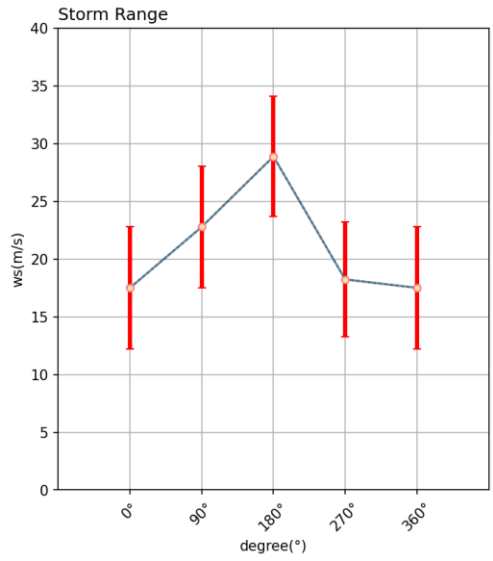

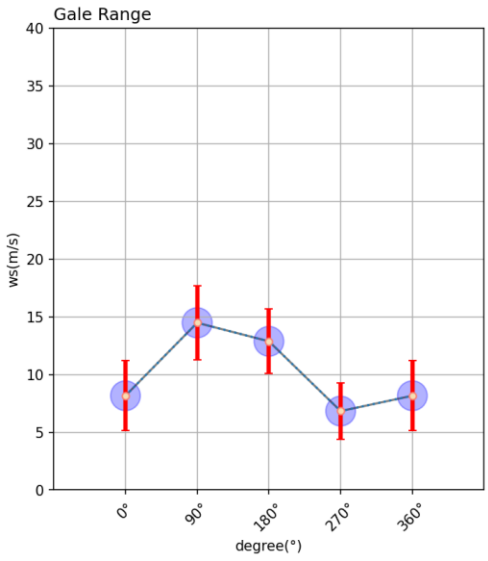

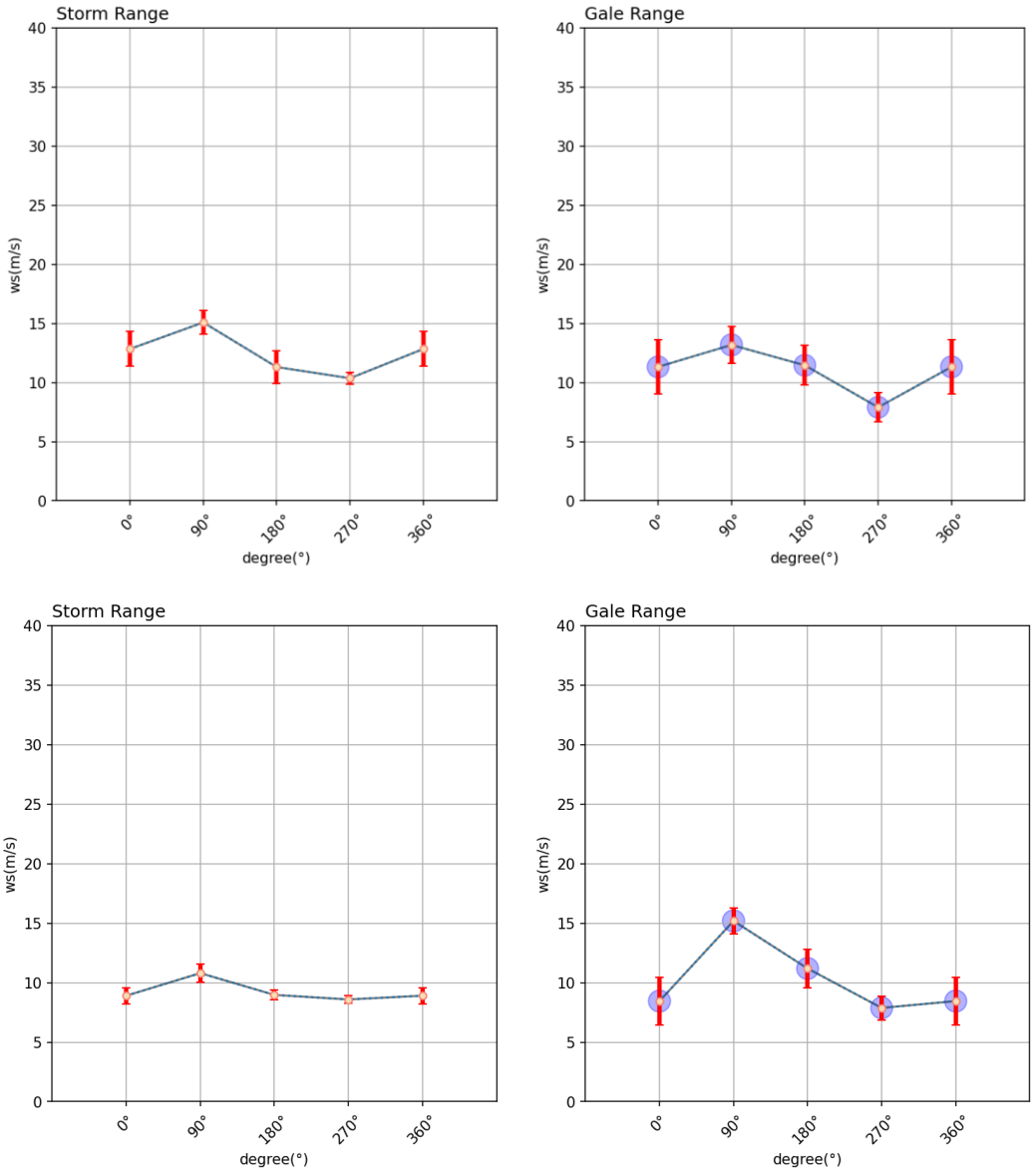

Fig.A-13 Aug.29 Wind speed distribution (the top set: CYGNSS; the second set: AMSR2; the third set: ERA5; the fourth set: CFSR2)

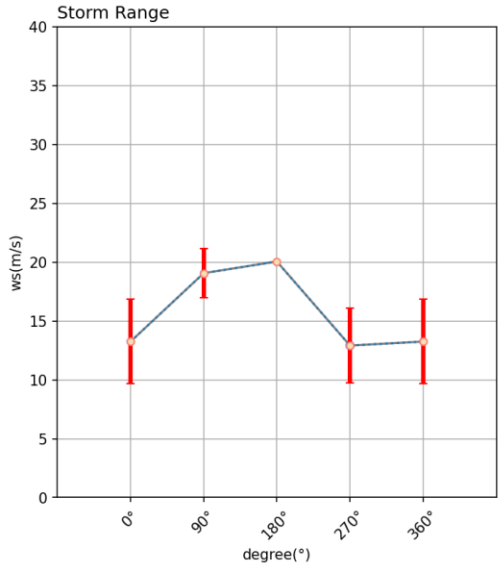
Storm Range
ws(m/s)
degree(°)
0°
90°
180°
270°
360°

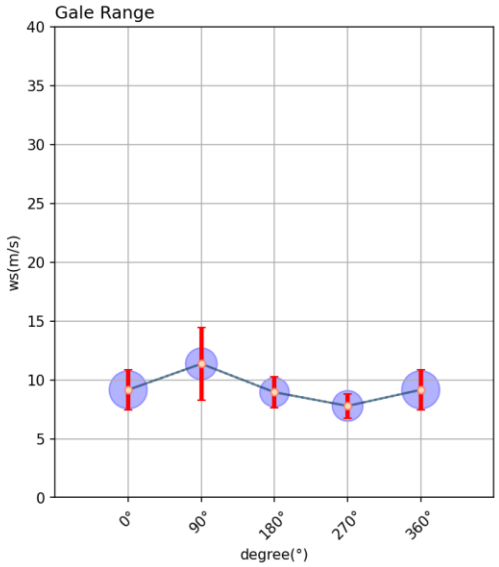
Gale Range
ws(m/s)
degree(°)
0°
90°
180°
270°
360°

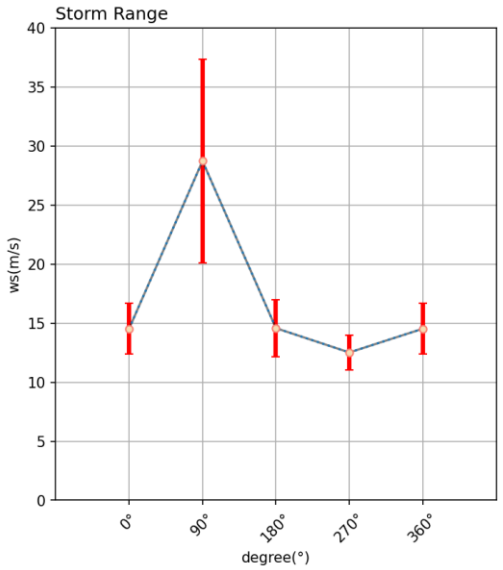
Storm Range
ws(m/s)
degree(°)
0°
90°
180°
270°
360°

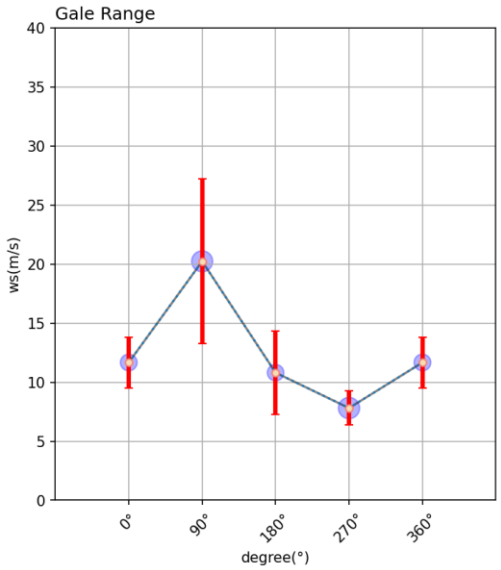
Gale Range
ws(m/s)
degree(°)
0°
90°
180°
270°
360°

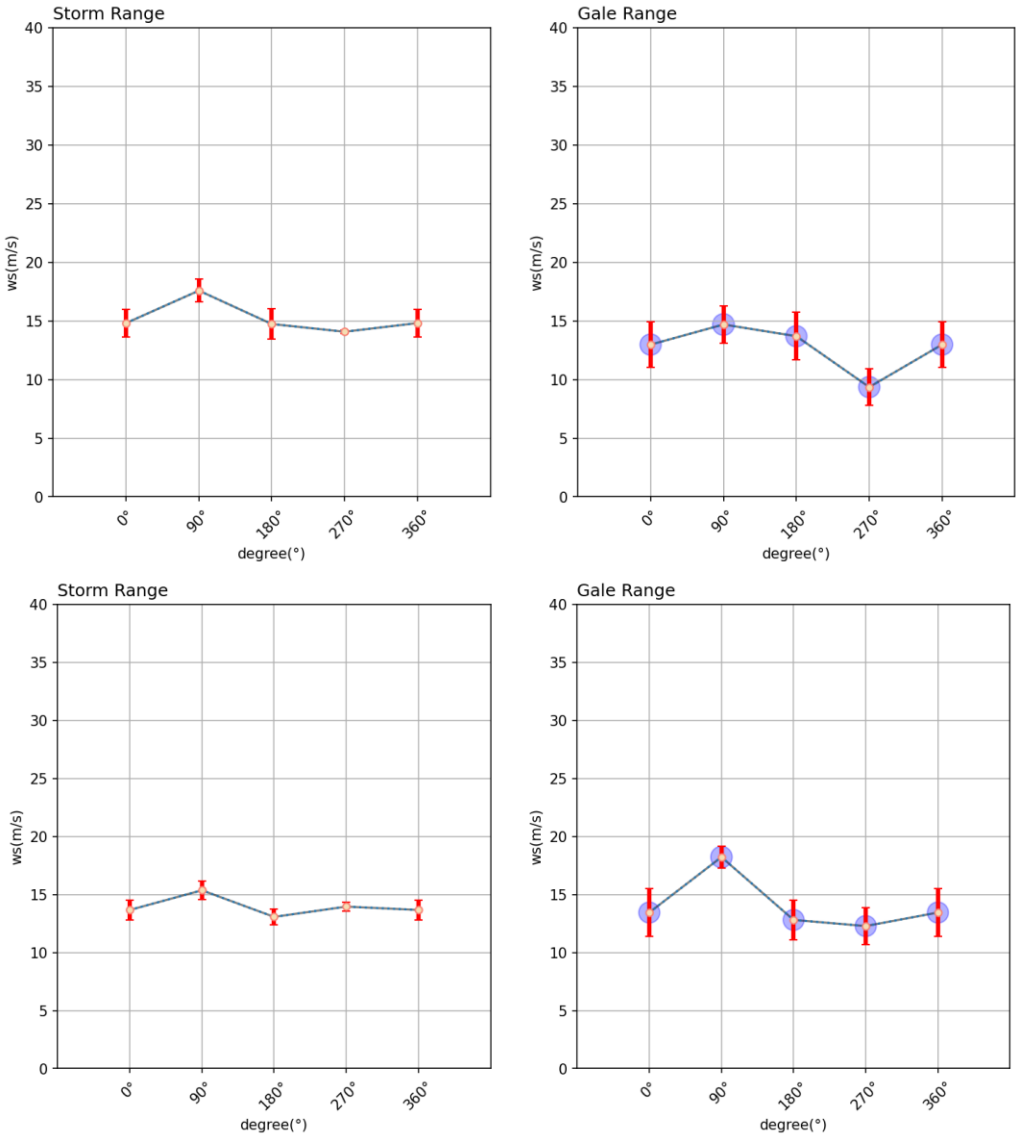

Fig.A-14 Aug.30 Wind speed distribution (the top set: CYGNSS; the second set: AMSR2; the third set: ERA5; the fourth set: CFSR2)

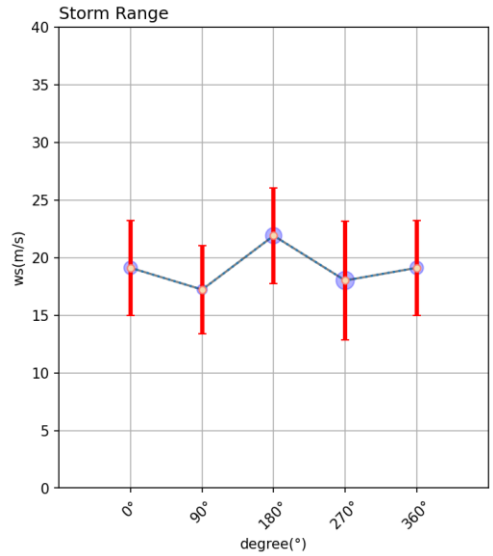
Storm Range
ws(m/s)
degree(°)
0°
90°
180°
270°
360°

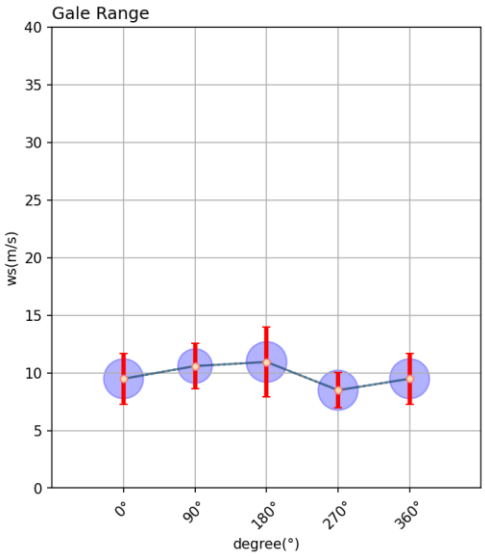
Gale Range
ws(m/s)
degree(°)
0°
90°
180°
270°
360°

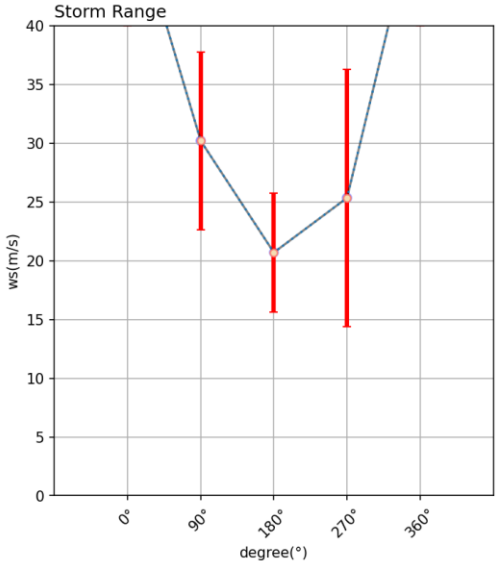
Storm Range
ws(m/s)
degree(°)
0°
90°
180°
270°
360°

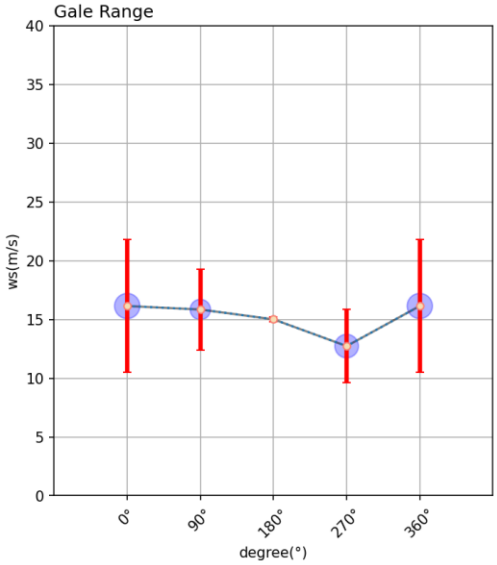
Gale Range
ws(m/s)
degree(°)
0°
90°
180°
270°
360°

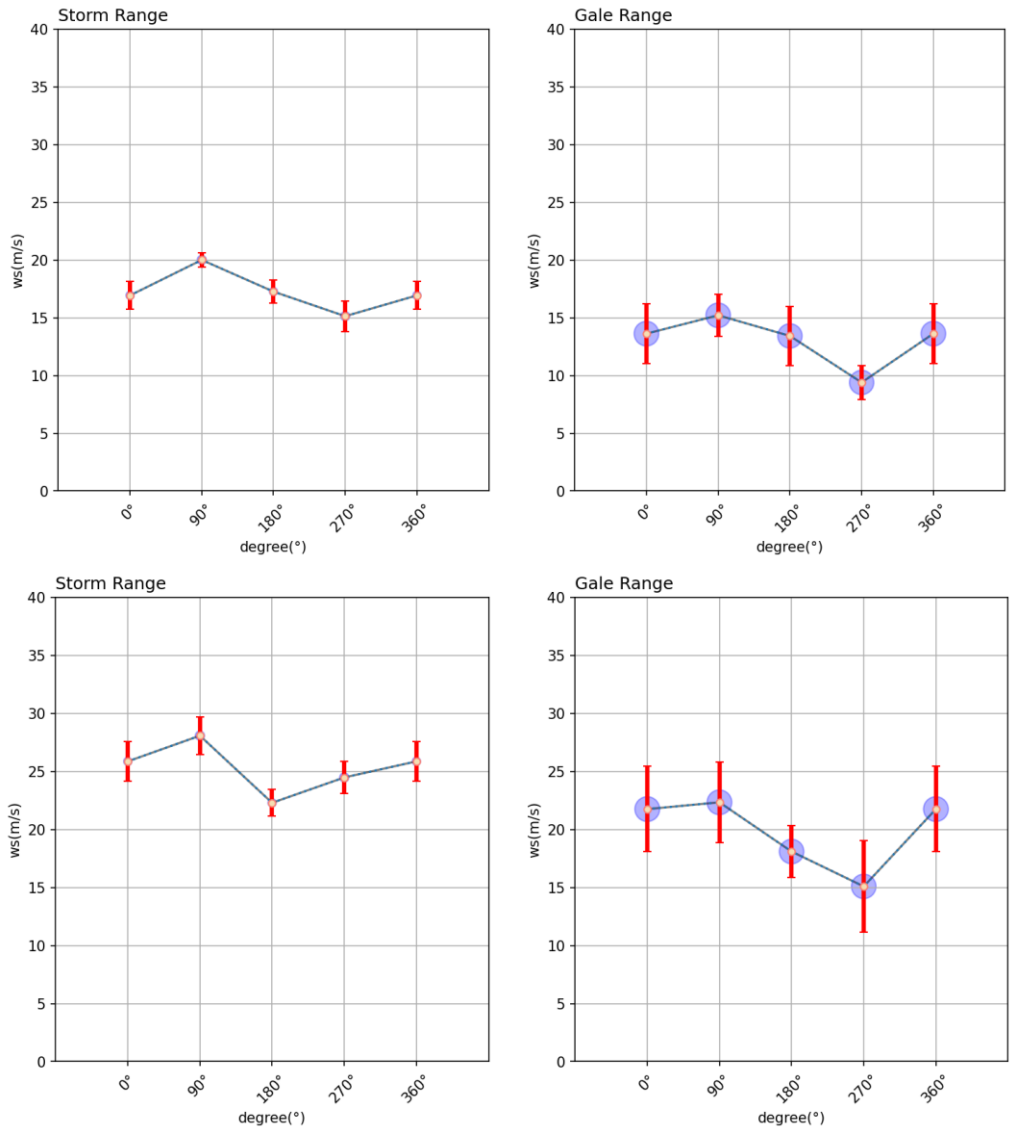

Fig.A-15 Aug.31 Wind speed distribution (the top set: CYGNSS; the second set: AMSR2; the third set: ERA5; the fourth set: CFSR2)

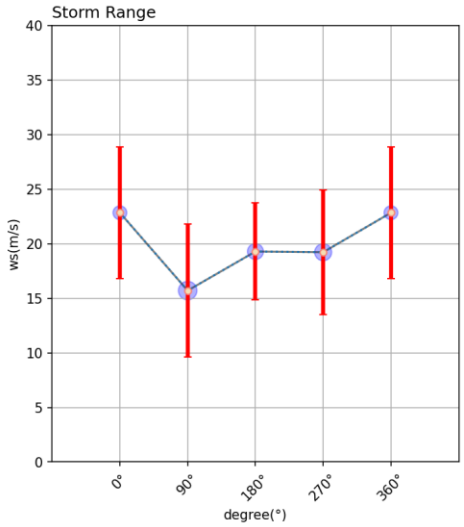
Storm Range
ws(m/s)
degree(°)
0°
90°
180°
270°
360°

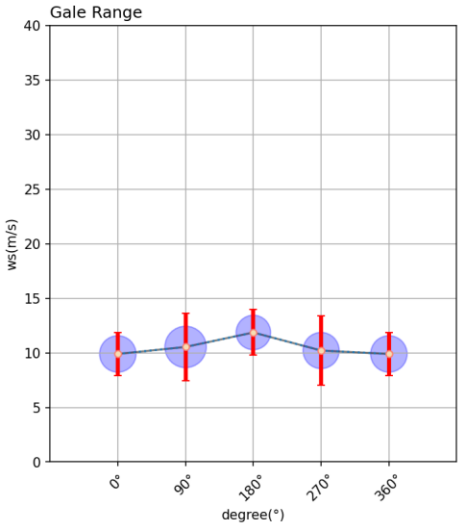
Gale Range
ws(m/s)
degree(°)
0°
90°
180°
270°
360°

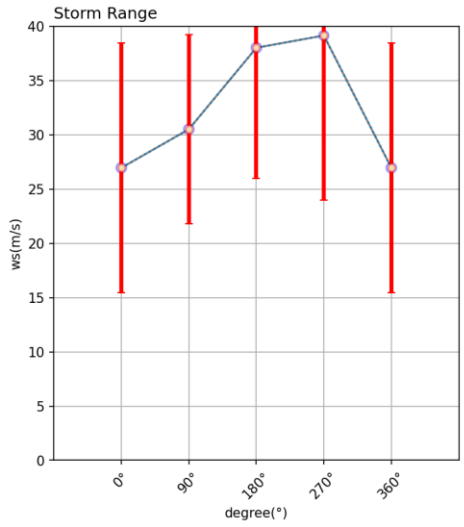
Storm Range
ws(m/s)
degree(°)
0°
90°
180°
270°
360°

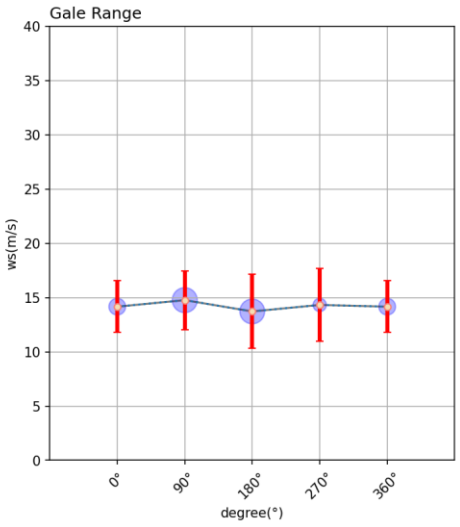
Gale Range
ws(m/s)
degree(°)
0°
90°
180°
270°
360°

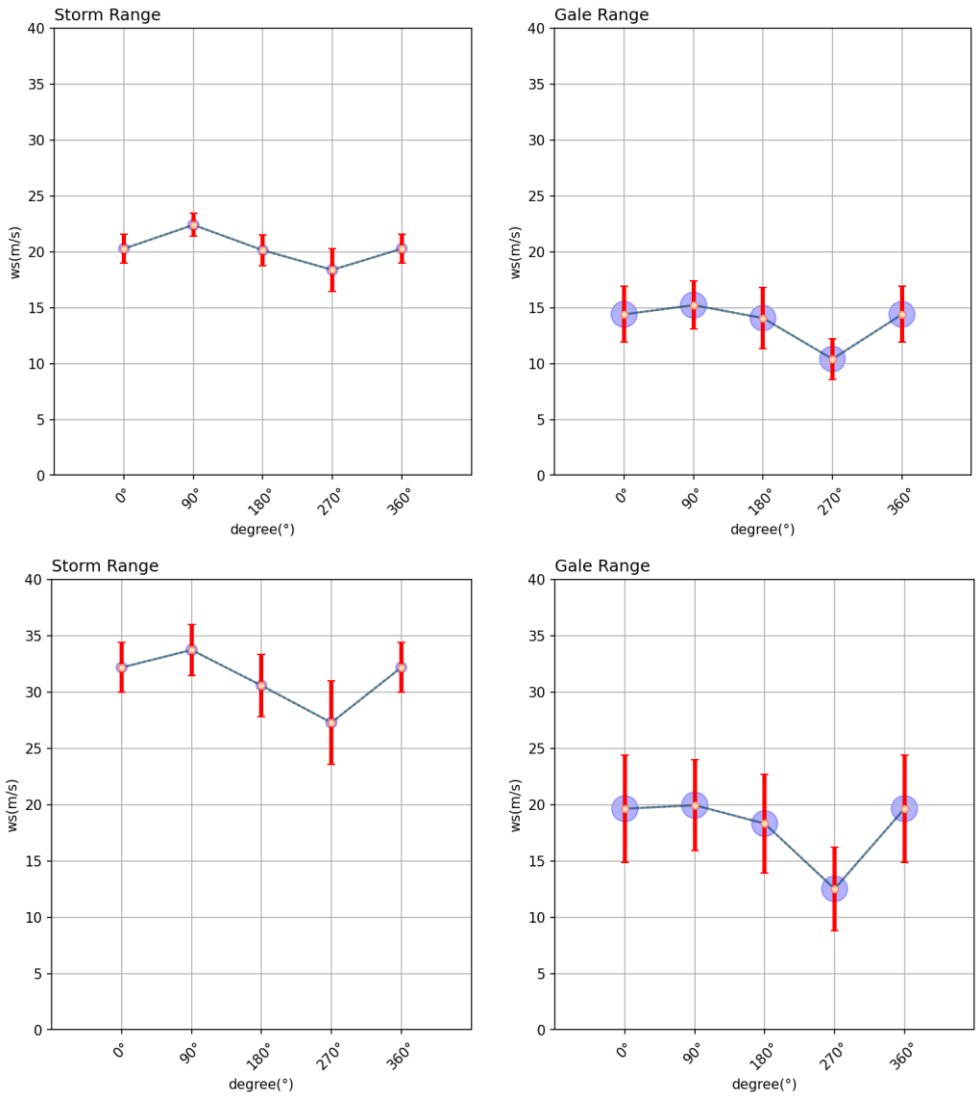

Fig.A-16 Sep.1 Wind speed distribution (the top set: CYGNSS; the second set: AMSR2; the third set: ERA5; the fourth set: CFSR2)

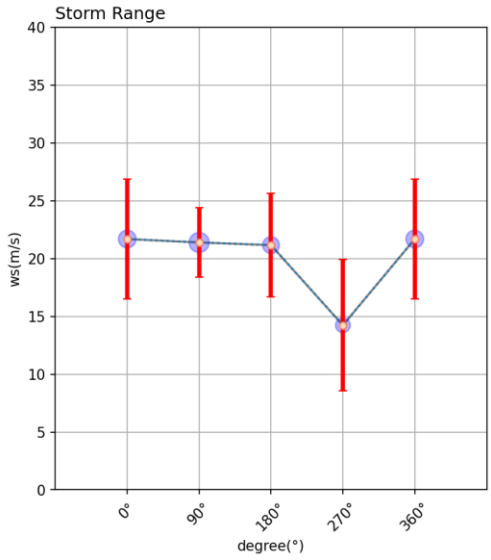
Storm Range
ws(m/s)
degree(°)
0°
90°
180°
270°
360°

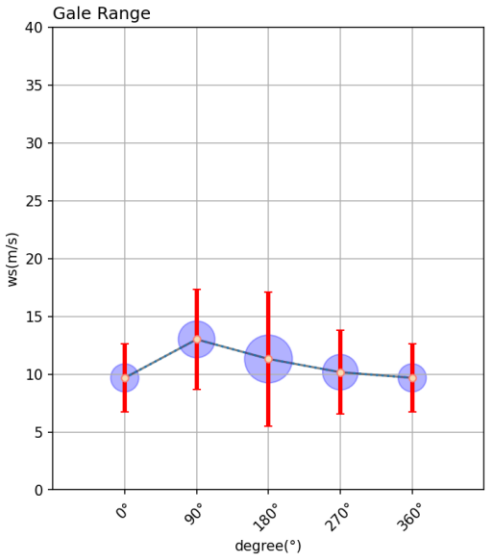
Gale Range
ws(m/s)
degree(°)
0°
90°
180°
270°
360°

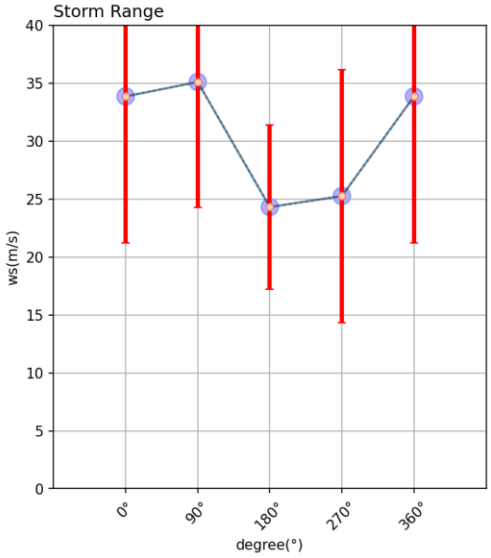
Storm Range
ws(m/s)
degree(°)
0°
90°
180°
270°
360°

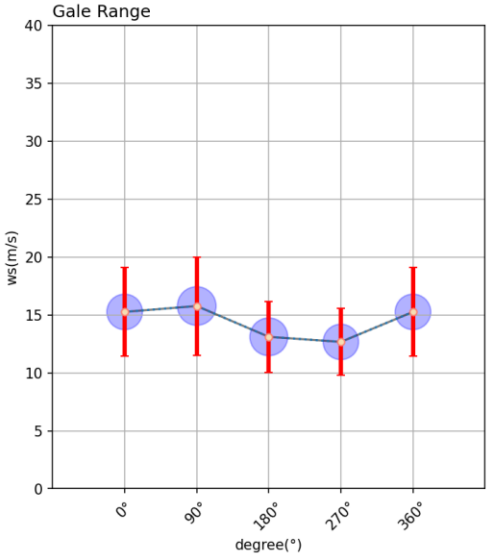
Gale Range
ws(m/s)
degree(°)
0°
90°
180°
270°
360°

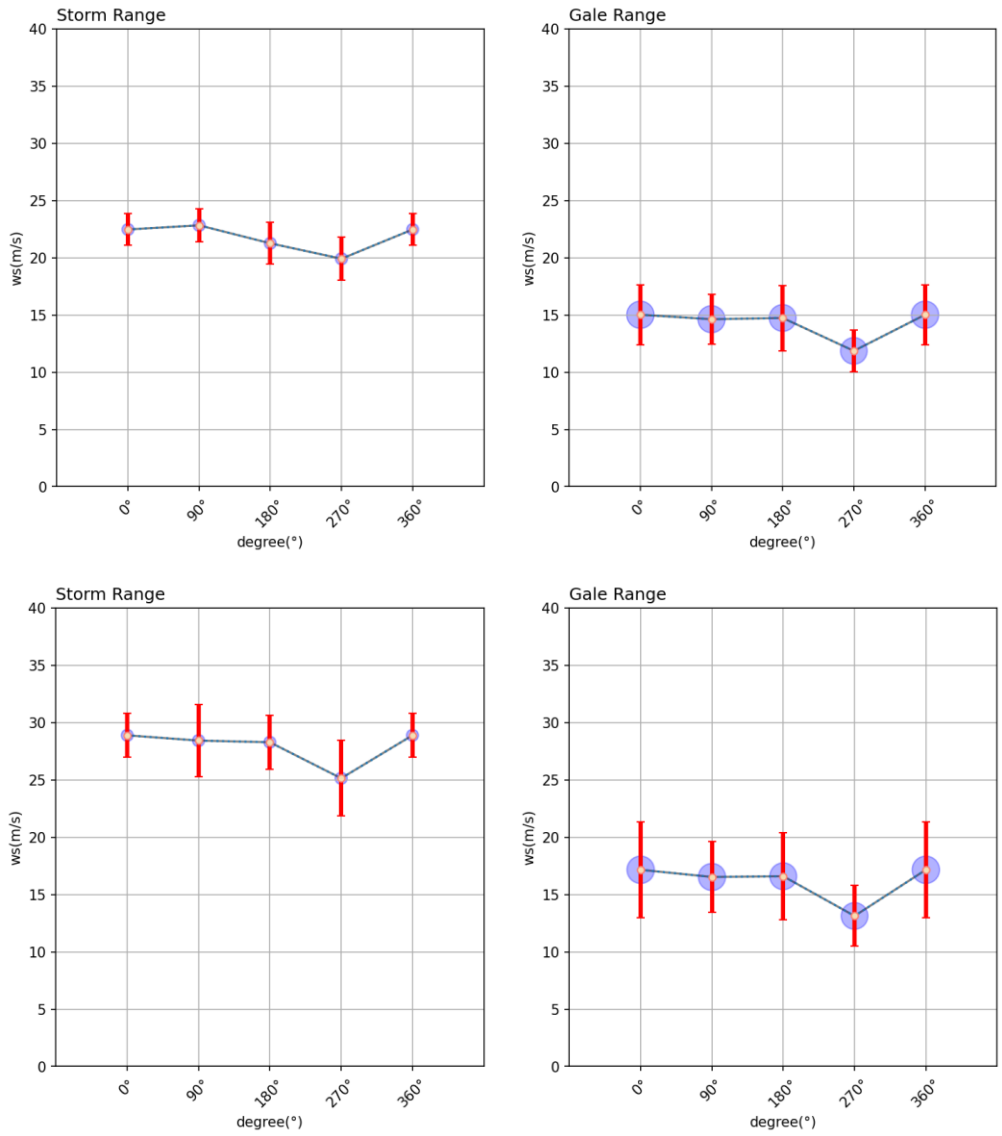

Fig.A-17 Sep.2 Wind speed distribution (the top set: CYGNSS; the second set: AMSR2; the third set: ERA5; the fourth set: CFSR2)

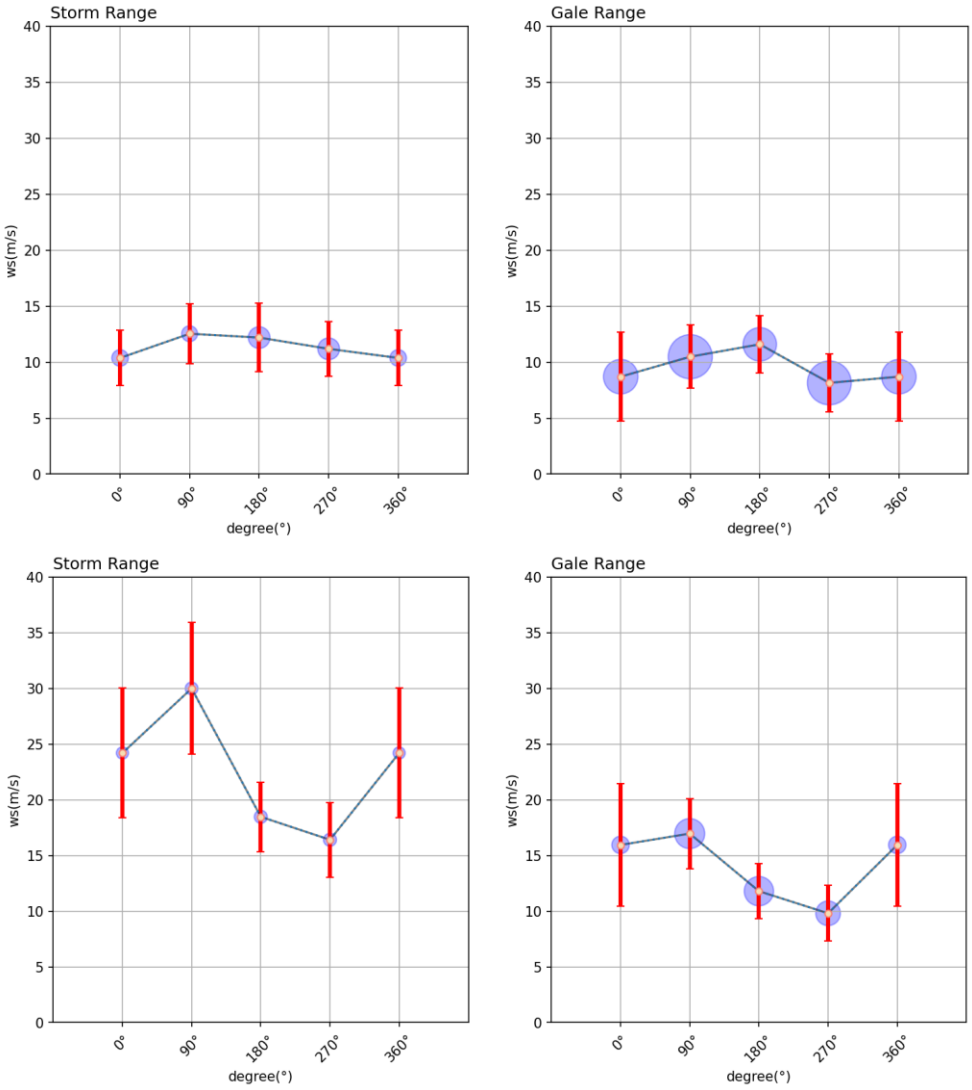
Storm Range
Gale Range
Storm Range
Gale Range
ws(m/s)
degree(°)
0°
90°
180°
270°
360°
0
5
10
15
20
25
30
35
40

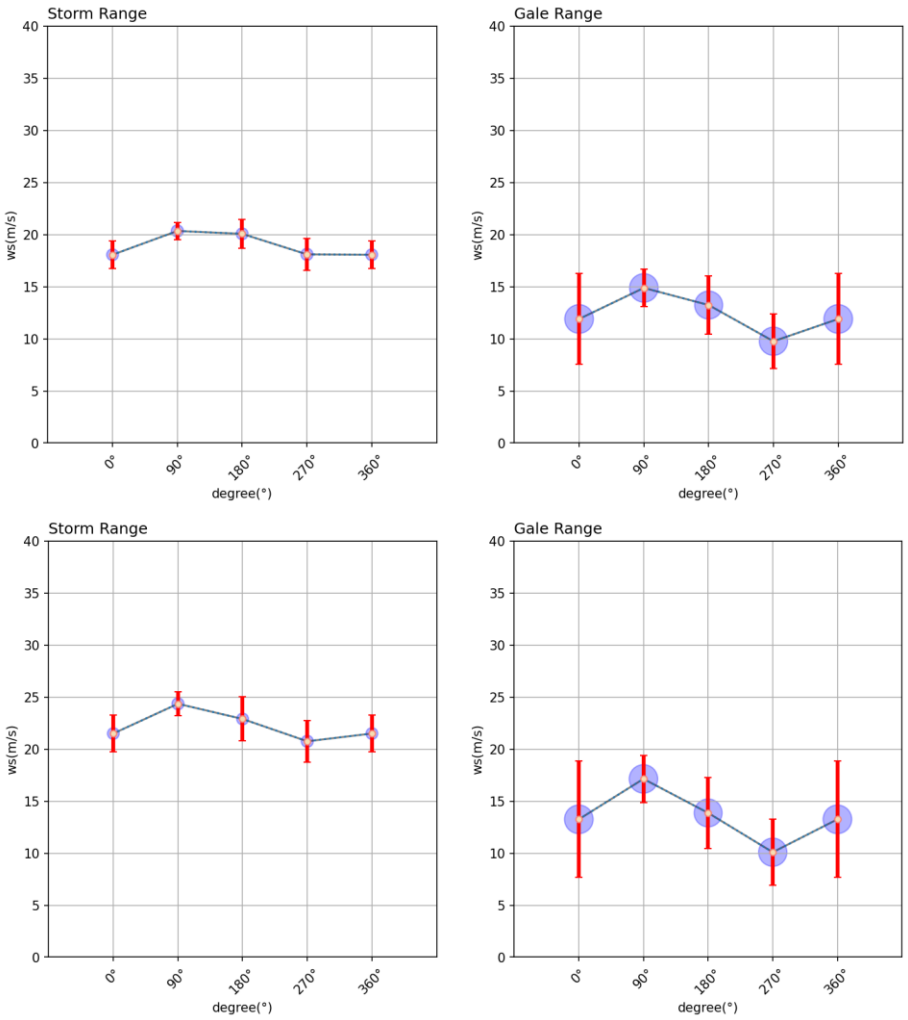

Fig.A-18 Sep.3 Wind speed distribution (the top set: CYGNSS; the second set: AMSR2; the third set: ERA5; the fourth set: CFSR2)

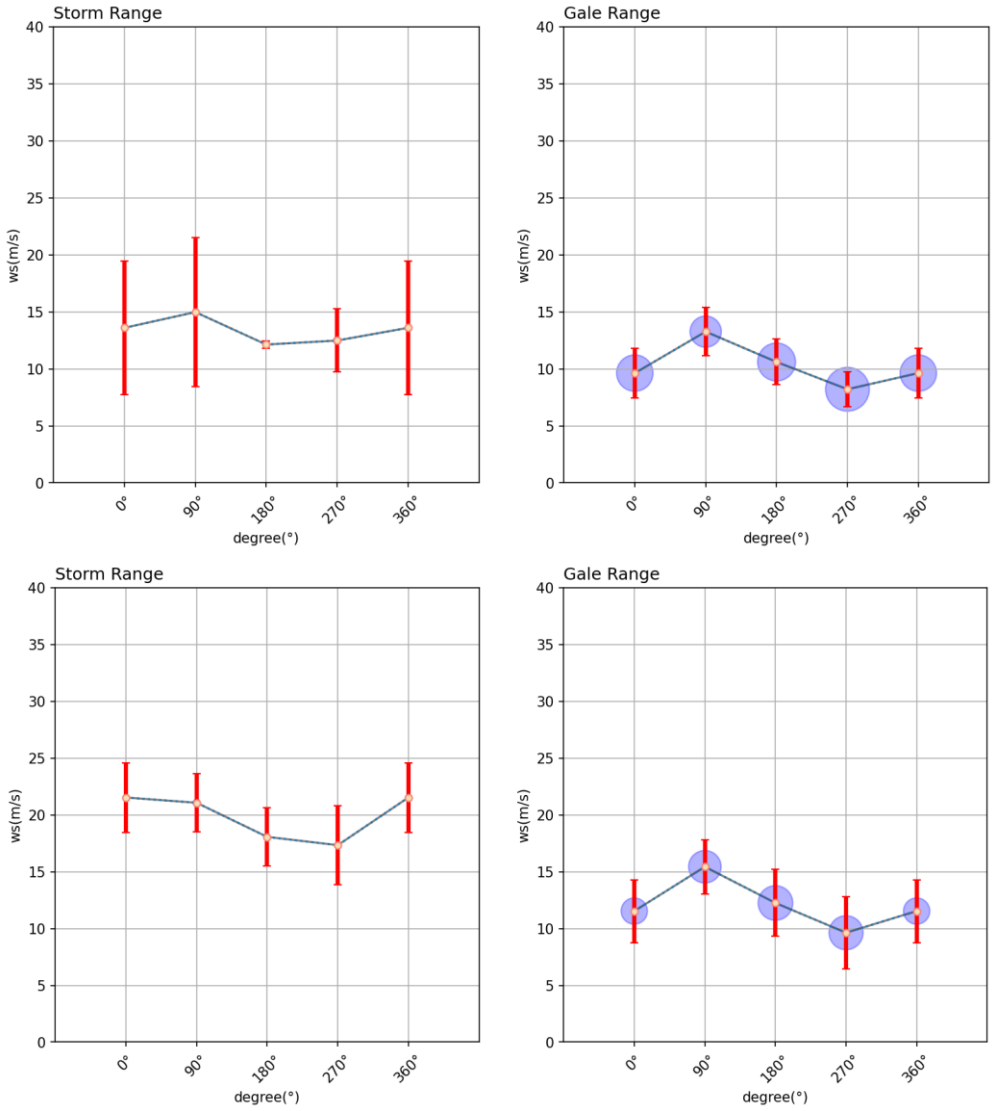
Storm Range
Gale Range
Storm Range
Gale Range
ws(m/s)
degree(°)
0°
90°
180°
270°
360°
0
5
10
15
20
25
30
35
40

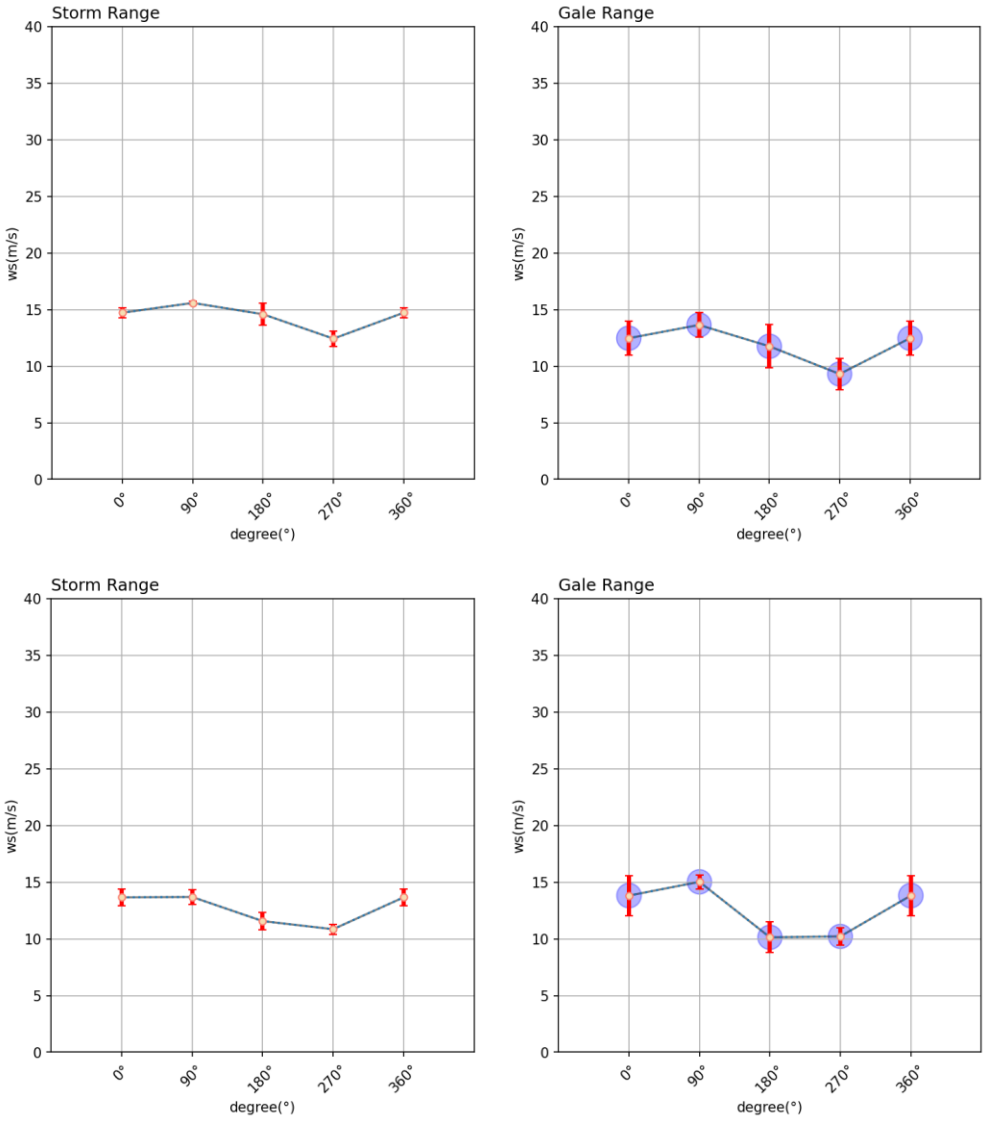

Fig.A-19 Sep.22 Wind speed distribution (the top set: CYGNSS; the second set: AMSR2; the third set: ERA5; the fourth set: CFSR2)

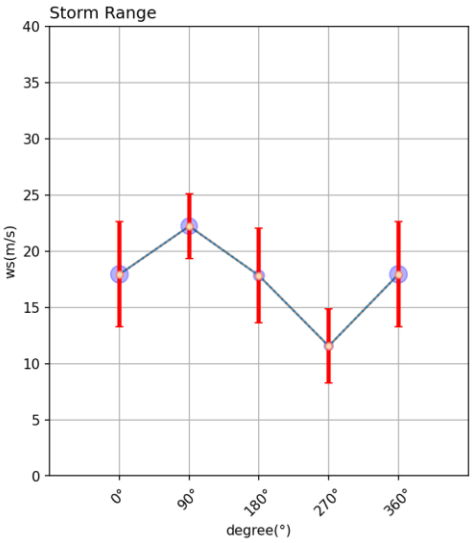
Storm Range
ws(m/s)
degree(°)
0°
90°
180°
270°
360°

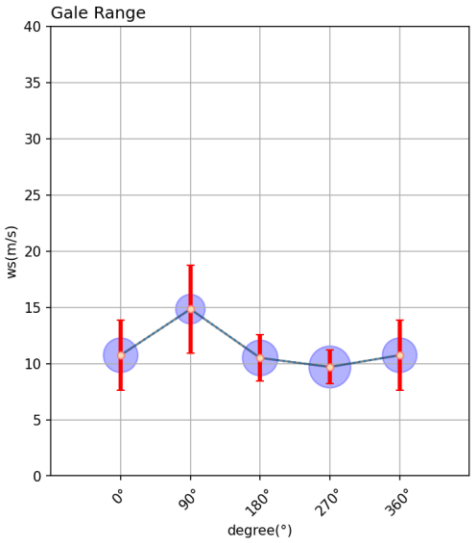
Gale Range
ws(m/s)
degree(°)
0°
90°
180°
270°
360°

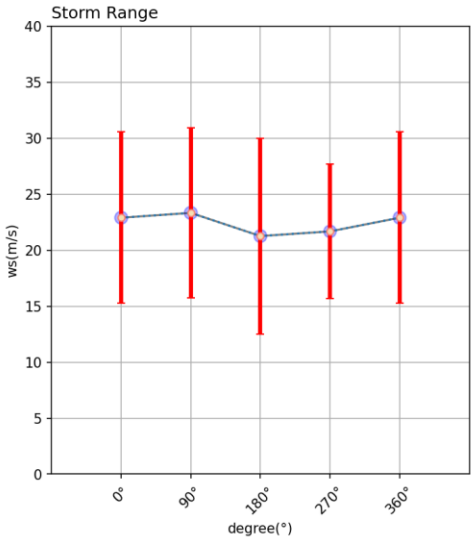
Storm Range
ws(m/s)
degree(°)
0°
90°
180°
270°
360°

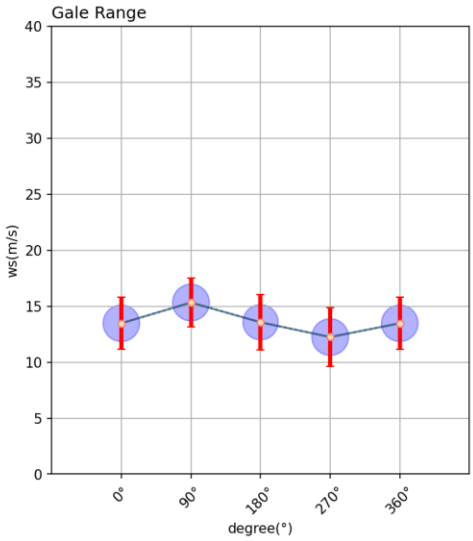
Gale Range
ws(m/s)
degree(°)
0°
90°
180°
270°
360°

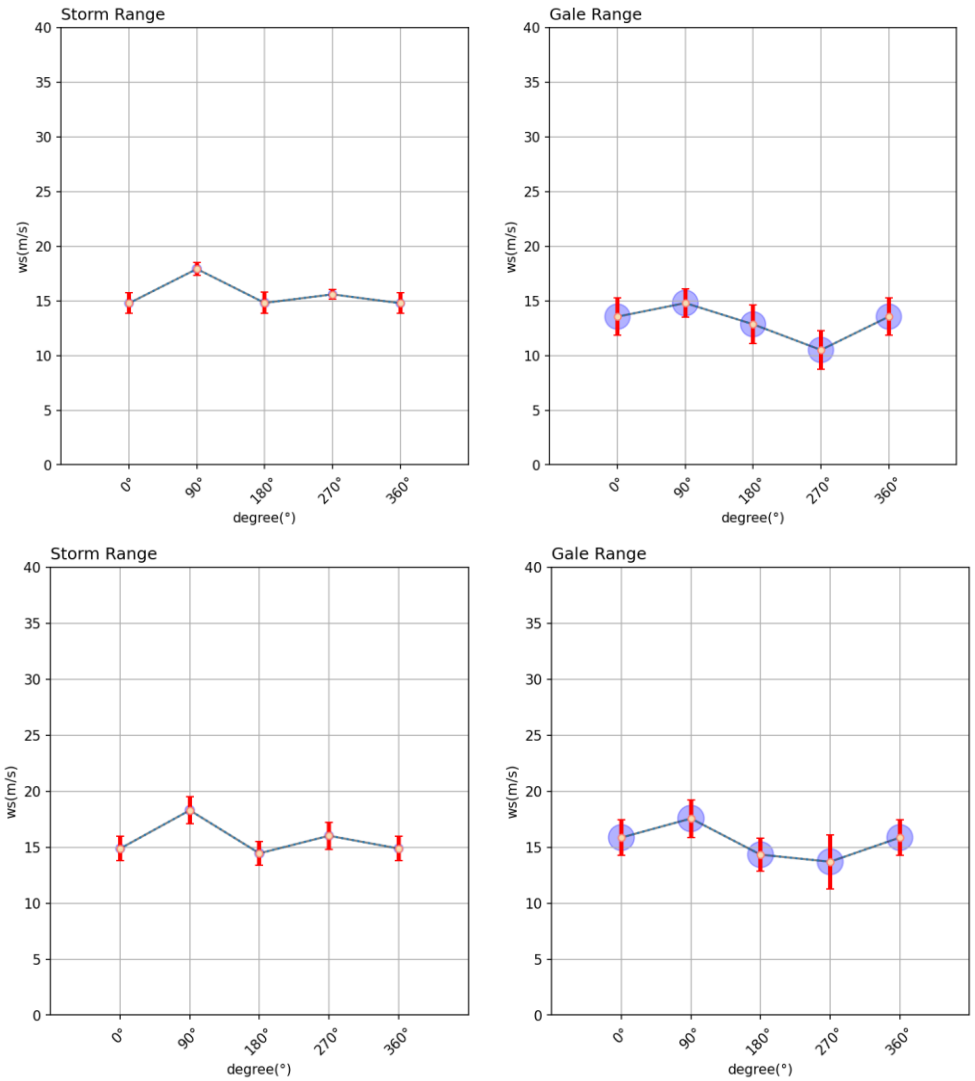

Fig.A-20 Sep.23 Wind speed distribution (the top set: CYGNSS; the second set: AMSR2; the third set: ERA5; the fourth set: CFSR2)

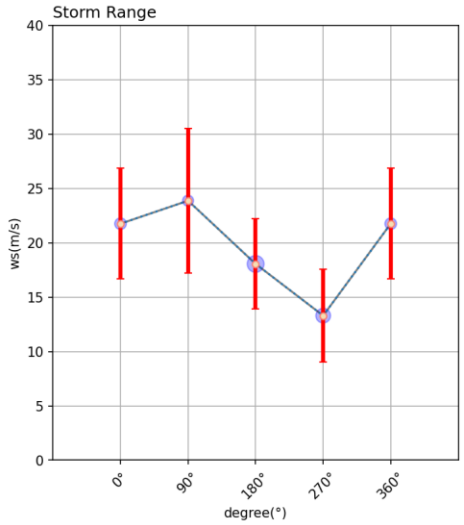
Storm Range
ws(m/s)
degree(°)
0°
90°
180°
270°
360°

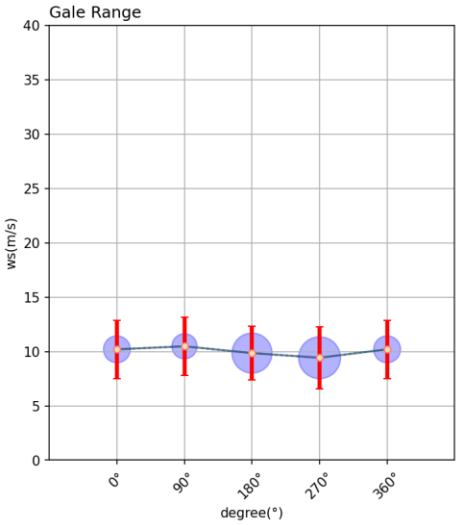
Gale Range
ws(m/s)
degree(°)
0°
90°
180°
270°
360°

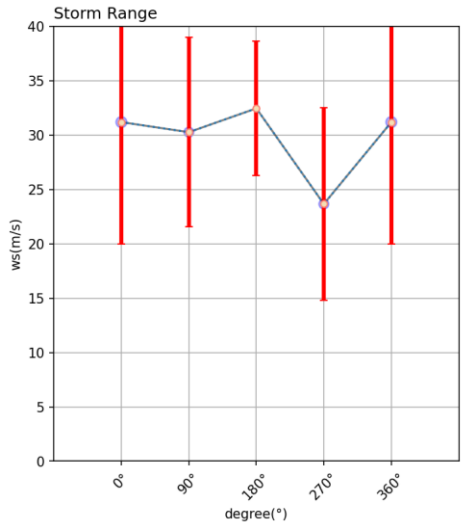
Storm Range
ws(m/s)
degree(°)
0°
90°
180°
270°
360°

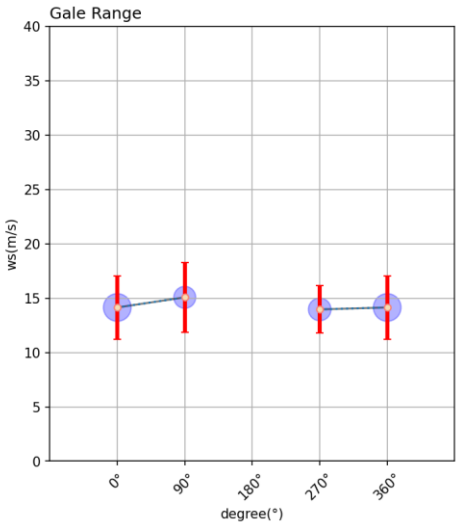
Gale Range
ws(m/s)
degree(°)
0°
90°
180°
270°
360°

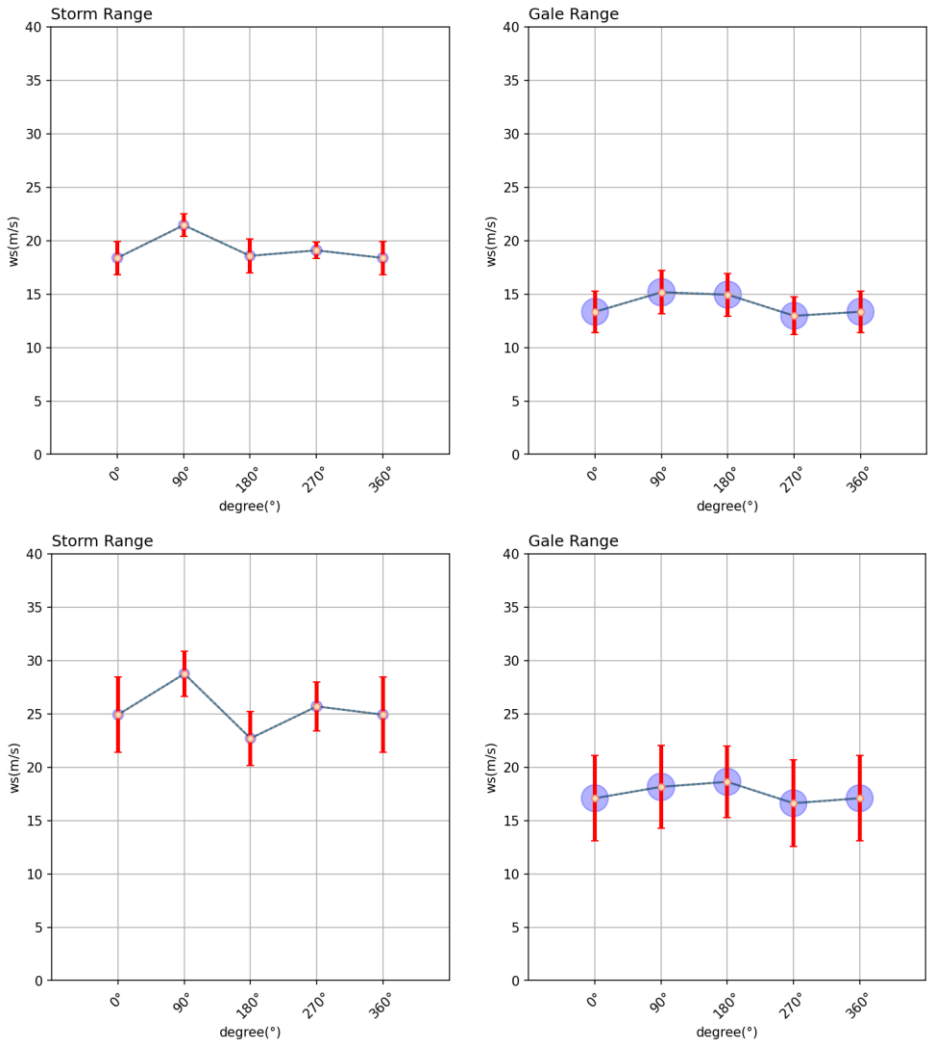

Fig.A-21 Sep.24 Wind speed distribution (the top set: CYGNSS; the second set: AMSR2; the third set: ERA5; the fourth set: CFSR2)

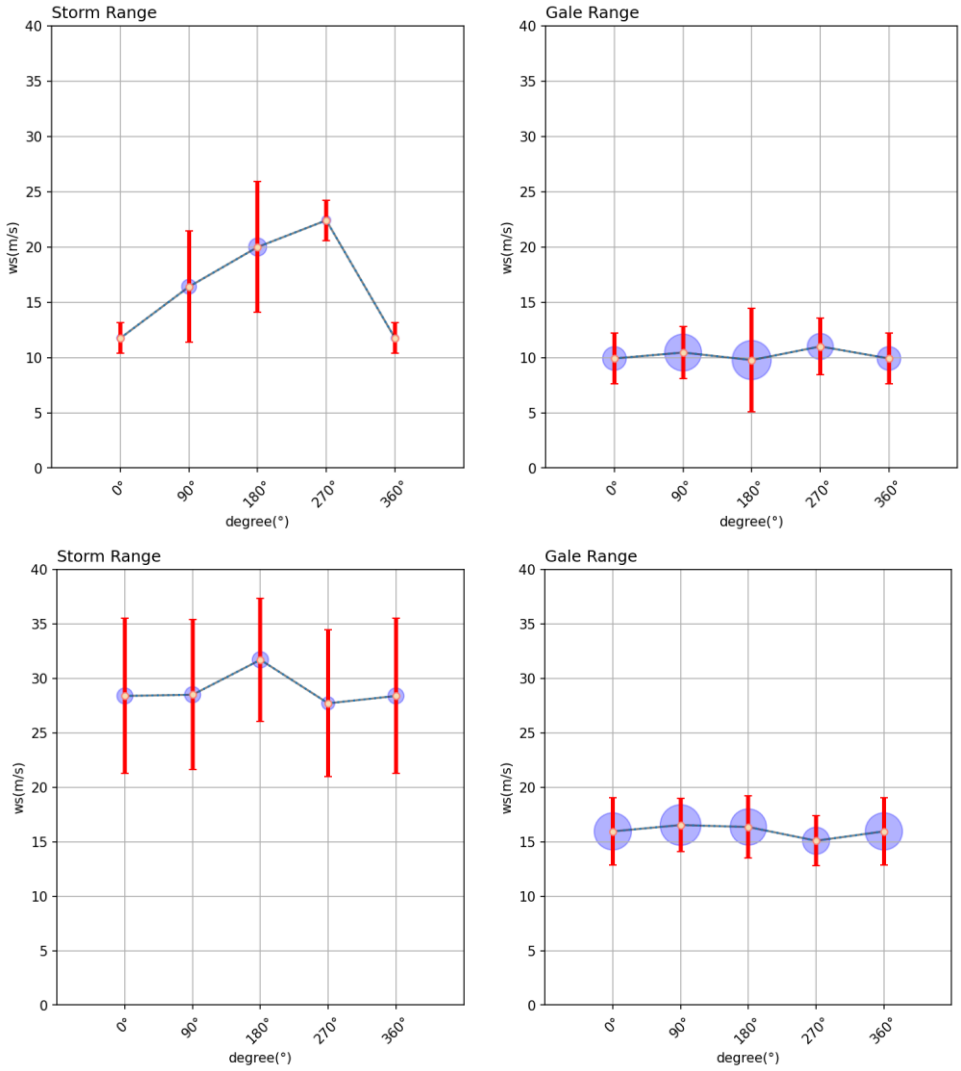
Storm Range
Gale Range
Storm Range
Gale Range
ws(m/s)
degree(°)
0°
90°
180°
270°
360°
0
5
10
15
20
25
30
35
40

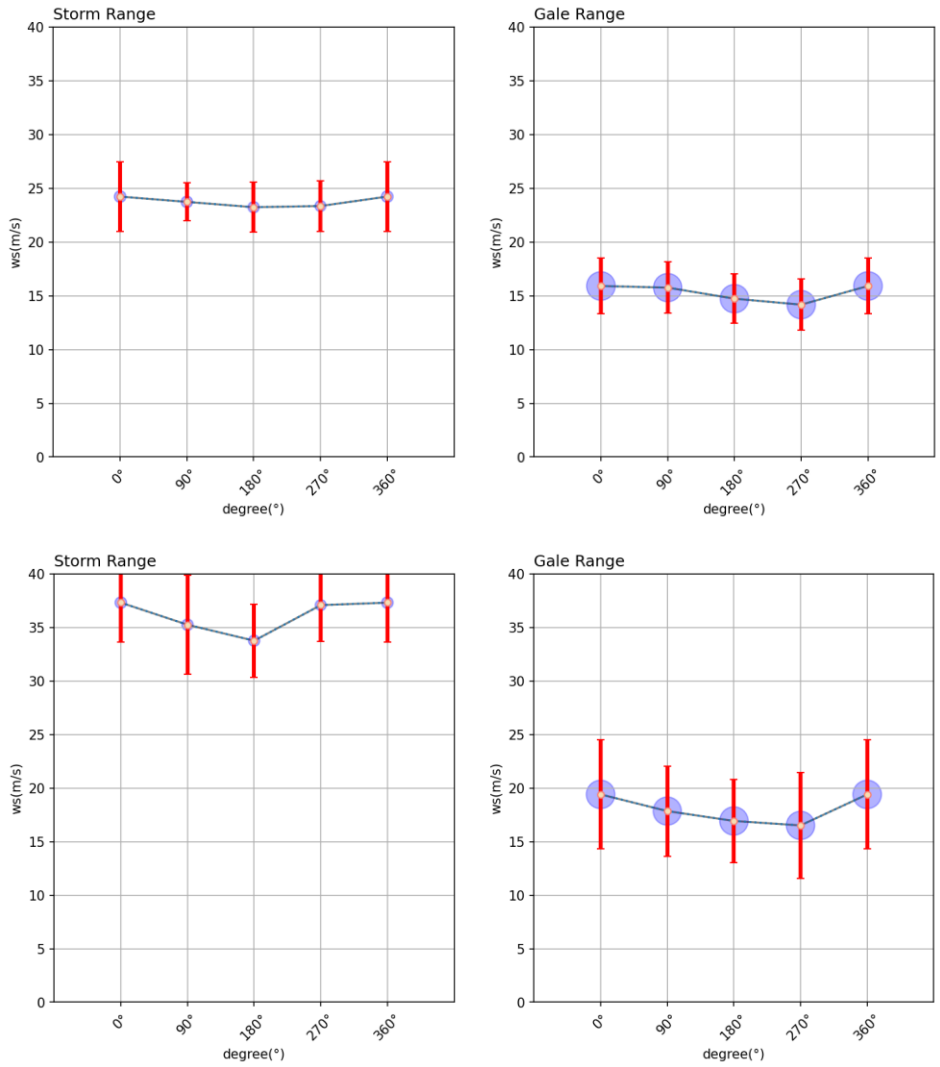

Fig.A-22 Sep.25 Wind speed distribution (the top set: CYGNSS; the second set: AMSR2; the third set: ERA5; the fourth set: CFSR2)

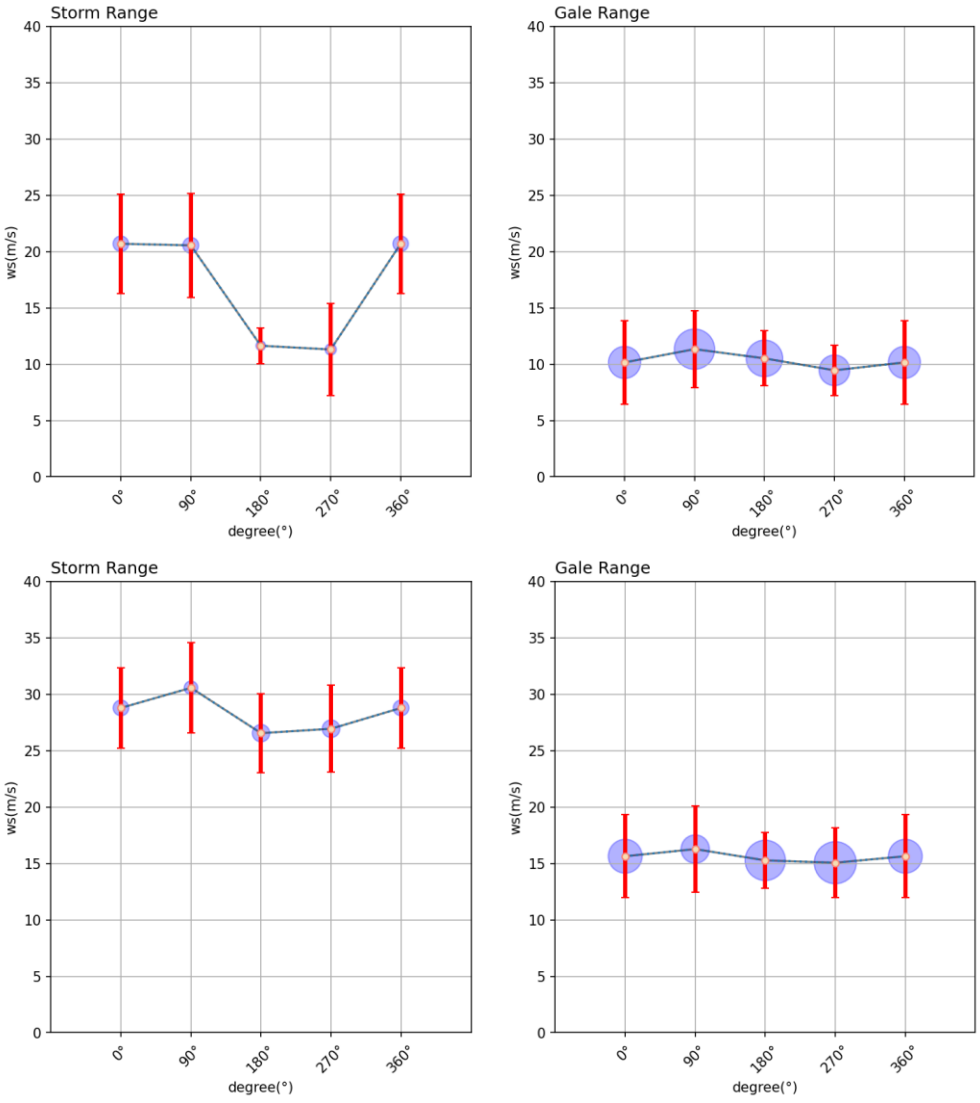
Storm Range
Gale Range
Storm Range
Gale Range
ws(m/s)
degree(°)
0°
90°
180°
270°
360°
0
5
10
15
20
25
30
35
40

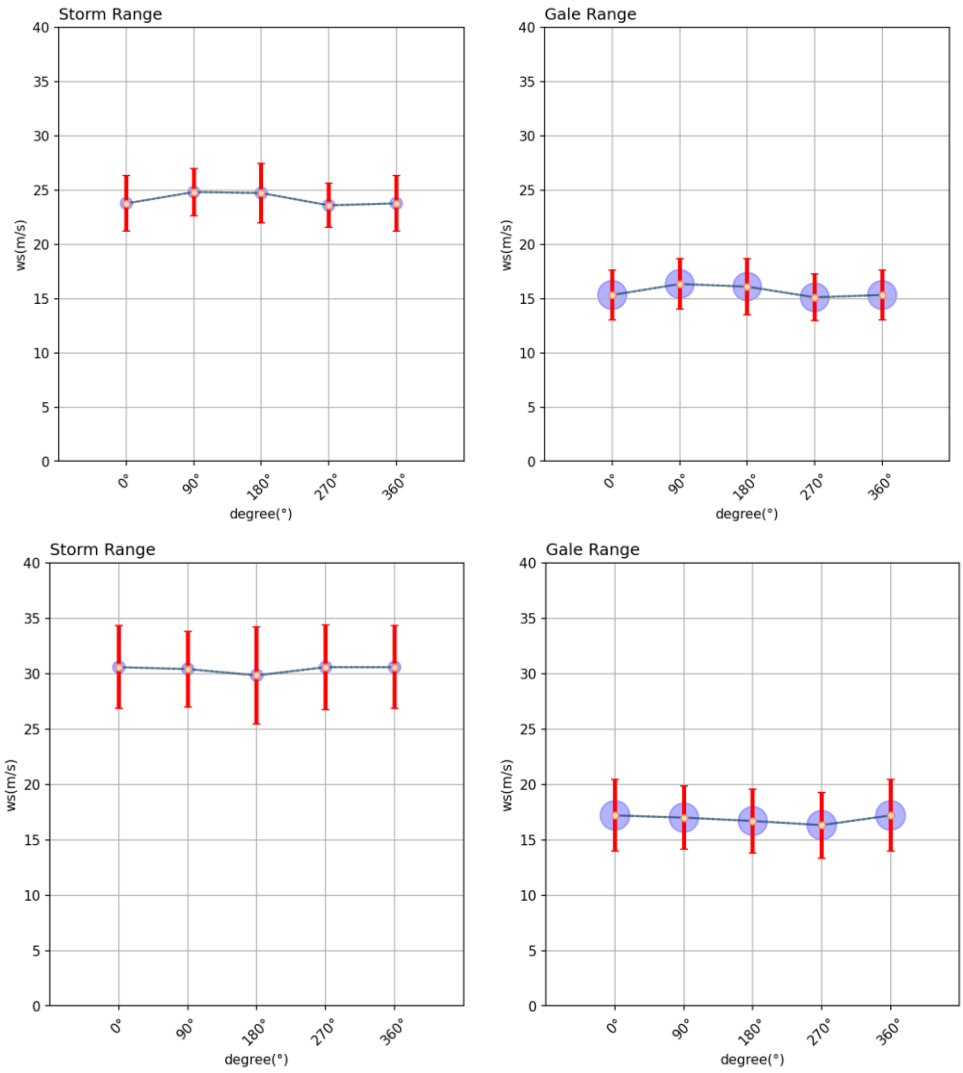

Fig.A-23 Sep.26 Wind speed distribution (the top set: CYGNSS; the second set: AMSR2; the third set: ERA5; the fourth set: CFSR2)

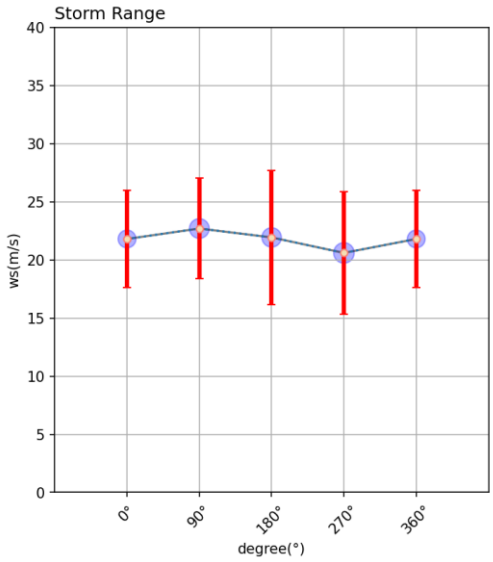
Storm Range
ws(m/s)
degree(°)
0°
90°
180°
270°
360°

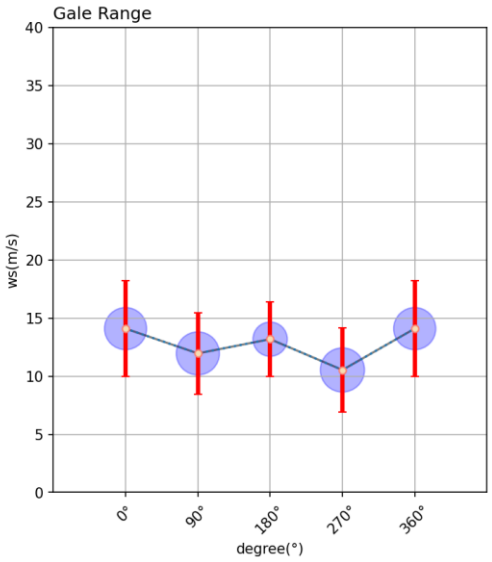
Gale Range
ws(m/s)
degree(°)
0°
90°
180°
270°
360°

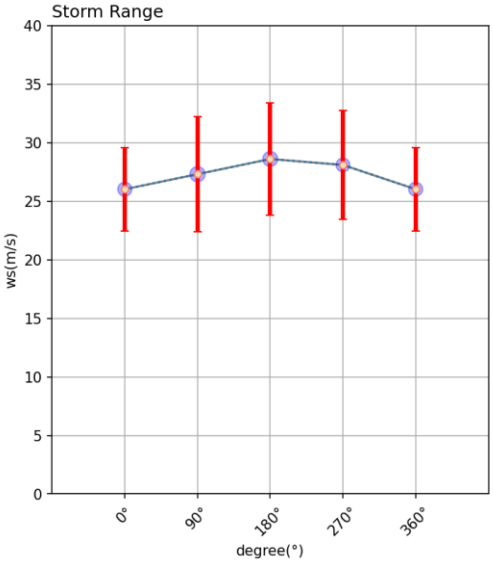
Storm Range
ws(m/s)
degree(°)
0°
90°
180°
270°
360°

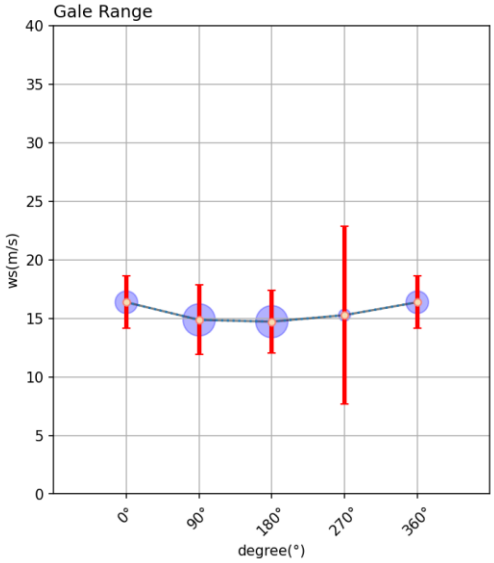
Gale Range
ws(m/s)
degree(°)
0°
90°
180°
270°
360°

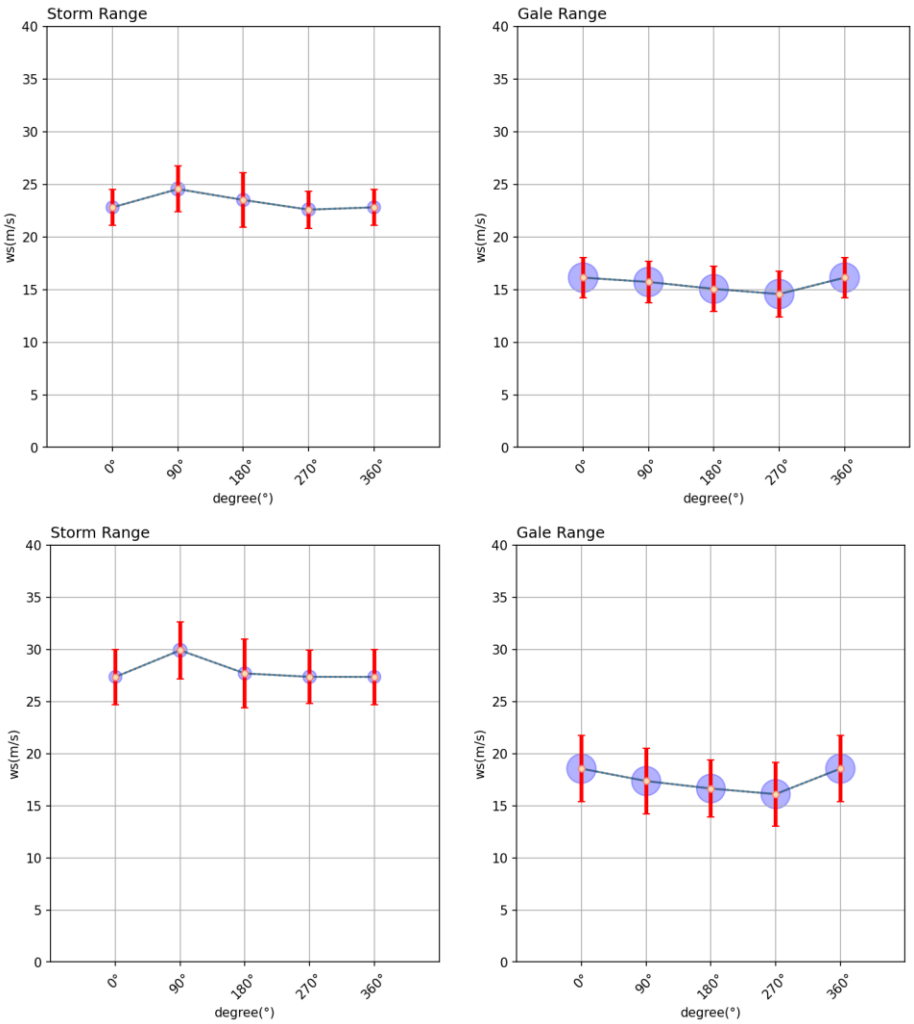

Fig.A-24 Sep.27 Wind speed distribution (the top set: CYGNSS; the second set: AMSR2; the third set: ERA5; the fourth set: CFSR2)